

# **Deciphering the role of human-specific genes in the development of the human neocortex**

Doctoral thesis  
to obtain a doctorate (PhD)  
from the Faculty of Medicine  
of the University of Bonn

**Fabio Marsoner**  
from Bolzano, Italy  
2024

Written with authorization of  
the Faculty of Medicine of the University of Bonn

First reviewer: Prof. Dr. Philipp Koch

Second reviewer: Prof. Dr. Susanne Schoch-McGovern

Day of oral examination: 29.11.2023

From the Hector Institute for Translational Brain Research (HITBR)

Director: Prof. Dr. Philipp Koch

From the Life and Brain Institute

Director: Prof. Dr. Oliver Brüstle

## TABLE OF CONTENTS

<b>LIST OF ABBREVIATION</b> .....	<b>- 5 -</b>
<b>1. INTRODUCTION</b> .....	<b>- 7 -</b>
1.1. THE MAMMALIAN CORTEX.....	- 7 -
1.1.1. <i>From the ectoderm to neural tube development</i> .....	- 7 -
1.1.2. <i>From the neural tube to brain region specification</i> .....	- 9 -
1.1.3. <i>Cortico genesis</i> .....	- 10 -
1.2. FEATURES OF THE HUMAN CORTICOGENESIS.....	- 14 -
1.2.1. <i>Emergence of the subventricular zone</i> .....	- 15 -
1.3. T-BOX BRAIN PROTEIN 2 ( <i>TBR2</i> ) SPECIFIC ROLE IN CORTICOGENESIS .....	- 17 -
1.4. THE ROLE OF <i>ARHGAP11B</i> IN THE HUMAN CORTICAL DEVELOPMENT .....	- 19 -
1.5. HUMAN BRAIN RESEARCH WITH <i>IN VITRO</i> MODELS .....	- 21 -
1.5.1. <i>Emergence of the induced pluripotent stem cells</i> .....	- 21 -
1.5.2. <i>Cortico genesis in two-dimensional (2D) cell cultures</i> .....	- 22 -
1.5.3. <i>Emergence of brain organoids</i> .....	- 24 -
1.5.4. <i>Forebrain organoids</i> .....	- 25 -
1.6. AIMS OF THE STUDY .....	- 26 -
<b>2. MATERIALS</b> .....	<b>- 28 -</b>
<b>3. METHODS</b> .....	<b>- 48 -</b>
3.1. CELL CULTURE PROTOCOLS .....	- 48 -
3.1.1. <i>Coating</i> .....	- 48 -
3.1.2. <i>Maintenance and passaging of human iPSCs (hiPSCs)</i> .....	- 48 -
3.1.3. <i>Generation of neural stem cells in 2D</i> .....	- 49 -
3.1.4. <i>Generation of dorsal forebrain organoids</i> .....	- 49 -
3.1.5. <i>Organoids single cell dissociation and RNA-sequencing</i> .....	- 50 -
3.1.6. <i>Fixation &amp; dehydration</i> .....	- 51 -
3.2. CRYOPRESERVATION AND CRYOSECTIONING.....	- 51 -
3.3. IMMUNOFLUORESCENCE (IF).....	- 51 -
3.4. DNA EXTRACTION.....	- 52 -
3.5. RNA ISOLATION.....	- 52 -
3.5.1. <i>Reverse Transcriptase for cDNA synthesis</i> .....	- 52 -
3.5.2. <i>Polymerase Chain Reaction (PCR)</i> .....	- 53 -
3.5.3. <i>Gene expression characterization by qRT-PCR</i> .....	- 54 -
3.6. WESTERN BLOT.....	- 54 -
3.7. STATISTICAL ANALYSES .....	- 54 -
<b>4. RESULTS</b> .....	<b>- 55 -</b>
4.1. GENERATION OF CRISPR/CAS9-BASED HIPSCS KO LINES.....	- 55 -
4.2. ORGANOID GENERATION AND CHARACTERIZATION .....	- 60 -
4.3. <i>ARHGAP11KO</i> .....	- 64 -
4.3.1. <i>ARHGAP11A vs ARHGAP11B</i> .....	- 68 -
4.4. <i>TBR2</i> .....	- 74 -
4.4.1. <i>Plane of division of apical radial glial cells</i> .....	- 74 -
4.4.2. <i>Cortico genesis</i> .....	- 76 -
4.5. CONTRIBUTORS .....	- 78 -
<b>5. DISCUSSION</b> .....	<b>- 79 -</b>
5.1. HUMAN <i>IN VITRO</i> GENE EDITING WITH ORGANIDS .....	- 79 -

5.2.	ROLE OF <i>ARHGAP11B</i> IN HUMAN BRAIN EVOLUTION .....	- 80 -
5.3.	<i>TBR2</i> IN CORTICOGENESIS .....	- 83 -
<b>6.</b>	<b>ABSTRACT .....</b>	<b>- 86 -</b>
<b>7.</b>	<b>LIST OF FIGURES .....</b>	<b>- 87 -</b>
<b>8.</b>	<b>LIST OF TABLES .....</b>	<b>- 88 -</b>
<b>9.</b>	<b>REFERENCES .....</b>	<b>- 89 -</b>
<b>10.</b>	<b>ACKNOWLEDGEMENTS .....</b>	<b>- 97 -</b>
<b>11.</b>	<b>CURRICULUM VITAE .....</b>	<b>- 98 -</b>

## List of Abbreviation

2D: 2 dimensional	GABA: Gamma-aminobutyric acid
3D: 3 dimensional	GFAP: Glial Fibrillary Acidic Protein
aIP: apical Intermediate Progenitors	GFP: Green Fluorescent Protein
ANR: Anterior Neural Ridge	GLAST: Glutamate Aspartate Transporter
ANT: Adenine Nucleotide Translocase	gRNA: guide RNA
aRG: apical Radial Glia	H: hour
ARHGAP: Rho GTPase Activating Protein	HDR: Homology Directed Repair
BCA: bicinthonic acid assay	HOPX: Homeodomain-only Protein
bIP: basal Intermediate Progenitors	Homeobox
BMP: Bone Morphogenic Protein	IF: Immunofluorescence
bRG: basal Radial Glia	INM; Interkinetic Nuclear Migration
BRN2: POU domain, class 3 transcription factor 2	INSM1: Insulinoma-associated 1 gene
BSA: Bovine Serum Albumin	IO: Isthmic Organizer
Cas9: CRISPR associated protein 9	IP: Intermediate Progenitors
CDH1: Cadherin1	iPSC: induced pluripotent stem cell
cMyc: Myc Proto-oncogene, bHLH transcription factor	IZ intermediate zone
CNS: Central Nervous System	ISVZ: Inner Subventricular Zone
CP: Cortical Plate	KLF4: Kruppel like factor 4
CRISPR: Clustered Regularly Interspaced Short Palindromic Repeats	KO: Knock-Out
CTIP2: (or BSL11B) B-cell lymphoma/leukemia11B	LGE: Lateral Ganglionic Eminence
CXCL: C-X-C Motif Chemokine Ligand	LHX2: LIM/homeobox protein 2
DAPI: 4',6'-diamidino-2-phenolindole	LMX1a: LIM homeobox transcription factor 1, alpha
DNA: deoxyribonucleic acid	LZTS1: Leucine Zipper Tumor Suppressor 1
EB: Embryoid Bodies	MCPH1: Microcephalin 1
EDTA: ethylenediamine tetra acetic acid	MGE: Medial Ganglionic Eminence
EMX2: Homeobox protein 2	min: minutes
ETV: translocation-Ets-leukemia virus	mPTP: mitochondrial Permeability Transition Pore
FAM107A: Family with Sequence Similarity 107 Member A	MST: Mitotic Somal Translocation
FGF: Fibroblastic Growth Factor	MZ: Marginal Zone
FOXP1: Forkhead box G1	NCS: Neural Stem Cell
	NE: Neuroepithelial cell
	NEUROD: Neurogenic Differentiation
	NIF1: Zinc Finger Protein 335

OCT4: Octamer-binding-transcription factor  
4

OTX2: homeobox protein OTX2

OSVZ: Outer Subventricular Zone

PAX6: Paired Box protein 6

PBS: Phosphate Buffered Saline

PCDH11Y: Protocadherin 11Y

PCR: Polimerase Chain Reaction

PFA: Paraformaldehyde

PP: Preplate

PPP1R17: Protein Phosphatase 1  
regulatory subunit 17

PTPRZ1: Protein Tyrosin Phosphatase  
Receptor Type Z1a

PVDF: polyvinylidene fluoride

pVIM: phosphorylated Vimentin

RA: Retinoic Acid

RFP: Red Fluorescent Protein

RG: Radial Glia

RhoGAP: Rho GTPase activating Protein

RI: Rho-associated coiled coil containing  
protein kinase Inhibitor

RNA: Ribonucleic acid

RT: Room Temperature

SATB2: Specia AT-rich sequence-binding  
protein 2

scRNA-seq: single cell RNA sequencing

SDS-PAGE: sodium dodecyl sulfate

polyacrylamide gel electrophoresis

SFEB: Serum-free culture of Embryoid  
Body-like

Shh: Sonic Hedgehog

SNP: Single Nucleotide Polymorphism

SOX2: SRY-Box Transcription Factor 2

SVZ: Subventricular Zone

TCA: Tricarboxylic Acid

TBR: T-box Brain Protein

TBST: Trisbuffered Saline with Tween20

TGF: Transforming Growth Factor

TMEM14B: Transmembrane Protein 14B

# **1. Introduction**

## **1.1. The mammalian cortex**

The brain is the most complex, stunning and mysterious organ in our body. Compared to non-human primates, the human brain went upon great enlargement during evolution. The genetic and cellular mechanisms responsible for this remain incompletely understood <sup>1</sup>. The neocortex, the central hub of neural integration and complex neural circuits, accounts for more than 75% of total human brain volume <sup>2-4</sup>. It is also the origin of higher functions, like consciousness, language, and memory <sup>4-6</sup>. Together with the pyriform, entorhinal cortex (paleocortex) and hippocampus (archicortex), the neocortex forms the cerebral cortex <sup>7</sup>. The neocortex represents 90% of the cortex, thus it is often and also in this thesis referred to as cortex.

The developed human cortex contains several neuronal populations organized into six distinct layers. 80% of the whole cortex is composed of glutamatergic excitatory neurons while the rest consists of GABA ( $\gamma$ -aminobutyric acid)-ergic inhibitory neurons and glial cells <sup>7-9</sup>. The neurons form connections to other brain regions, generating several complex networks that underly crucial information processing activities. The human cortex is also referred to as grey matter, since most of the somas are collected there, while the neuronal myelinated extensions are mostly located in the subcortical area also called white matter <sup>7</sup>. To fully understand the following work, it is important to understand the development of the human cortex.

### ***1.1.1. From the ectoderm to neural tube development***

The first phase of brain development starts a few weeks post conception <sup>10</sup>, when in the embryo three cell layers can be detected: endoderm, mesoderm and ectoderm <sup>11-13</sup>. From the endoderm all internal organs will be generated, the mesoderm gives rise to bones and muscles, while the entire nervous system and skin arise from the ectoderm. In particular, the human nervous system develops from the neuroectoderm, a portion of the ectoderm cell layer that receives specific bone morphogenic protein (BMP) -inhibiting signals from the underlying axial mesoderm <sup>14,15</sup>. This signaling follows a thickening of the neuroectoderm and the generation of the neural plate. At this point a process called

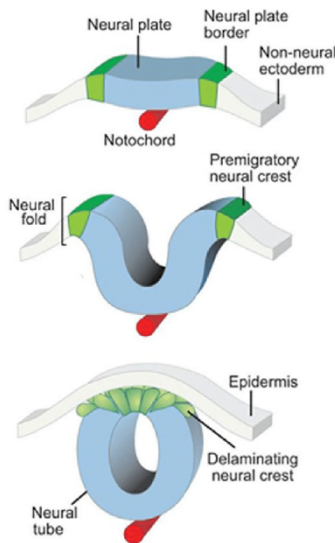


**Figure 1 NEURULATION.**

The formation of the neural tube is called neurulation. It takes place when a thin layer of cells, the neuroectoderm, starts to thicken. A subsequent invagination of this layer leads to the formation of the neural groove. Here the invaginated neuroectoderm is flanked by the premigratory neural crest cells and the non-neural ectoderm. The closure of the neural groove gives rise to the neural tube. Ventrally the notochord is releasing specific morphogens facilitating the process. Dorsally the ectoderm layer is merged, and the neural crest cells can be seen located between the neural tube and the ectoderm. Adapted from Simoes-Costas and Bronner, 2015

neurulation takes place <sup>16</sup> (Figure 1). Invagination of the neural plate establishes the so-called neural groove. Folding and fusion of the neural groove generates the first 3D neuronal structure: the neural tube <sup>13,17-19</sup>. Several cells and structures are present or generated around the neural tube, including: the notochord, located ventrally and later in development responsible for the generation of peripheral neurons; neural crest cells, located dorsally at the edge of the neural tube fusion; the somites, mesoderm regions located at both sides of the neural tube; the epidermal ectoderm, located dorsally and later responsible of the skin generation <sup>20</sup>.

Neurulation is guided by morphogens present at different concentrations along the dorso-ventral and rostro-caudal axis of the neural tube <sup>21,22</sup>. Dorsally, the epidermal ectoderm releases BMP, a member of the Transforming Growth Factor  $\beta$  (TGF- $\beta$ ) family <sup>22-24</sup> which specify the roof plate. Here BMP also activates an additional morphogen, namely Wingless related integration site (Wnt). Two isoforms: Wnt response 1 and 3a (Wnt1 and Wnt3a) are highly expressed in the roof plate <sup>25</sup>. Ventrally, the notochord is responsible for the release of Sonic Hedgehog (Shh) and floor plate induction (Figure 2) <sup>21,26-28</sup>. All the cells between the roof and floor plate experience a gradient of those



morphogens and the presence of BMP/Wnt or Shh will determine the dorsal or ventral fate of the cells, as illustrated in Figure 2<sup>18,21,25</sup>.

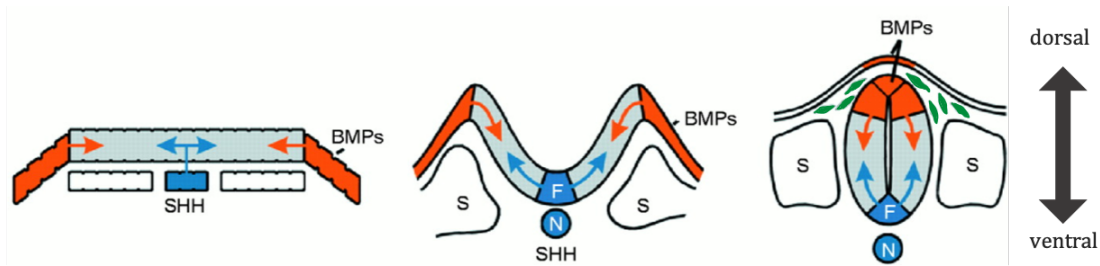


**Figure 2 MORPHOGENS PATTERNING THE NEURAL TUBE.**

The neural tube formation is driven by morphogens secreted by the epidermal ectoderm and the notochord. The epidermal ectoderm initially and the roof plate later on, release BMP, inducing the dorsal identity. On the other hand, the notochord initially and the floor plate later on release Shh, inducing the ventral identity. BMP: Bone Morphogenic Protein; SHH: Sonic Hedgehog; F: floorplate; S: somites; N: notochord. Adapted from Tanabe and Jessell, 1996.

### 1.1.2. From the neural tube to brain region specification

Proliferation of the cells in the neural tube results in the formation of three primary vesicles<sup>7,29</sup>. The *prosencephalon* (forebrain) that is the most rostral part, the *mesencephalon* (midbrain) develops posteriorly from the previous one, followed by the *rhombencephalon* (hindbrain) as most caudal structure. Over time the *prosencephalon* subdivides into two additional vesicles, the *telencephalon* and *diencephalon* and so does the *rhombencephalon* giving rise to the *metencephalon* and *myelencephalon*. Caudally, the narrow tube becomes the spinal cord. In a fully developed brain, the *telencephalon* is the largest part of the brain, and it includes the cerebral cortex, the hippocampus, the olfactory bulb, and the basal ganglia<sup>7</sup>. The *mesencephalon* includes the tectum, the cerebral aqueduct, the tegmentum, and the cerebral peduncles, while the cerebellum, the pons, the medulla, and the brainstem are part of the *rhombencephalon*.

Morphogens also play a key role for the rostro-caudal development of the neural tube in the different vesicles. To achieve the correct morphogen gradients at the correct location, three secondary organizers arise in the developing neural tube. The organizers are regions that delimit the vesicles and secrete morphogens to help the regionalization of the neural tube. They are called: anterior neural ridge (ANR), zona limitans intrathalamica (ZLI) and isthmic organizer (IO) (Figure 3)<sup>30</sup>. ANR is the most anterior

secondary organizer, and is important to specify forebrain identity<sup>30</sup> by secretion of BMP/Wnt<sup>24,31</sup>, and also through Fibroblastic Growth Factors (FGFs). An example is FGF8, which is able to induce Forkhead box G1 (FOGX1) expression, a marker of forebrain identity<sup>24,30,32</sup>.

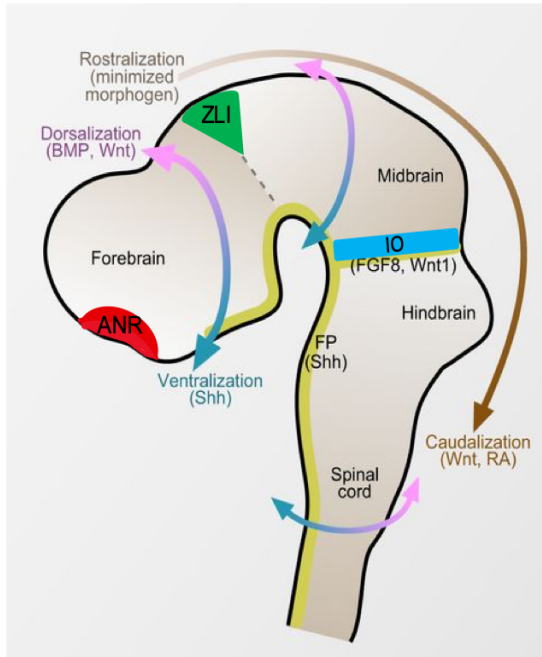


**Figure 3 DETERMINATION OF BRAIN REGIONAL IDENTITIES**

During early development the brain is subjected to different morphogens, determining the different brain regional identities. Secondary organizers help in the process delimiting those areas and secreting specific morphogens. The anterior neural ridge (ANR) induces the forebrain identity; the zona limitans intrathalamica (ZLI) is located in the forebrain-midbrain boundary and the Isthmic organizer (IO) delimits the midbrain to the hindbrain. In addition to BMP, Wnt and Shh influencing the dorso-ventral axis, Wnt and Retinoic acid increase their concentration caudally. BMP: Bone Morphogenic Protein; SHH: Sonic Hedgehog; FP: floor plate; FGF: Fibroblastic Growth Factor; RA: Retinoic Acid. Adapted from: Suzuki and Vanderhaeghen, 2015.

The ZLI is important to establish the diencephalon through the expression of Shh, Wnt and the FGF family<sup>33–36</sup>. The IO is located between the midbrain and the hindbrain. It functions as a boundary and expresses caudally FGF8 to induce hindbrain identity and Wnt1 rostrally to sustain the midbrain development<sup>37,38</sup>. An additional morphogen known to play a role in the hindbrain patterning is retinoic acid, present in the whole brain at low concentrations and more abundant in the most caudal region<sup>39</sup>. Its' role in forebrain patterning has yet to be fully characterized<sup>40–43</sup>.

### **1.1.3. Corticogenesis**

Neuroepithelial cells (NEs) proliferate and generate a packed region organized in layers around a central cavity, called the ventricle. This organization of NEs around the ventricle is referred to as the ventricular zone (VZ). (Figure 4)<sup>44</sup>. NEs are highly proliferative cells meant to increase the surface area and the thickness of the neocortex<sup>45</sup>. They undergo so-called symmetric cell division during which one cell gives rise to two daughter cells with the same characteristics<sup>46–48</sup>. Once the thickness of the neocortex

increases, the NE population develop into a new progenitor subtype, referred to as radial glial (RG) cells <sup>44,49</sup>.

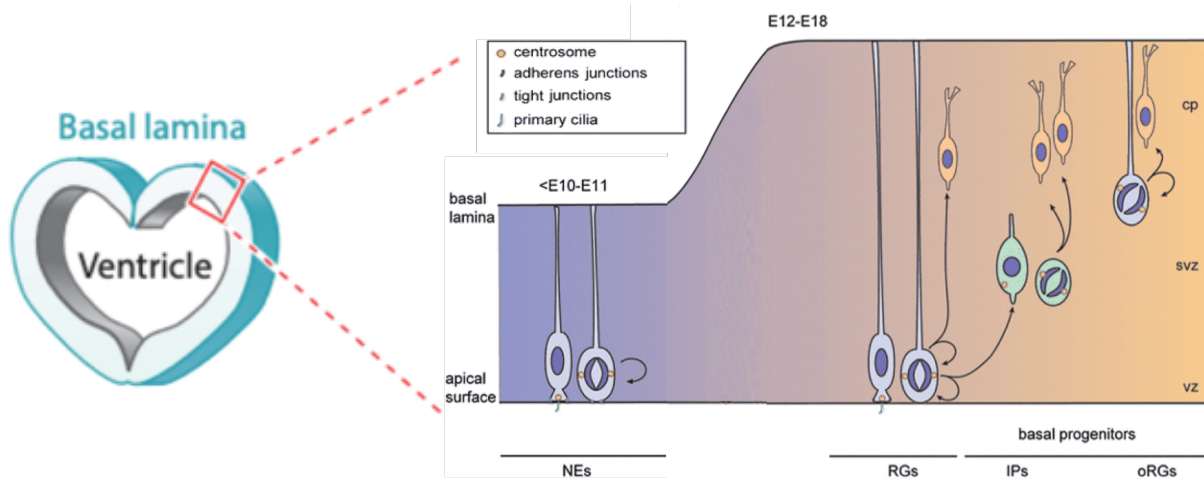


**Figure 4 GROWTH OF THE NEURAL TUBE**

Neuroepithelial cells (NEs) are the first cells to populate the neural tube. They undergo symmetrical cell division to self-renew and generate a thick layer of cells spanning the apical-basal axis. Over time those cells develop into radial glial cells (RGs). Those can also divide asymmetrically, giving rise to basal progenitors and eventually neurons. IPs: intermediate progenitors; oRGs: outer radial glial cells; VZ: ventricular zone; SVZ: subventricular zone; CP: cortical plate; E: Embryonic day. Adapted from: Laguesse et al., 2015; Taverna et al., 2014.

RGs have the ability to span throughout the entire neuroepithelium. RGs extend their end feet to the pial surface (basal side), while maintaining their soma close to the apical surface (ventricle) <sup>44,50</sup>. Those cells are still expressing the typical progenitor markers SRY-Box Transcription Factor 2 (SOX2) and Paired Box protein 6 (PAX6), but also astroglia markers, like Glial Fibrillary Acidic Protein (GFAP) and Glutamate Aspartate Transporter (GLAST), or intermediate filament proteins like Nestin and Vimentin <sup>51–54</sup>. RGs can be divided into apical (aRG) or basal (bRG, or oRG) based on the location of their mitoses. Unlike NEs, RGs do not undergo symmetrical division indefinitely. One RG can for example give rise to intermediate progenitors (IPs), bRGs or neurons.

All those cellular subtypes use the long process of the aRG, spanning through the apical-basal neocortex, to migrate to different locations. aRG can self-expand through symmetrical proliferation or generate neurons with asymmetrical or oblique cellular division. Interestingly, based on the cleavage plane, one progenitor cells can either give rise to two progenitor cells (symmetrical division through the vertical plane) or generate one progenitor and one neuron (asymmetrical division through the horizontal or oblique

plane) (Figure 5)<sup>44,55,56</sup>. Initially, aRGs mostly undergo symmetrical divisions and can give rise to RG or IP cells. Subsequently, their divisions mostly become asymmetrical and they start to also give rise to neurons<sup>45,57,58</sup>.

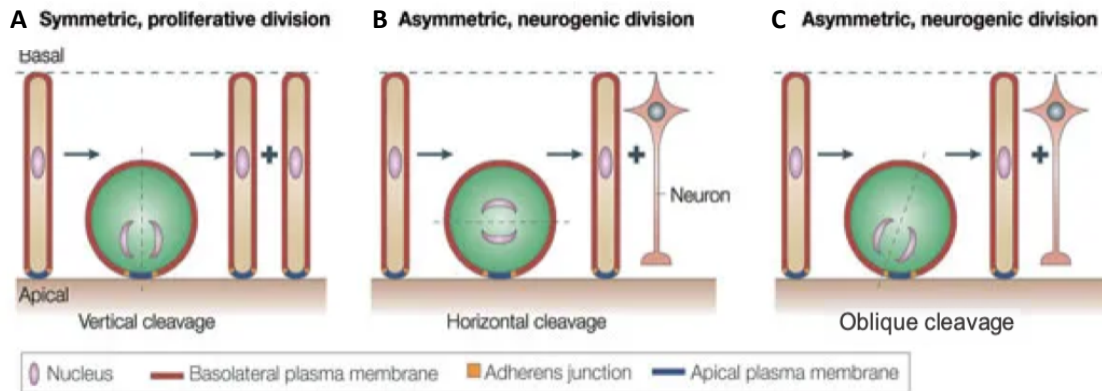


**Figure 5 SYMMETRIC VS ASYMMETRIC DIVISION OF RADIAL GLIAL CELLS**

On the apical plane RG cells go upon cell division. An RG cell can generate two identical daughter cells when the division is symmetrical, and these divisions take place on the vertical cleavage plane. We refer here to the proliferative division (A). An asymmetrical division in the horizontal (B) or oblique (C) cleavage plane generate a progenitor cell and a neuron and is thus it is also called neurogenic division. Adapted from: Götze and Huttner, 2005

NEs and aRGs developed a peculiar motion to properly distribute in the ventricular zone, called interkinetic nuclear migration (INM). During this process the cells' soma moves on its apical-basal axis according to the cell cycle stage they are in. During the G1 phase, the soma moves basally until the S phase is reached. At this point an opposite motion starts, lasting the entire G2 phase at the end of which the soma returns back to the apical surface. Here the cells divide and restart the cycle, resulting in a pack layering of cells in the VZ (Figure 6)<sup>46,56,59</sup>. This motion has the important function of saving space in the developing brain and allowing more cells to proliferate<sup>60</sup>. Another theory suggests that INM might be important to expose the cells to different signaling gradients along the apical-basal axis<sup>61</sup>.

Following asymmetric divisions, the first neurons migrate on the apical-basal axis forming a layer of precursor neurons, referred to as the preplate (PP) and located between the VZ and the pia. (Figure 7)<sup>62,63</sup>. From this thin layer, initially mostly composed by Reelin expressing-Cajal-Retzius cells and progenitor projection neurons, the whole gray and white matter of the cortex will develop<sup>64,65</sup>. As neurons accumulate, the PP divides into

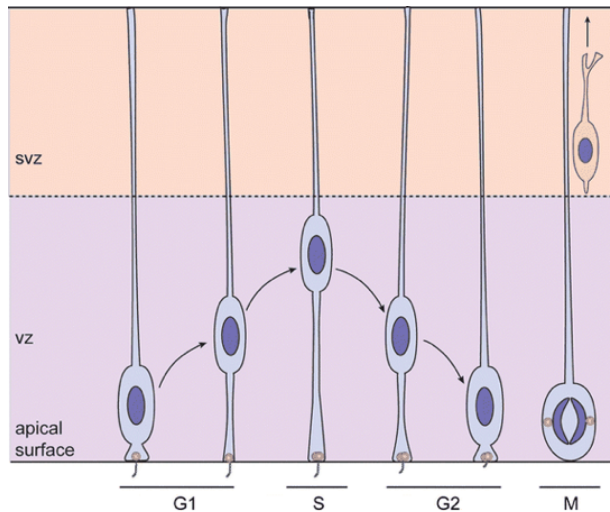


**Figure 6 INTERKINETIC NUCLEAR MIGRATION IN THE VENTRICULAR ZONE**

Radial glial cells having an attachment at the apical surface of the ventricular zone undergo INM to efficiently distribute the some in this packed region. The process is characterized by the migration of the nuclei on the apical-basal axis of the cell according to the cell cycle phase the cells is in. SVZ: subventricular zone; VZ: ventricular zone; G1, S, G2, M: cell cycle stages. Adapted from Laguesse et al. 2015

intermediate zone (IZ) and subplate (SP) and the VZ divides into VZ and subventricular zone (SVZ) <sup>66</sup>. The SVZ in development contains the bRG cells and IP, while the VZ is reduced to a single cell layer over time and it is the area where ultimately ependymal cells reside <sup>67</sup>. The IZ soon becomes the area where neuronal myelinated processes will accumulate, the white matter <sup>68</sup>. The SP in contrast is a heterogeneous population of pyramidal neurons and glial cells containing early-born cells, that over time will also merge in the white matter <sup>69,70</sup>.

At week 8 of development, migrating pyramidal neurons start to accumulate in the pial surface, giving rise to the CP. Here, over time the six-layered mature cortex will reside. The cortex develops in an inside-out process, where the layer VI neurons are the first to be originated, followed by layer V, IV and so on. The name inside-out is based on the fact that the cells from every new layer migrate from the VZ to the outermost region of the developing cortex, even beyond the previously generated layers. A pyramidal neuron from the layer III, for example, will be generated after the neurons from layer IV and to reach its final destination, it will need to migrate from the VZ to the CP and here pass-through layer VI, V, and IV to find its final destination. In fact the uppermost layer will be named as layer I and is also where the youngest neurons are located <sup>71</sup>. The neurons generated at this stage are mainly excitatory glutamatergic neurons, although in the adult cortex other neuronal subtypes are also found. Those originate in other regions of the developing brain and then migrate in the cortex. Inhibitory GABAergic interneurons or

oligodendrocytes, for example, migrate from the ventrolateral telencephalon to the cortex (Figure 7A) <sup>72</sup>.

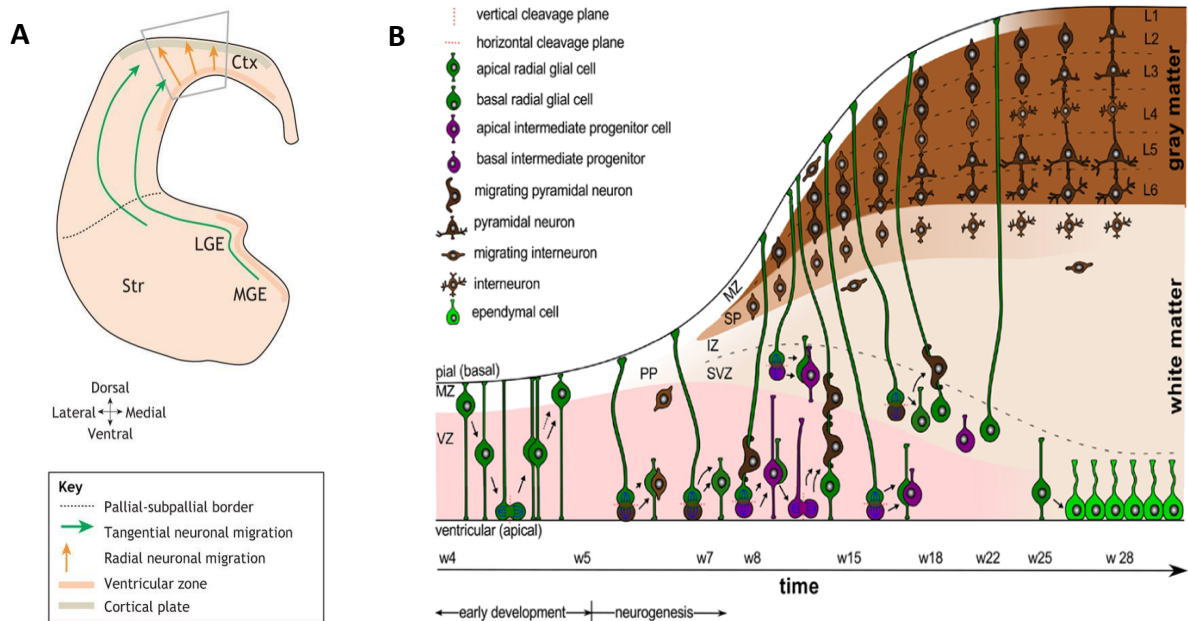


**Figure 7 CELL MIGRATION AND CORTICOGENESIS**

(A) Every brain region originates specific cell populations, which can migrate to their final location through tangential or radial migration (B). An example of radial migration is what happens in the cortex. Here, in the first weeks, symmetrical divisions increase the progenitor pool. After some weeks the radial migration of progenitors gives rise to the SVZ, while the neurons generate the preplate. This turns in the cortical zone, where over time neurons are organized in 6 layers. Ctx: cerebral cortex; LGE: lateral ganglionic eminence; MGE: medial ganglionic eminence; Str: striatum; VZ: ventricular zone; MZ: marginal zone; PP: preplate; SVZ: subventricular zone; IZ: intermediate zone; SP: subplate; L: layer; w: week. Adapted from Buchsbaum and Cappello 2019; and Budday et al 2015

## 1.2. Features of the human corticogenesis

Corticogenesis has mostly been investigated using various animal models, like rodents or ferrets. This has shown that several basic mechanisms of human brain development are highly conserved during evolution. Neurogenesis or cortical layering are, for example, observed and studied also in mice <sup>73,74</sup>. The human cortex has gyri and sulci, characteristic of gyrencephalic brains, which are absent in lissencephalic brains, like in rodents. The human cortex constitutes up to 80% of the total brain volume as compared to 40% of the mouse brain <sup>5,75,76</sup>. This difference is due to increase in surface area and gyrification of the human cortex (Figure 8) <sup>4,77</sup>. Ferrets are widely used as one of the most reliable models to study gyrification, as they contain an extended neocortex and a diversity

of neural progenitor cells. Nonetheless, they fail to recapitulate many aspects of human brain development<sup>78–81</sup>. Even taking our closest living relatives, the chimpanzees, they do not have the same cell network and brain size as human and the spatiotemporal proliferation of RG cells in the earliest phase of development was found out to be different<sup>82</sup>. To better understand what evolutionary changes took place in the human brain the focus must be on the development of the subventricular zone.

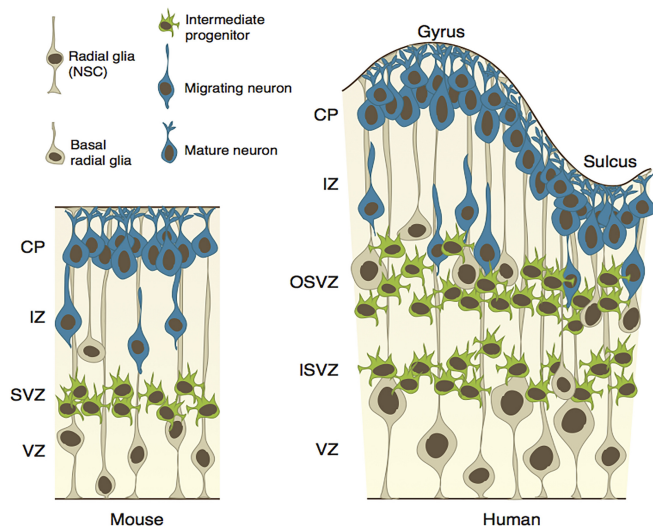


**Figure 8 MOUSE VS HUMAN CORTEX**

During development the mouse and human cortex consists of similar cells and zones. Although it can be observed how the subventricular zone in human is bigger and divided in inner and outer subventricular zone. Here there is a high abundance of intermediate progenitors as well as basal radial glial cells, just sparsely present in the mouse cortex. The increased thickness of this region results in the formation of gyri. CP: cortical plate; IZ: intermediate zone; SVZ: subventricular zone; VZ: ventricular zone; OSVZ: outer subventricular zone; ISVZ: inner subventricular zone. From Kaleva and Lancaster 2016

### 1.2.1. Emergence of the subventricular zone

The SVZ is the region, where dividing IPs and bRGs are located. This area can be divided into the inner SVZ (iSVZ) or outer SVZ (oSVZ, referred as SVZ in this work)<sup>67,83,84</sup>. The iSVZ consists of mostly transitioning IPs, while the oSVZ is the area where most of the transit-amplifying cells are located.

IPs delaminate from the VZ and after a first proliferation round in the iSVZ, they further migrate to populate the oSVZ (Figure 9)<sup>45,85–87</sup>. In mice IPs undergo one or maximal two rounds of division before differentiating into cortical neurons. In humans their proliferative capacity is increased, and they can greatly amplify their progenitor pool and thus increase the SVZ thickness before differentiating<sup>47,58,88</sup>.

bRGs reside exclusively in the oSVZ. The molecular mechanisms regulating bRGs generation have been partially uncovered. In ferret brain it has been observed how the weakening of cell adhesion in the ventricular lining mediated through a reduction of *Cdh1* expression, leads to increased oblique division and thus delamination of the radial glial

cells<sup>89</sup>. Similarly, also *Lzts1* overexpression induces bRGs generation through oblique division<sup>90</sup>. bRG undergo mitotic somal translocation (MST), which is a rapid movement of the soma along its basal process prior to mitosis<sup>91</sup>. Compared to IPs, bRG can undergo many more proliferation rounds which supports the expansion of the cortex and importantly creates a scaffold to allow the basal migration of the newborn neurons<sup>80,81</sup>. Morphologically, bRG can differ from monopolar to multipolar and express most of the aRG markers but also some additional ones like Homeodomain-only Protein Homeobox (HOPX), Family With Sequence Similarity 107 Member A (FAM107A) and Protein Tyrosine Phosphatase Receptor Type Z1a (PTPRZ1A)<sup>92,93</sup>.

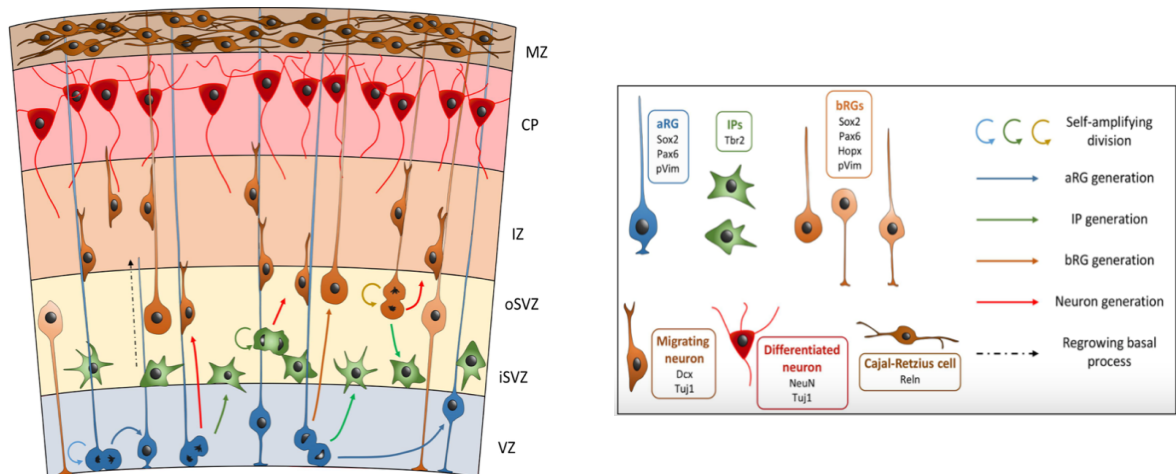


**Figure 9 CELL DYNAMICS IN HUMAN CORTEX DEVELOPMENT**

Cells in the developing embryonic cortex have specific dynamics from proliferation and generation of new subtypes to radial migration (left). Every cell is characterized by the expression of specific markers (right). VZ, ventricular zone; iSVZ, inner subventricular zone; oSVZ, outer subventricular zone; IZ, intermediate zone; CP, cortical plate; MZ, marginal zone. aRG, apical radial glial cell; bRGs, basal radial glial cells (different bRG morphotypes are shown); IP, intermediate progenitor. Adapted from Panisson et al.2019

Cell proliferation in the SVZ has been shown to underly increased cortical thickness and folding<sup>3</sup> in gyrencephalic brains. In contrast, lissencephalic brains, do not demonstrate a wide SVZ and bRG cells are barely present<sup>94,95</sup>. Gyri or folding in the cortex are regulated by several proteins which are mostly expressed in bRG cells, including the Transmembrane Protein 14B (TMEM14B)<sup>96</sup> or though specific pathways, such as Notch signaling<sup>97</sup>. The recent discovery of this bRGs can contribute to further understanding the underlying mechanisms of cortical expansion<sup>98</sup>.



### 1.3. T-box brain protein 2 (*Tbr2*) specific role in corticogenesis

IPs are generated during corticogenesis from RGs <sup>58,88</sup> and they can be divided into apical intermediate progenitor cells (aIPs) and basal intermediate progenitor cells (bIPs). The difference between those two populations resides in the morphology and position in the developing cortex. aIPs are mono- or bi-polar and have their soma in the VZ. Whereas, bIPs are multipolar and located in the SVZ (Figure 10) <sup>45,87,99</sup>. Both these subpopulations have in common the expression of *Tbr2* (also called Eomesodermin or *Eomes*), considered their hallmark <sup>86</sup>. *Tbr2*, is a transcription factor part of the T-Box brain protein gene family and located on chromosome 3p24.1. This gene family is characterized by a shared DNA-binding motif, the T-box domain, and the sequence is conserved throughout different species in the evolution <sup>100</sup>.

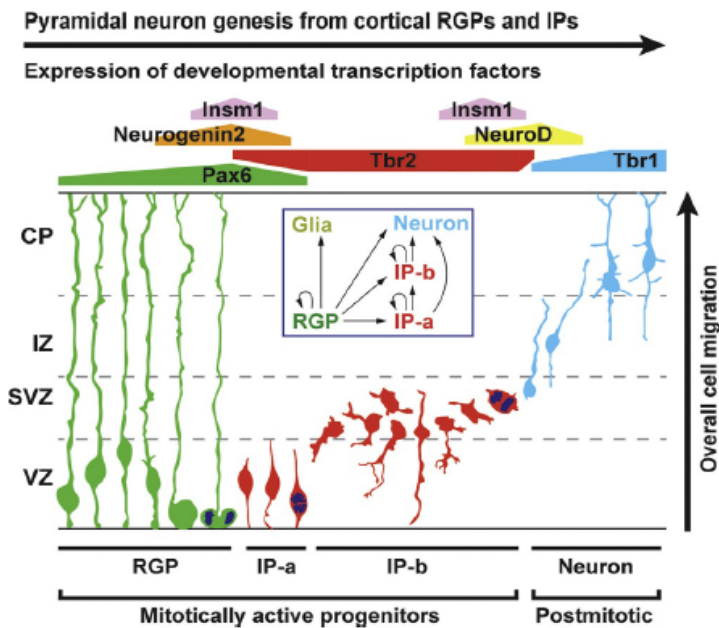


**Figure 10 TRANSCRIPTION FACTORS TRANSITION DURING CORTICOGENESIS**

Cells can be characterized according to the expression pattern of specific transcription factors. For example, *Tbr2* is the hallmark for IPs, *Pax6* for the RG.

RGP: radial glial progenitors; IP-a: apical intermediate progenitors; IP-b: basal intermediate progenitors; VZ: ventricular zone; SVZ: subventricular zone; IZ: intermediate zone; CP: cortical plate. From Mihalas and Havner 2017

Several studies in mice have elucidated the role of *Tbr2* during fetal development. Firstly, homozygous knockout (KO) of *Tbr2* results in the inability to develop the trophoblast and is therefore lethal <sup>101,102</sup>. Conditional KO of *Tbr2*, on the other side, results in decreased IPs and cortical neurons, dysregulation of cortical layer formation, specifically of layers IV, V, and VI <sup>100,101,103,104</sup>. In the same model *Pax6* and *Insulinoma-associated 1* gene (*Insm1*), crucial genes to maintain the progenitor pool during

neurogenesis, show increased expression as compared to wild type animals. These findings suggest that *Tbr2* may inhibit expression of genes crucial to maintain the progenitor like state and thus promotes neuronal differentiation. Furthermore, it has been demonstrated that *Tbr2* plays an important role in rostro-caudal patterning during development of the cortex<sup>105</sup>. Ferrets are the only model organism in which the role of *Tbr2* in gyrencephalic cortices has been studied. KO of *Tbr2* has been associated, in this model, to a reduced cortical size and a decreased folding<sup>78</sup>. Consistent with these observations, also in other studies *Tbr2* depletion resulted in differences in cortex enlargement<sup>106,107</sup>. Overexpression of *Tbr2* has been shown to result in increased gyrification in ferrets as well as increased cortical surface in mice<sup>79</sup>. A single human case study of an individual that lacked *TBR2* expression due to a chromosomal translocation, reported that this patient presented microcephaly and polymicrogyria<sup>108</sup>. GABAergic interneurons and microglia do not originate in the cortex, and it is thought that *Tbr2* plays a role to attract these cells to the developing cortex<sup>99,104,109–111</sup>, through the expression of the chemokine C-X-C Motif Chemokine Ligand 12 (Cxcl12)<sup>112</sup>.

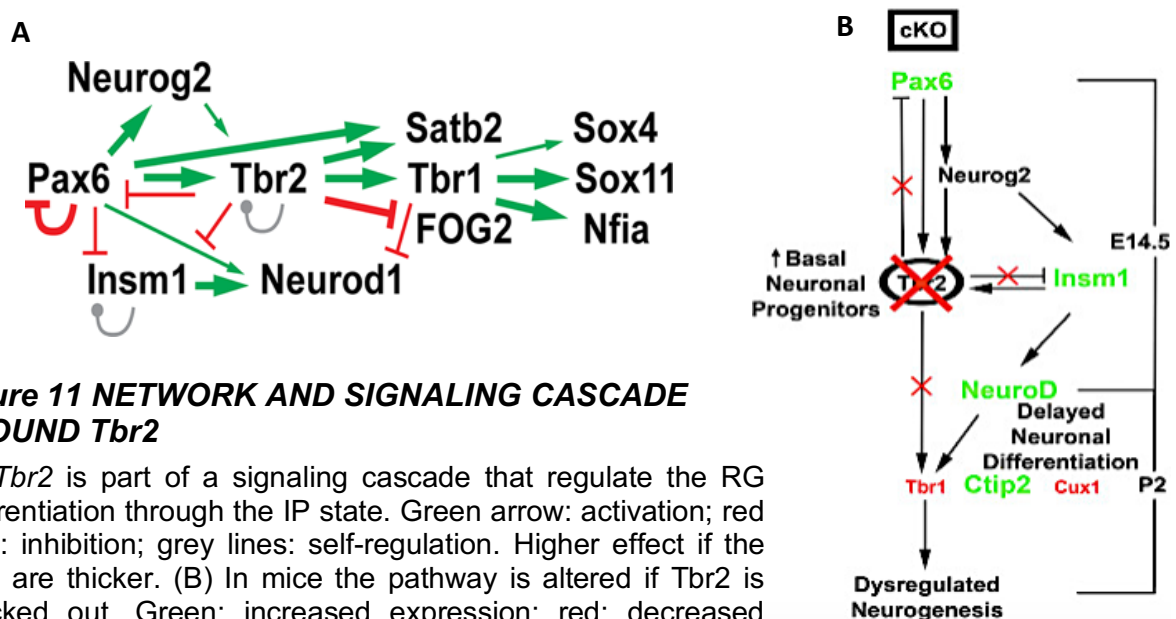


**Figure 11 NETWORK AND SIGNALING CASCADE AROUND *Tbr2***

(A) *Tbr2* is part of a signaling cascade that regulate the RG differentiation through the IP state. Green arrow: activation; red lines: inhibition; grey lines: self-regulation. Higher effect if the lines are thicker. (B) In mice the pathway is altered if *Tbr2* is knocked out. Green: increased expression; red: decreased expression. Adapted from Hevner 2019 and Mihalas 2016.

Due to its central role in a variety of complex signaling pathways, a lot of research in mice has focused on understanding the molecular mechanisms regulating *Tbr2* expression. Englund *et al.* (2006) first proposed a pathway where *Pax6*, *Tbr2* and *Tbr1* are the key players controlling RG differentiation to neurons (Figure 11)<sup>86</sup>. Hevner (2006)


confirmed the network between *Pax6*, *Tbr2* and *Tbr1*, but demonstrated how many other genes are involved. Indeed, while those three key players have a direct interaction with each other, every gene also regulates other transcription factors generating the complex signaling cascade as demonstrated in Figure 11A<sup>113,114</sup>. In line with that, Mihalas (2016) proposed the effect of *Tbr2*KO in the network (Figure 11B). The first effect is the increased expression of those transcription factors, who are inhibited by *Tbr2*, namely *Pax6* and *Insm1*. On the contrary, the expression of the transcription factors directly activated by *Tbr2*, like *Tbr1*, are downregulated. Eventually this results in delayed neuronal differentiation due to *Pax6*, *Insm1* and Neurogenic Differentiation 1 (*NeuroD*) over-expression, and dysregulated neurogenesis due to repression of *Tbr1*<sup>104</sup>. No human data are currently available to verify if this network is conserved during evolution.

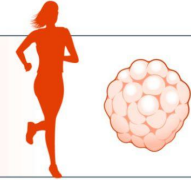
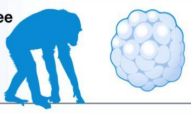
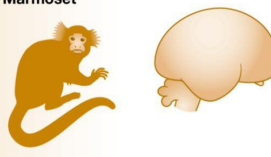


## **1.4. The role of ARHGAP11B in the human cortical development**

ARHGAP11B arose about 5 million years ago after a partial duplication of the highly conserved ARHGAP11A gene, encoding a Rho GTPase activating protein (RhoGAP). Following duplication, a C to G point mutation in the GAP domain occurred, inducing a new splice donor site and thus the novel human-specific C-terminal sequence, characteristic of the modern ARHGAP11B gene. Its recent evolution attracted the attention of evolutionary biologists to further characterize its function. The expression of ARHGAP11B has been induced in several species, including mice, ferrets, marmoset and chimpanzees, to understand the extent of the involvement of this gene in the human brain evolution (Figure 12)<sup>115</sup>.

In a pioneer study, expression of ARHGAP11B in the mouse neocortex, resulted in enrichment of bRGs, increased cortical plate area and gyrification<sup>116</sup>. Recently, ARHGAP11B has been demonstrated to induce the bRG expansion through mitochondrial regulation. Molecular analysis elucidated how it interacted with adenine nucleotide translocase (ANT) to regulate the opening of the mitochondrial permeability transition pore (mPTP)<sup>117</sup>. In specific, the opening of the pores was delayed in the presence of ARHGAP11B, causing an increased  $\text{Ca}^{2+}$  concentration in the mitochondria and activation of the enzyme  $\alpha$ -ketoglutarate dehydrogenase. This resulted in an increased conversion

of a-ketoglutarate in succinyl-CoA through the TCA cycle. The consequence of this was a glutamine-dependent increase in mitochondrial respiration and thus higher bRG proliferation (Figure 13). Neither the parental gene ARHGAP11A or a mutated ARHGAP11B version (reverting the C → G mutation occurred during evolution) was able to interact with the mitochondria, confirming the specificity of ARHGAP11B in the glutamine-related increased mitochondrial respiration of bRG cells.



MODEL	APPROACH	PHENOTYPES
<b>Human</b> 	<b>Loss of function</b> <ul style="list-style-type: none"> <li>• Electroporation, dominant negative ARHGAP11A220</li> <li>• CRISPR ARHGAP11A/B dKO and rescue by overexpression</li> </ul>	<b>Cellular</b> BP abundance ↓ BP proliferation ↓
<b>Chimpanzee</b> 	<b>Overexpression</b> <ul style="list-style-type: none"> <li>• Electroporation, CAG promoter</li> </ul>	<b>Cellular</b> BP abundance ↑ BP proliferation ↑ Upper-layer neurons ↑
<b>Marmoset</b> 	<b>Physiological expression</b> <ul style="list-style-type: none"> <li>• Transgenics, human ARHGAP11B promoter</li> </ul>	<b>Tissue</b> Neocortex size ↑ Cortical folding ↑ Cortical plate thickness ↑ oSVZ thickness ↑  <b>Cellular</b> BP abundance ↑ BP proliferation ↑ Upper-layer neurons ↑
<b>Mouse</b> 	<b>Overexpression</b> <ul style="list-style-type: none"> <li>• Electroporation, CAG promoter</li> <li>• Microinjection, mRNA</li> </ul> <b>Physiological-like expression</b> <ul style="list-style-type: none"> <li>• Transgenics, endogenous ARHGAP11A locus</li> </ul>	<b>Behavioral</b> Memory flexibility ↑  <b>Tissue</b> Neocortex size ↑ Cortical folding ↑ SVZ thickness ↑  <b>Cellular</b> BP abundance ↑ BP proliferation ↑ Upper-layer neurons ↑
<b>Ferret</b> 	<b>Overexpression</b> <ul style="list-style-type: none"> <li>• Electroporation, CAG promoter</li> </ul>	<b>Tissue</b> Neocortex size ↑ Neurogenic period ↑  <b>Cellular</b> BP abundance ↑ BP proliferation ↑ Upper-layer neurons ↑

**Figure 12 ARHGAP11B IMPACT IN DIFFERENT MODELS**

ARHGAP11B is present and expressed exclusively in the human brain. In order to understand its role in the evolution, ARHGAP11B has been expressed in different animal models. Observation aligns in increased BP abundance on a cellular level and increased cortical size and folding on a systemic level. BP: basal progenitors; SVZ: subventricular zone. From Ding and Pollen, 2022.

Kalebic and collaborators investigated the effect of ARHGAP11B in ferrets <sup>118</sup>. They observed human associated features in the ferret brain development, such as increased proliferative bRG cells, lengthening of neurogenic period and increased cortical plate size, mostly due to an enhanced number of deep layers neurons (like Brn2+

neurons) <sup>118</sup>. Consistent results were also observed in marmoset animals expressing *ARHGAP11B* <sup>119</sup>.

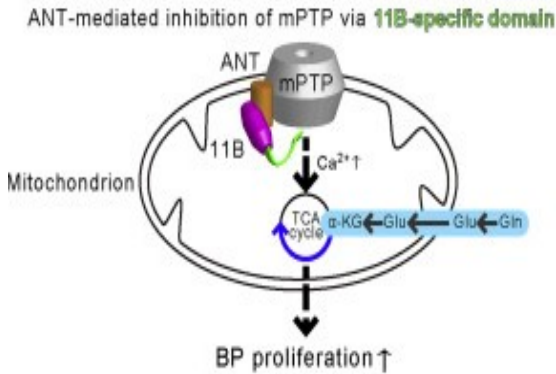


### Figure 13 IMPACT OF ARHGAP11B IN MITOCHONDRIA

ARHGAP11B interacts with ANT to postpone the opening of mPTP. This causes an increased Ca<sup>2+</sup> in the mitochondria and subsequent activation of the TCA cycle, glutamine mediated. The higher respiration leads to basal progenitor proliferation. ANT: adenine nucleotide translocase; mPTP: mitochondrial permeability transition pore; α-KG: α-ketoglutarate; GLU: glucose; GLN: glutamine; BP: basal progenitors. From: Namba 2020

Brain organoids generated from the closest human relative, the chimpanzee shows results in line with those observed in rodent models *in vivo*. ARHGAP11B expression increased bRG abundance and proliferation as well as upper layer neurons generation. These data support the hypothesis that ARHGAP11B potentially contributes to the evolutionary enlargement of the human brain as compared to non-human primates <sup>120</sup>.

## 1.5. Human brain research with *in vitro* models

The study of human brain development has always been a major challenge. Animal models allow us to gain fundamental knowledge about molecular mechanisms, physiological and anatomical features of the brain, however many observations in model organisms do not translate to humans <sup>73,74</sup>. The use of post-mortem human tissue has for decades been the only possibility to investigate the human brain <sup>121</sup>, but the discovery and use of embryonic stem cells first, and induced pluripotent stem cells more recently, drastically changed the approach of human brain research *in vitro*.

### 1.5.1. Emergence of the induced pluripotent stem cells

In 2007 the first human somatic cells have been reprogrammed into the so-called human induced pluripotent stem cells (iPSCs). Following the successful experiment in mouse cells, <sup>122</sup> Yamanaka and his team changed the fate of human somatic cells into primordial pluripotent cells with the use of four transcription factors; *SOX2*, *OCT4*, *KLF4* and *cMYC*, also referred to as the Yamanaka factors <sup>123</sup>.

Expression of these four factors in human fibroblasts with retroviral delivery system resulted in colonies of pluripotent cells after a few weeks' in culture <sup>123</sup>. The use of retroviral vectors has as consequence the integration of those sequences into the reprogrammed cells, raising safety concerns for clinical applications. Thus, in the last decade the delivery system has been optimized to allow a transient or episomal expression of the Yamanaka factors. The use of the Sendai virus, for example, avoids integration of DNA sequences, thus maintaining the genome unaltered <sup>124,125</sup>. iPSC are able to differentiate into all three germ layers <sup>126</sup>. Additionally, iPSCs can be generated from any person, allowing not only to study general human cellular or molecular processes but also making them highly relevant for personalized medicine.

### **1.5.2. Corticogenesis in two-dimensional (2D) cell cultures**

The generation and maintenance of neural stem cell (NSCs) has been a main goal for many scientists in the last decades. A variety of methods have been employed to generate these. The first protocols generated NSC in 3D systems, referred to as neurospheres, attempting to generate a niche or microenvironment to allow their self-renewal <sup>127,128</sup>. NSCs can nowadays be efficiently generated in 2D with or without an intermediate neurosphere step, and their maintenance and expansion *in vitro* has been greatly increased using combinations of growth factors <sup>129-131</sup>.

In 2008 Elkabetz et colleagues characterized NSCs grouping in very specific structures, namely neural rosettes <sup>132</sup>. These are the 2D *in vitro* counterpart of the neural tube, resembling some structural and molecular aspects. For example, neural rosettes cells radially distribute around an empty area and proliferate into different progenitors and neuronal subtypes according to the morphogens present in the cultivation media. Cells in neural rosettes self-organize in a precise spatiotemporal manner mimicking what has been observed *in vivo*. It is nowadays possible to grow neural rosettes in a dish for weeks, allowing the generation of apical-basal polarity, cells going upon INM and differentiation into electrophysiological active neurons of all cortical layers <sup>133</sup>.

NSCs can be differentiated, starting from iPSCs, following the activation of similar molecular mechanisms and pathways observed *in vivo* <sup>134,135</sup>. The most common induction of neuroectoderm is based on the dual SMAD inhibition. As the names suggest, two molecules, Noggin and SB431542 are used to inhibit SMAD thereby inhibiting the

signaling pathways of BMP and TGF $\beta$  that rely on SMAD for signal transduction <sup>134</sup>. Interestingly, PSCs cultured without morphogens also have the tendency to initiate neuroectodermal differentiation and even generate cortical neurons in some extent <sup>136</sup>.

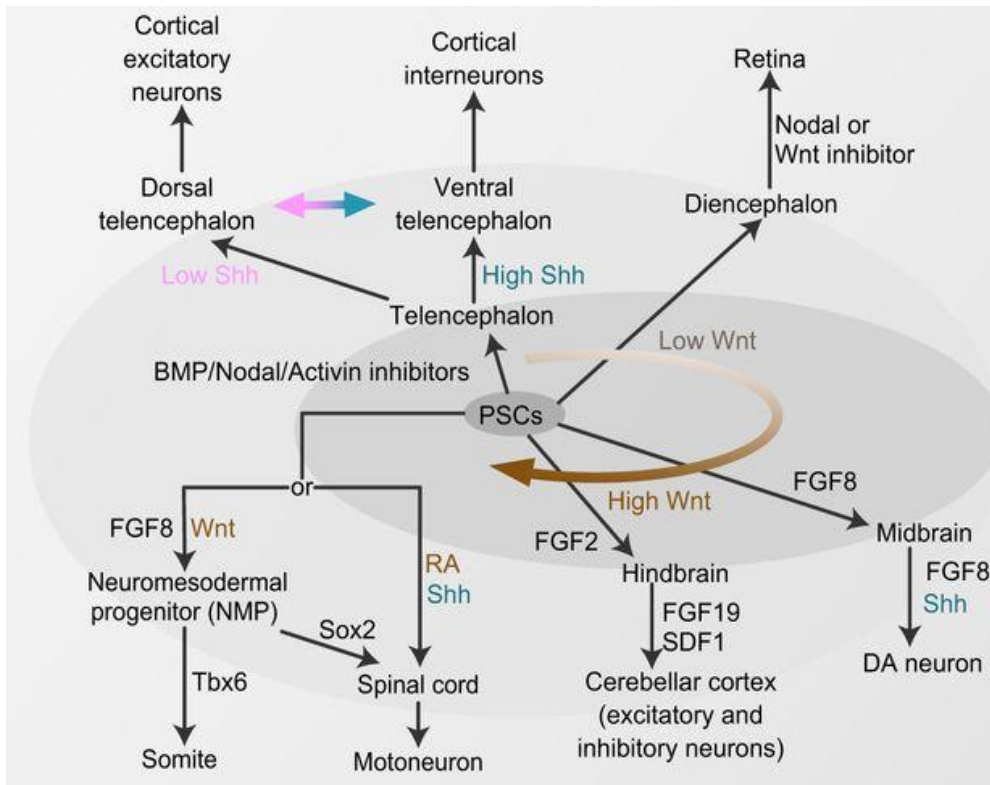


**Figure 14 PATTERNING OF PLURIPOTENT STEM CELL DERIVED NEURONS**

Pluripotent stem cells (PSCs) can be induced in neuronal fate and then differentiated in a variety of neurons. The patterning is mediated by morphogens like Wnt, regulating the rostro-caudal pattern. Other morphogens highly used are Shh, RA and the FGF family. From Suzuki and Vanderhaegen 2015

In human corticogenesis some important morphogens such as BMP, Wnt or Shh are fundamental for the spatiotemporal determination. Similarly, *in vitro*, the presence of these factors at different concentrations can induce one or the other fate. For example, BMP inhibition leads to rostral identity; Wnt activation with higher gradients lead to caudalization while lower levels to rostralization; Shh activation results in ventralization <sup>137</sup>. Every population of progenitors generated with these gradients can be further patterned into the final neural population of interest (Figure 14). The current challenge in the field is to obtain homogeneous cultures and reduce the time needed for the neuronal differentiation. The ongoing process of optimizing culturing protocols holds promise for

the near future, as it may enable the rapid generation of nearly any type of neurons while preserving their physiological characteristics intact.

Although in the last decade enormous progress has been made in the field, it is important to understand the limitation of 2D *in vitro* neuronal culturing. Not only these methods require a lot of work from operators and expensive culturing materials, but they also fail to recapitulate complex interactions and the migration of cells derived from different progenitors. Even if this can be partially addressed with the co-culture of different cell types, the temporal and spatial organization of the cells *in vitro* still cannot recapitulate what can be observed *in vivo* <sup>138</sup>.

### **1.5.3. Emergence of brain organoids**

To address the absence of spatial organization in *in vitro* cultures as well as increasing the complexity and the interaction between cell types, 3D brain organoids have been developed. In 2005 Watanabe and colleagues characterized the self-organization of mouse embryonic stem cells into embryoid bodies (EB) <sup>139</sup> and later observed the formation of embryoid body-like aggregate in serum-free culture (SFEBs) <sup>140</sup>. In the presence of Wnt and Nodal antagonists, these 3D structures developed a forebrain identity. Following this observations, the first human PSCs-derived 3D floating culture with forebrain identity was reported in 2011 <sup>141</sup>.

The term 'brain organoids' was first coined in 2013, when Madeline Lancaster and colleagues published a non-guided protocol to generate a single 3D entity resembling several human brain regions <sup>142</sup>. A decade later a multitude of protocols (summarized in <sup>143</sup>) have been established and published to efficiently generate organoids resembling several brain regions together, known as whole-brain organoids, or single or specific region, known as patterned organoids (Figure 15). Compared to whole brain organoids, patterned organoids show less diversity in cell types but higher consistency and homogeneous differentiation <sup>144</sup>. Nowadays it is possible to generate forebrain <sup>145-147</sup>, midbrain <sup>148,149</sup>, hypothalamic <sup>149</sup> and retinal <sup>150</sup> patterned organoids. Furthermore, different region-specific organoids may be fused together to study the interaction between distinct brain areas, to form assembloids <sup>151</sup>.



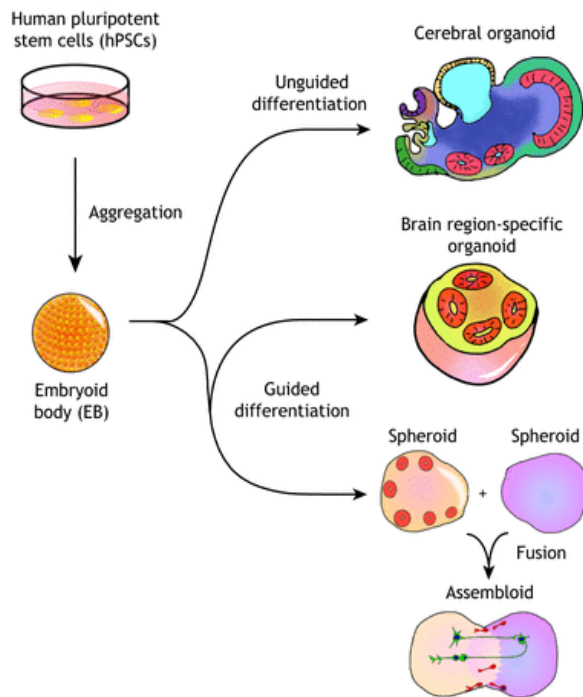


**Figure 15 3D NEURONAL CULTURES IN VITRO**

Human pluripotent stem cell can be aggregated in embryoid bodies. Differentiation to neuronal cultures can be unguided to generate cerebral organoids or guided to generate region-specific organoids or spheroids. Fusion of spheroids of different brain regions are called assembloids. Cortical loops are depicted in red.

From: Qian et al. 2019

Organoids have been used in the last decade for many different purposes, from studying human brain development and evolution to establishing models for human diseases. From a developmental point of view, organoids have made it possible to visualize and study processes of corticogenesis, such as the formation of stratified neuroepithelial layers,<sup>146</sup> or developing bRGs<sup>152</sup>. With the help of bioengineers, brain organoids have been tested in different cultivation devices, from bioreactors to spinning discs, from orbital shaker to simple cell suspension as spheroids<sup>142,149,153</sup>. The Zika outbreak in 2015 was a perfect springboard for the exploitation of brain organoid as disease models. Microcephaly associated to Zika virus was one of the first diseases modelled employing organoids, as they proved to be a new and effective tool to elucidate the mode of action and mechanisms behind the viral infection during the viral outbreak<sup>154–157</sup>. Additionally, brain organoids have been used to gain a better understanding of specific brain disorders, such as lissencephaly<sup>145,158</sup>, microcephaly<sup>142,159</sup> and even familial Alzheimer's disease<sup>160</sup>.

#### **1.5.4. Forebrain organoids**

Forebrain organoids consist of progenitor cells as well as neurons and glial cells<sup>135,142,148,152</sup>. Comparison of transcriptomic and epigenetic data suggests a high homology

between forebrain organoids and human fetal forebrain development in the first trimester<sup>151,161,162</sup>. As discussed previously, the human brain develops from the neural tube and neural rosettes are the closest 2D *in vitro* model for the human neural tube development. In organoids the counterpart of the 2D neural rosettes is the formation of cortical loops. They are complex 3D structures of progenitor cells, where layers of NEs initially and RGs later are radially disposed around a cavity. In a single organoid, several cortical loops are generated and each loop is a model of one human cortex<sup>163</sup>. The cavity is considered to be a ventricular-like structure and the cells close to it represent the dense progenitor-populated ventricular-like zone. Once those structures develop in size, a subventricular-like zone can be observed, with similar cell composition and structure to the developing human cortex. Neurons are generated and migrate on the apical-basal axis to give rise to the cortical plate<sup>147,164</sup>. Altogether, forebrain organoids can be a good model for human brain development, even if they also present some limitations, including the formation of necrotic core, restrained growth size, absence of cells derived from non-ectoderm layers. Furthermore, the reproducibility and homogeneity of the culture is often challenging, highlighting the need for better protocols and cultivation techniques to achieve a high-throughput generation of organoids.

## 1.6. Aims of the study

From an evolutionary point of view, the human brain shows an increased complexity compared to non-human primates. At a cellular level it is thought that the increased complexity is due to different proliferation rates and physiological characteristics of RGs during the development of the neocortex<sup>82</sup>. However, the genetic mechanisms underlying these cellular mechanisms remains undetermined.

The objective of this study was to investigate whether new genes emerge in RGs during human brain evolution, or if the existing genes altered their role or expression pattern during human brain development. Over the years the development of computational tools has facilitated the generation of databases for comparing the human genome with that of our ancestors. In this project, a group of genes were selected that: (i) were human-specific, or (ii) had an increased expression in the human brain compared to non-human primates. The final 5 candidates from this list were: *ARHGAP11B*, *TBR2*, *NIF1*, *PCDH11Y*, and *MCPH1*. Genetically engineered CRISPR/CAS9 based KO-

human iPSC (hiPSC) derived organoids were used to model human cortical evolution<sup>137,142,151,165,166</sup> and understand the role of the candidate genes in human brain development. The aims of this work are as follows:

- i. Generation of hiPSC KO lines for ARHGAP11B, TBR2, NIF1, PCDH11Y, and MCPH1;
- ii. Validation of dorsal forebrain organoids as model for the human neocortex development;
- iii. Morphological, functional and transcriptomic analysis of the KO-lines;
- iv. Identify a potential role of these genes during human brain development.

## 2. Materials

**Table 1: CELL LINES**

NAME	CELL LINE	ORIGIN	REPROGRAMMING / EDITING
A40	ID GM08680	5-month-old male	Sendai Virus, CRISPR/CAS
80#6	ID GM08680	5-month-old male	Sendai Virus
T3	ID GM08680	5-month-old male	Sendai Virus
A23		44-years-old female	Sendai Virus, CRISPR/CAS
28#4		44-years-old female	Sendai Virus

**Table 2: CELL CULTURE**

PRODUCT	CAT. #	MANUFACTURER
2-Mercaptoethanol	31350010	Thermo Fisher Scientific Inc. (Waltham, Massachusetts, USA)
A 83-01	2939	Tocris Bioscience (Bristol, UK)
B-27® Supplement	17504-044	Thermo Fisher Scientific Inc. (Waltham, Massachusetts, USA)
BSA Solution	15260037	Thermo Fisher Scientific Inc. (Waltham, Massachusetts, USA)
Cyclic adenosine monophosphate	A9501-1G	SIGMA-ALDRICH (St. Louis, Missouri, USA)
DMEM + GlutaMAX™-I	61965-026	Thermo Fisher Scientific Inc. (Waltham, Massachusetts, USA)
DMEM/F-12 + L-Glutamine	11320-074	Thermo Fisher Scientific Inc. (Waltham, Massachusetts, USA)
DMEM/F12(1:1) + L-Glutamine + 15mM HEPES	11330-032	Thermo Fisher Scientific Inc. (Waltham, Massachusetts, USA)
DMSO	D5879	Carl Roth GmbH & Co. KG (Karlsruhe, Deutschland)
EBSS (1X)	24010-043	Thermo Fisher Scientific Inc. (Waltham, Massachusetts, USA)
EDTA pH 8.0 UltraPure™	15575020	Invitrogen (Waltham, Massachusetts, USA)
Ethanol	32205	SIGMA-ALDRICH (St. Louis, Missouri, USA)
FGF-2 (147)	GFH28	Cell Guidance Systems Ltd (Cambridge, UK)

FGF-2 (154)	GFH146	Cell Guidance Systems Ltd (Cambridge, UK)
GelTrex™	A1413302	Thermo Fisher Scientific Inc. (Waltham, Massachusetts, USA)
GDNF	GFH2	Cell Guidance Systems Ltd (Cambridge, UK)
D(+)-Glucose	HN06.3	Carl Roth (Karlsruhe, Germany)
GlutaMAX™-I	35050038	Thermo Fisher Scientific Inc. (Waltham, Massachusetts, USA)
Heparin	H3149-25KU	SIGMA-ALDRICH (St. Louis, Missouri, USA)
Holo-Transferrin, human	T3705-1G	SIGMA-ALDRICH (St. Louis, Missouri, USA)
Human Recombinant Insulin	91077C-1G	SIGMA-ALDRICH (St. Louis, Missouri, USA)
Human TGF-β1	GFH39	Cell Guidance Systems Ltd (Cambridge, UK)
Knockout™-SR	10828010	Thermo Fisher Scientific Inc. (Waltham, Massachusetts, USA)
L-Ascorbic Acid	A4544	SIGMA-ALDRICH (St. Louis, Missouri, USA)
L-Ascorbic acid 2-phosphate	A8960	SIGMA-ALDRICH (St. Louis, Missouri, USA)
L-Cysteine	168149-2.5g	SIGMA-ALDRICH (St. Louis, Missouri, USA)
LDN-193189	72148	Miltenyi Biotec B.V. & Co. KG (Bergisch Gladbach, Germany)
LM22A	SML0848-25mg	SIGMA-ALDRICH (St. Louis, Missouri, USA)
LM22B	6037	Tocris Bioscience (Bristol, UK)
MEM Non-Essential Aminoacids	11140035	Thermo Fisher Scientific Inc. (Waltham, Massachusetts, USA)
Papain from papaya latex	P3125-250mg	SIGMA-ALDRICH (St. Louis, Missouri, USA)
PBS (-CaCl <sub>2</sub> -MgCl <sub>2</sub> )	D8537-500ML	SIGMA-ALDRICH (St. Louis, Missouri, USA)
PBS (-CaCl <sub>2</sub> -MgCl <sub>2</sub> )	10010-015	Thermo Fisher Scientific Inc. (Waltham, Massachusetts, USA)
Penicillin/Streptomycin	15140122	Thermo Fisher Scientific Inc. (Waltham, Massachusetts, USA)
Pluronic® F-127	P2443	SIGMA-ALDRICH (St. Louis, Missouri, USA)

Progesterone	P8783	SIGMA-ALDRICH (St. Louis, Missouri, USA)
Puromycin	540222	EMD Millipore (Burlington, USA)
Putrescine	51799	SIGMA-ALDRICH (St. Louis, Missouri, USA)
Sodium Selenite	S5261	SIGMA-ALDRICH (St. Louis, Missouri, USA)
TrypLE™ Express	12605-028	Thermo Fisher Scientific Inc. (Waltham, Massachusetts, USA)
XAV939	13596	Enzo Life Sciences, Inc. (New York, USA)
Y-27632	SM02	Cell Guidance Systems Ltd (Cambridge, UK)

**Table 3: CELL CULTURE MEDIUM COMPOSITION**

MEDIUM	COMPONENT	CONCENTRATION
Stem cell medium	DMEM/F12(1:1) + L-Glutamine + 15mM HEPES	
	Pen/Strep	1% (v/v)
	LAAP	64 µg/ml
	Sodium selenite	14 ng/ml
	FGF-2 (154)	100 ng/ml
	Insulin	20 µg/ml
	TGF-β1	2 ng/ml
	Transferrin	10 µg/ml
Cell freezing medium	KOSR	70% (v/v)
	Cytobuffer	20% (v/v)
	DMSO	10% (v/v)
	Y-27632	10 µM
Neural progenitor induction medium	DMEM/F-12 + L-Glutamine	
	Pen/Strep	1% (v/v)
	GlutaMAX™-I	1% (v/v)
	NEAA	1% (v/v)
	B27 supplement	1% (v/v)
	N2 supplement	0.5% (v/v)
	cAMP	1.5 µg/ml
	D-Glucose	0,4 µg/ml
	2-Mercaptoethanol	50 nM
A83	500 nM	

	LDN193189	200 nM
	XAV939	2 µM
Neural differentiation medium	DMEM/F-12 + L-Glutamine	
	Pen/Strep	1% (v/v)
	GlutaMAX™-I	1% (v/v)
	NEAA	1% (v/v)
	B27 supplement	1% (v/v)
	N2 supplement	0.5% (v/v)
	cAMP	1.5 µg/ml
	D-Glucose	0,4 µg/ml
	2-Mercaptoethanol	50 nM
Forebrain organoids induction medium	DMEM/F-12 + L-Glutamine	
	Pen/Strep	1% (v/v)
	GlutaMAX™-I	1% (v/v)
	NEAA	1% (v/v)
	B27 supplement	1% (v/v)
	N2 supplement	0.5% (v/v)
	cAMP	1.5 µg/ml
	D-Glucose	0,4 µg/ml
	2-Mercaptoethanol	50 nM
	A83	500 nM
	LDN193189	200 nM
	XAV939	2 µM
	Heparin	10 µg/ml
	KOSR	2% (v/v)
Forebrain organoids differentiation medium	DMEM/F-12 + L-Glutamine	
	Pen/Strep	1% (v/v)
	GlutaMAX™-I	1% (v/v)
	NEAA	1% (v/v)
	B27 supplement	1% (v/v)
	N2 supplement	0.5% (v/v)
	cAMP	1.5 µg/ml
	D-Glucose	0,4 µg/ml
	2-Mercaptoethanol	50 nM

	Insulin	2,5 µg/ml
Forebrain organoids maturation medium	DMEM/F-12 + L-Glutamine Pen/Strep GlutaMAX™-I NEAA B27 supplement N2 supplement cAMP D-Glucose 2-Mercaptoethanol Insulin GDNF LM22A LM22B L-Ascorbic Acid GelTrex™	 1% (v/v) 1% (v/v) 1% (v/v) 1% (v/v) 0.5% (v/v) 1.5 µg/ml 0,4 µg/ml 50 nM 2.5 µg/ml 10 ng/ml 1 µM 1 µM 0.2 mM 1% (v/v)
N2 supplement	DMEM/F-12 Transferrin Insulin Putrescine Progesterone Sodium Selenite	 50 mg/ml 5 mg/ml 80.6 mg/ml 50 µg/ml 70 µg/ml
Papain Buffer	EBSS (1X) EDTA L-Cysteine Papain	 40ml 0.5 mM 50 mM 29,4 µl/ml
Pluronic solution	Pluronic® F-127 PBS	 2 g 40 ml
Tissue embedding	PBS Sucrose Gelatine	 10% 7.5%
Wash medium	DMEM + GlutaMax™-I Pen/Strep	 1% (v/v)
Cytobuffer	Myo-Inositol	240 mM



	Polyvinylalcohol	5 mg/ml
	PBS	0.2X

**Table 4: EQUIPMENT**

<b>DEVICE</b>	<b>MANUFACTURER</b>
10X Vortex Adapter	10X Genomics (San Francisco, USA)
10X Magnetic Separator	10X Genomics (San Francisco, USA)
2100 Bioanalyzer Laptop Bundle	Agilent (Waldbronn, Germany)
4200 Tape Station	Agilent (Waldbronn, Germany)
Agarose gel electrophoresis chamber Easy Phor Midi	Biozym (Hessisch Oldendorf, Germany)
Agarose Gel imaging System, GeneFlash	Syngene (Bangalore, India)
Analytical Balance BP121-S	Sartorius Stedim Biotech S. A. (Aubagne Cedex, France)
Centrifuge 5415D	Eppendorf AG (Hamburg, Germany)
Centrifuge Z216MK	HERMLE Labortechnik GmbH (Wehingen, Germany)
Chromium Controller	10X Genomics (San Francisco, USA)
Chromium Next GEM Secondary Holder	10X Genomics (San Francisco, USA)
CM3050S cryostat	Leica Biosystems (Wetzlar, Germany)
CO2 Incubator HERAcCell 150i	Thermo Fisher Scientific Inc. (Waltham, Massachusetts, USA)
Double Edge Stainless Razor Blade	Science Services (München, Germany)
Electrophoresis Power Supply EPS 301	Amersham Pharmacia Biotech (Little Chalfont, UK)
Extraction hood mc6® das Laborsystem	Waldner GmbH & Co (Wangen, Germany)
Fluorescence Microscope Axioskop 2 plus	Zeiss Microscopy GmbH (Oberkochen, Germany)
Fluorescence Microscope Celldiscoverer 7	Zeiss Microscopy GmbH (Oberkochen, Germany)
Freezer Hera Freeze -80°C	Thermo Fisher Scientific Inc. (Waltham, Massachusetts, USA)
Freezer VIP plus -150°C	Panasonic, (Kadoma, Japan)

Freezing container, Mr. Frosty™	Thermo Fisher Scientific Inc. (Waltham, Massachusetts, USA)
Heraeus Sorvall Four Place Swinging Bucket Rotor 6445	Thermo Fisher Scientific Inc. (Waltham, Massachusetts, USA)
Heraeus® Herasafe™ 2030i Biological Safety Cabinet	Thermo Fisher Scientific Inc. (Waltham, Massachusetts, USA)
Heraeus® Labofuge® 400R Centrifuge	Thermo Fisher Scientific Inc. (Waltham, Massachusetts, USA)
HiSeq 4000 Sequencing system	Illumina (San Diego, USA)
Illumina Nova Seq 6000 system	Illumina (San Diego, USA)
Inverted Leica DMIL LED Microscope	Leica Microsystems GmbH, (Mannheim Germany)
Light-Sheet-Microscope	Leica Microsystems GmbH (Mannheim, Germany)
LiCor Odyssey	LI-COR Bioscience (Lincoln, Nevada, USA)
Liquid Nitrogen Store Cryotech	Thermo King (Minneapolis, USA)
Luna™ Automated Cell Counter	Logos Biosystems (Gyeonggi-do, Southkorea)
Micro Balance iso9001	Sartorius Stedim Biotech S. A. (Aubagne Cedex, France)
Microscope Cell discoverer7	Carl Zeiss (Oberkochen, Germany)
Microscope DM6 B	Leica (Wetzlar, Germany)
Micropipettes Research ® plus (2 µl, 10 µl, 20 µl, 100 µl, 200 µl, 1000 µl)	BioTek (Bad Friedrichshall, Germany)
MilliQ Integral Water Treatment System	Merck Millipore (Burlington, Massachusetts, USA)
Mikrotomklingen, Schmalband 819	Leica Microsystems GmbH (Mannheim, Germany)
MJ Research PTC-200 Thermal Cycler	Biozym Diagnostik GmbH (Oldendorf, Deutschland)
Nanodrop™ ND-1000 Spectrophotometer	Thermo Fisher Scientific Inc. (Waltham, Massachusetts, USA)
NovaSeq™ 6000 sequencing system	Illumina (San Diego, USA)

Odyssey Imaging System	LI-COR Bioscience (Lincoln, Nevada, USA)
Orbital shaker KS 250 basic	IKA Labortechnik ® Gmbh, Staufen (Germany)
pH-Meter Profi Lab WTW pH597	SIGMA-ALDRICH (St. Louis, Missouri, USA)
Pipetboy, pipetting aid	Integra Biosciences AG. (Zizers, Switzerland)
PowerWave XS	BioTEK (Winooski, Vermont, USA)
PTC-200 Peltier Thermal Cycler	Marshall Scientific (Hampton, New Hampshire, USA)
QuantStudio 7 Flex Real-Time PCR System	Thermo Fisher Scientific Inc. (Waltham, Massachusetts, USA)
Qubit 4.0 Fluorometer	Thermo Fisher Scientific Inc. (Waltham, Massachusetts, USA)
Sonifier Branson 250	Thermo Fisher Scientific Inc. (Waltham, Massachusetts, USA)
Sunlab Roll Mixer SU 1400	Sustainable lab instruments (Heidelberg, Germany)
Thermal Cycler C1000 Touch (with 96-deep well reaction module)	Bio-Rad Laboratories (Essen, Germany)
Thermal Master Cycler Pro	Eppendorf AG (Hamburg, Germany)
Thermal Cycler MJ Research PTC-200	Biozym Diagnostik GmbH (Oldendorf, Deutschland)
Thermal Cycler Veriti (96-well)	Thermo Fisher Scientific Inc. (Waltham, Massachusetts, USA)
Thermomixer comfort 5355	Eppendorf AG (Hamburg, Deutschland)
Thunder Imager 3D Tissue, DM6B	Leica Microsystems GmbH, (Mannheim, Germany)
Trans-Blot Turbo	BioRad (Berkley, California, USA)
Vortex Reax control	Heidolph Instruments GmbH & CO. KG, Schwabach (Germany)
Warm bath ED-17	JULABO Labortechnik GmbH (Seelbach, Deutschland)

Warm bath for cell culture	Köttermann GmbH & Co. KG (Uetze/Häningsen, Germany)
----------------------------	--

**Table 5 CONSUMABLES**

CONSUMABLE	SIZE	CAT. #	MANUFACTURER
Tissue Culture dish	Ø 3.5 cm	83.3900	Sarstedt (Nümbrecht, Germany)
	Ø 10 cm, Cell+	83.3902.300	
Tissue Culture plates	6-well	833.920.005	Sarstedt (Nümbrecht, Germany)
	12-well, Cell+	833.921.300	
	24-well, Cell+	833.922.300	
	48-well, Cell+	83.3923.300	
	96-well, Cell+	83.3924.005	
Blotting membrane	0.2 µm PVDF Nitrocellulose	10600001	GE Healthcare Life Science (Chicago, USA)
Bottle top filter	500 ml	15983307	Thermo Fisher Scientific Inc. (Waltham, Massachusetts, USA)
	1000 ml	15993307	
Cell scraper		sc-395251	Santa Cruz Biotechnology (Dallas, USA)
Coverslips	12 mm	631-1577	VWR (Radnor, USA)
Cryotubes	1 ml	123280	Greiner (Frickenhausen, Germany)
Luna™ reusable slide		L12008	Logos Biosystems, Inc. (Gyeonggi-do, South Korea)
Luna™ reusable coverslips		L12010	
MACS® SmartStainers	30 µm	130-098-458	Miltenyi Biotec B.V. & Co. KG (Bergisch Gladbach, Germany)
Microscopy slides		H868.1	Carl Roth (Karlsruhe, Germany)
Molds, disposable vinyl	10mm x 10mm x 5mm	4565	Tissue Tek (Tokio, Japan)
Pasteur pipette	3 ml	7691061	Th. Geyer (Renningen, Germany)
PCR strip tubes	8 x 200 µl	710971	Biozym (HESsisch Oldendorf, Germany)
Petri dish	Ø 10 cm	633180	Greiner (Frickenhausen, Germany)

Pipette tip	10 µl	70.1130	Sarstedt (Nümbrecht, Germany)
	200 µl	70.760.002	
	1250 µl	701.186	
Pipetting reservoir	25 ml	B3125-50	Parmer GmbH (Cole- Wertheim, Germany)
qPCR plate	96-well	4ti-0910/C	Steinbrenner Laborsysteme (Wiesenbach, Germany)
qPCR plate seal		4ti-0500	Steinbrenner Laborsysteme (Wiesenbach, Germany)
Reaction tubes	0.2 ml	72.737.002	Sarstedt (Nümbrecht, Germany)
	0.5 ml	72.699	
	1.5 ml	72.690.001	
	2.0 ml	72.695.200	
Scalpel Cutfix®		9409814	Th. Geyer (Renningen, Germany)
Screw cap tube	15 ml	62.554.502	Sarstedt (Nümbrecht, Germany)
	50 ml	62.547.254	
Serological pipettes	5 ml	861.253.001	Sarstedt (Nümbrecht, Germany) Th. Geyer (Renningen, Germany)
	10 ml	861.254.001	
	25 ml	861.685.001	
	50 ml	7695555	
Syringe	50 ml	946.077.137	Sarstedt (Nümbrecht, Germany)
Syringe filter	0.2 µm	831.826.001	Sarstedt (Nümbrecht, Germany)
Western blot filter tissue		115-2166	VWR (Radnor, USA)

**Table 6 REAGENTS AND CHEMICAL COMPOUNDS**

CHEMICAL	CAT. #	MANUFACTURER
2-Mercaptoethanol	805740	Merck Millipore (Darmstadt, Germany)
2-Propanol	1157	Th. Geyer (Renningen, Germany)
30 % Bis/acrylamide	3029.1	Carl Roth (Karlsruhe, Germany)
Acetic acid	33209	Sigma-Aldrich (St. Louis, USA)
Agar (Bacto™)	214010	BD Biosciences (Franklin Lakes, USA)
Agarose	A9539	Sigma-Aldrich (St. Louis, USA)
Agarose Low Melt	6351.5	Carl Roth (Karlsruhe, Germany)

Ammonium persulfate	A3678	Sigma-Aldrich (St. Louis, USA)
Ampicillin	A9518	Sigma-Aldrich (St. Louis, USA)
Bacto-Tryptone	211705	BD Biosciences (Franklin Lakes, USA)
Boric acid	15583	Life Technologies (Carlsbad, USA)
Bovine serum albumin (BSA)	A3294	Sigma-Aldrich (St. Louis, USA)
Bromophenol blue	B8026	Sigma-Aldrich (St. Louis, USA)
CaCl <sub>2</sub>	31307	Sigma-Aldrich (St. Louis, USA)
Chloroform	32211	Sigma-Aldrich (St. Louis, USA)
DABCO	0718.2	Carl Roth (Karlsruhe, Germany)
DEPC	K028.1	Carl Roth (Karlsruhe, Germany)
EDTA	E3889	Across organics (Fair Lawn, USA)
Ethanol	2246.1000	Th. Geyer (Renningen, Germany)
Fetal bovine serum (FBS)	10270-106	Thermo Fisher (Waltham, USA)
Gelatin, from porcine skin	G1890	Sigma-Aldrich (St. Louis, USA)
Glycerol	15523	Sigma-Aldrich (St. Louis, USA)
Glycine	10070150	Thermo Fisher (Waltham, USA)
Histodenz	D2158	Sigma-Aldrich (St. Louis, USA)
Hydrochloric acid	836.1000	Th. Geyer (Renningen, Germany)
KH <sub>2</sub> PO <sub>4</sub>	1648	Th. Geyer (Renningen, Germany)
KCl	1632	Th. Geyer (Renningen, Germany)
LB medium powder	X968.4	Carl Roth (Karlsruhe, Germany)
MgCl <sub>2</sub>	A351B	Promega (Madison, USA)
MgSO <sub>4</sub>	105886	Merck (Darmstadt, Germany)
Methanol	0082.1	Carl Roth (Karlsruhe, Germany)
Milk powder	T145.3	Carl Roth (Karlsruhe, Germany)
Mowiol®4-88	0713.1	Carl Roth (Karlsruhe, Germany)
NaOH	1310-73-2	Sigma-Aldrich (St. Louis, USA)
NaH <sub>2</sub> PO <sub>4</sub>	S9638	Merck (Darmstadt, Germany)
Na <sub>2</sub> HPO <sub>4</sub>	8622	Th. Geyer (Renningen, Germany)
NaCl <sub>2</sub>	1367	Th. Geyer (Renningen, Germany)
OCT™ Tissue-freezing medium	4583	Tissue Teck (Tokio, Japan)
Paraformaldehyde (PFA)	16005	Sigma-Aldrich (St. Louis, USA)

Phosphatase inhibitor mini tablets	A32957	Thermo Fisher (Waltham, USA)
Poly-L-lysine hydrobromide (MW 30,000-70,000)	P2636	Sigma-Aldrich (St. Louis, USA)
Protease inhibitor mini tablets	A32955	Thermo Fisher (Waltham, USA)
Puromycin dihydrochloride	540222	Merck Millipore (Darmstadt, Germany)
Roti Liquid Barrier Marker	AN92.1	Carl Roth (Karlsruhe, Deutschland)
SDS, pellets	CN30.1	Carl Roth (Karlsruhe, Germany)
Sodium hydroxide, pellets	6771.2	Carl Roth (Karlsruhe, Germany)
TEMED	T9281	Sigma-Aldrich (St. Louis, USA)
THEED	87600	Merck (Darmstadt, Germany)
TRIS-HCl pH 8.5	4855.5	Carl Roth (Karlsruhe, Germany)
Triton X-100	1.08603.1000	Merck Millipore (Darmstadt, Germany)
Trypan Blue	17-942E	Lonza (Basel, Switzerland)
Tween® 20	P2287	Sigma-Aldrich(Darmstadt, Germany)
Yeast Extract	212750	BD Biosciences (Franklin Lakes, USA)
Urea	57-13-6	Merck (Darmstadt, Germany)

**Table 7 SELF-MADE BUFFER AND SOLUTIONS**

<b>BUFFER / SOLUTION</b>	<b>COMPONENT</b>	<b>CONCENTRATION</b>
DAPI staining solution	DAPI	300 nM in PBS
DNA sample buffer (10x)	Tris-HCl, pH 7.6	50 mM
	Bromphenol blue	0.25% (w/v)
	Glycerol	60%
gDNA isolation lysis buffer	Tris-HCl, pH 8.5	100 mM
	EDTA	5 mM
	SDS	0.2% (w/v)
	NaCl	200 mM
Mounting solution	Tris-HCl, pH 8.5	100 mM
	Glycerol	25%
	Mowiol	10%
	DABCO®	0.6%
PBS	NaCl	137 mM

	KCl Na <sub>2</sub> HPO <sub>4</sub> KH <sub>2</sub> HPO <sub>4</sub>	2.7 mM 10.0 mM 1.8 mM
Protein lysis buffer	Tris-HCl, pH 7.4 NaCl SDS EDTA Phosphatase inhibitor tablet Protease inhibitor tablet	50 mM 150 mM 0.2% (w/v) 25 mM 1 tablet / 10 ml 1 tablet / 10 ml
RIMS (pH 7.5)	Phosphate Buffer Histodenz Tween-20	30ml 0.02M 40g 0.1%
Sca/eCUBIC-1	Urea THEED Triton X-100	25% (250mg/ml) 25% (250mg/ml) 15%
SDS-PAGE Anode buffer (1x)	Tris-HCl, pH 8.8	200 mM
SDS-PAGE sample buffer (6x)	Tris-HCl, pH 6.8 SDS Glycerol 2-Mercaptoethanol Bromphenol blue	93.75 mM 6% 6% 9% 0.25%
SDS-PAGE gel buffer	Tris-HCl pH 8.45 SDS	3 M 0.3% (w/v)
SDS-Polyacrylamide separating gel	SDS-PAGE gel buffer Bis/Acrylamide Glycerol Ammonium persulfate TEMED	33.3% (v/v) 10% (v/v) 10% (v/v) 0.028% (w/v) 0.09% (v/v)
SDS-Polyacrylamide stacking gel	SDS-PAGE gel buffer Bis/Acrylamide Ammonium persulfate TEMED	24.8% (v/v) 3.84% (v/v) 0.0672% (w/v) 0.224% (v/v)
TAE (1x), agarose gel buffer	Tris, pH 8.0 EDTA	200 mM 1 mM



	Glacial acetic acid	0.114%
TBS (10x)	Tris-HCl, pH 7.4	248 mM
	NaCl	1.37 M
	KCl	26.8 mM
TBST (1x)	TBS (10x)	10% (v/v)
	Tween® 20	0.1% (v/v)
Western Blot transfer buffer	Tris-glycine buffer (10x)	10% (v/v)
	Methanol	20% (v/v)
	SDS	0.08% (v/v)

**Table 8 COMMERCIAL BUFFER AND SOLUTIONS**

<b>BUFFER / SOLUTION</b>	<b>CAT. #</b>	<b>MANUFACTURER</b>
DNA polymerase buffer (10x)	311611	Biozym Diagnostik GmbH (Oldendorf, Deutschland)
Restriction buffer 2.1 (10x)	B7202S	New England Biolabs (Ipswich, USA)
T4 DNA ligase buffer (10x)	B0202S	New England Biolabs (Ipswich, USA)
TriFast™ peqGold	30-2010	VWR (Radnor, USA)
Tris-Tricine-SDS buffer (10x)	T1165	Sigma-Aldrich (St. Louis, USA)

**Table 9 ENZYMES**

<b>ENZYME</b>	<b>CAT. #</b>	<b>MANUFACTURER</b>
DNase I, amplification grade	AMPD1-1KT	Sigma-Aldrich (Darmstadt, Germany)
DNase I, cell culture	10104159001	Sigma-Aldrich (Darmstadt, Germany)
GoTaq® G2 Flexi DNA polymerase	M780B	Promega (Madison, USA)
LongAmp Taq DNA Polymerase		New England Biolabs (Ipswich, USA)
Phusion® High-Fidelity DNA Polymerase	M0530S	New England Biolabs (Ipswich, USA)
Proteinase K	405-001	GeneON Bioscience (Ludwigshafen, Germany)
T4 DNA Ligase	M0202L	New England Biolabs (Ipswich, USA)
T4 PNK	M02015S	New England Biolabs (Ipswich, USA)
Taq DNA polymerase	331610	Biozym (Hessisch Oldendorf, Germany)

**Table 10 REAGENTS**

<b>NAME</b>	<b>CAT. #</b>	<b>MANUFACTURER</b>
1 kb marker, Quick-Load®	N0468S	New England Biolabs (Ipswich, USA)
100 bp marker, Quick-Load®	N0467S	New England Biolabs (Ipswich, USA)
Adult brain total RNA, human	R1234035-50-BC	BioCat (Heidelberg, Germany)
ARHGAP11B CRISPR/Cas9 KO Plasmid	sc-416795	Santa Cruz Biotechnology (Dallas, USA)
ARHGAP11B HDR Plasmid	sc-416795 - HDR	Santa Cruz Biotechnology (Dallas, USA)
dNTPs	147850010	Steinbrenner (Laborsysteme Wiesenbach, Germany)
EOMES CRISPR/Cas KO Plasmid	sc-403485	Santa Cruz Biotechnology (Dallas, USA)
EOMES HDR Plasmid	sc-40348 - HDR	Santa Cruz Biotechnology (Dallas, USA)
Fetal brain total RNA, human	1F01-50	Tebu Bio (Le-Perray-en-Yvelines, France)
peqGREEN DNA/RNA binding dye	peq137-5010	VWR (Radnor, USA)
Protein marker PS 10 plus	310003	GeneOn (Ludwigshafen am Rhein, Germany)
ROX	A351513	GENAXXON (Ulm, Germany)
Rnase AWAY	10666421	Thermo Fisher (Waltham, USA)
SYBR® Green nucleic acid stain	S9430	Sigma-Aldrich (Darmstadt, Germany)

**Table 11 KITS**

<b>KIT</b>	<b>CAT. #</b>	<b>MANUFACTURER</b>
BCA Protein-Assay	23228	Thermo Fisher 8 Waltham, USA)
Biozym Taq DNA Polymerase kit	331610	Biozym (Hessisch Oldendorf, Germany)
Cell Line Nucleofector Kit V	VCA-1003	Lonza (Basel, Switzerland)

Chromium Next GEM Chip G Single Cell Kit	1000120	10X Genomics (San Francisco, USA)
DNase I, amplification grade	AMPD1-1KT	Sigma-Aldrich(Darmstadt, Germany)
EXTRACTME® GENOMIC DNA KIT	EM13-050	BLIRT S.A. (Gdańsk, Poland)
Gel extraction, peqGOLD	12-2501-01	VWR (Radnor, USA)
GoTaq® G2 Flexi	M780B	Promega (Madison, USA)
iScript™ cDNA synthesis kit	17088991BUN	Bio-Rad Laboratories (Hercules, USA)
Plasmid midiprep kit, PureLink™ HiPure	K210015	Thermo Fisher (Waltham, USA)
Plasmid miniprep kit, peqGOLD	732-2780	VWR (Radnor, USA)
RNA 6000 Nano kit	5067-1511	Agilent Technologies (Santa Clara, USA)

**Table 12 DATA PROCESSING**

<b>COMPUTER PROGRAM</b>	<b>SUPPLIER</b>
ApE – A plasmid editor	M. Wayne Davis
BioRender	BioRender (Toronto, Canada)
Excel 2019	Microsoft (Redmond, USA)
ImageJ (FIJI)	National Institutes of Health (NIH) (Rockville, USA)
Image Studio v 2.0	Li-Cor (Lincoln, USA)
Leica Application Suite AF	Leica (Wetzlar, Germany)
Leica Application Suite X	Leica (Wetzlar, Germany)
PowerPoint 2019	Microsoft (Redmond, USA)
Prism6	GraphPad (San Diego, USA)
QuantStudio qPCR software	Thermo Fisher (Waltham, USA)
SPSS Statistics 25/26	IBM (USA)
Word 2019	Microsoft (Redmond, USA)
ZEN	Carl Zeiss (Oberkochen, Germany)

**Table 13 PRIMERS**

PRIMER	FORWARD	REVERSE	SIZE
18S	ATTCTTGGACCGGCGCAA	GCCGCATCGCCGGTCGG	143
CORIN	CATATCTCCATCGCCTCAGTTG	GGCAGGAGTCCATGACTGT	106
FOXA2	CCACCACCAACCCACAAAATG	TGCAACACCGTCTCCCCAAAGT	294
FOXG1	CCCTCCCATTCTGTACGTTT	CTGGCGGCTCTTAGAGAT	204
OTX2	ACAAGTGGCCAATTCCTCC	GAGGTGGACAAGGGATCTGA	122
PAX6	TGGTATTCTCTCCCCCTCCT	TAAGGATGTTGAACGGGCAG	126
TBR2 control	CGGGCACCTATCAGTACAGC	CCAGTGGTTGGGGTCCG	1388
TBR2- Cassette	CGGGCACCTATCAGTACAGC	ACCCGTTGCGAAAAAGAACG	1701

**Table 14: PRIMARY ANTIBODIES**

ANTIBODY	HOST	DILUTION	MANUFACTURER
Anti- Homeobox protein Nkx-2.1 (NKX.2.1)	rabbit	1:500	Zytomed Systems GmbH (Berlin, Germany,)
Anti- sex determining region Y-box 2 (SOX2)	Rabbit	1:400	Cell Signalling (Danvers, Massachusetts, USA)
Anti- $\beta$ -III-Tubulin	Rabbit	1:3000	Cell Signalling (Danvers, Massachusetts, USA)
Anti- $\beta$ -III-Tubulin	Mouse	1:500	Synaptic Systems (Goettingen, Germany)
Anti-B-cell CLL/lymphoma 11B (CTIP2)	Rabbit	1:500	Abcam (Cambridge, UK)
Anti-empty spiracles homeobox 1 (EMX1)	Guinea pig	1:400	Takara Bio Inc. (Shiga, Japan)
Anti-Family With Sequence Similarity 107 Member A (FAM107A)	Mouse	1:500	SIGMA-ALDRICH (St. Louis, Missouri, USA)

Anti-Octamer-binding transcription factor 4 (OCT4)	Mouse	1:1000	Abcam (Cambridge, UK)
Anti-Orthodenticle homeobox 2 (OTX2)	Rabbit	1:200	Developmental Studies Hybridoma Bank (Iowa City, Iowa, USA)
Anti-Paired Boxed 6 (PAX6)	Rabbit	1:500	Synaptic system (Goettingen, Germany)
Anti-Paired Boxed 6 (PAX6)	Mouse	1:500	Biologend (San Diego, California, USA)
Anti-Phosphorylated vimentin (pVIM)	Mouse	1:1000	MBL International (Woburn, Massachusetts, USA)
Anti-Reelin (Reelin)	Mouse	1:400	MBL International (Woburn, Massachusetts, USA)
Anti-Special AT-Rich Sequence-Binding Protein (SATB2)	Rabbit	1:500	Abcam (Cambridge, UK)
Anti-Stage-specific embryonic antigen 4 (SSEA4)	Mouse	1:200	Developmental Studies Hybridoma Bank (Iowa City, Iowa, USA)
Anti-T-box protein 1 (TBR1)	Mouse	1:500	Abcam (Cambridge, UK)
Anti-T-box protein 2 (TBR2)	Mouse	1:200	Abcam (Cambridge, UK)
Anti-T-box protein 2 (TBR2)	Rat	1:100	Ebioscience, Inc. (San Diego, California, USA)
Anti-T-box protein 2 (TBR2)	Chicken	1:100	Merck Millipore (Burlington, Massachusetts, USA)
Anti-Targeting protein for Xklp2 (TPX2)	Rabbit	1:500	Novus Biologicals (Littleton, Colorado, USA)

**Table 15: SECONDARY ANTIBODIES**

<b>ANTIBODY</b>	<b>HOST</b>	<b>DILUTION</b>	<b>MANUFACTURER</b>
Alexa Fluor® 555 anti-goat	donkey	1:1000	Life technologies (Carlsbad, California, USA)
AlexaFluor® 488 anti-mouse	goat	1:1000	Life technologies (Carlsbad, California, USA)
AlexaFluor® 647 anti-mouse	goat	1:1000	Life technologies (Carlsbad, California, USA)
AlexaFluor® 647 anti-rabbit	goat	1:1000	Life technologies (Carlsbad, California, USA)
AlexaFluor™ 488 anti- rabbit	goat	1:1000	Invitrogen (Waltham, Massachusetts, USA)
AlexaFluor™ 555 anti-mouse	goat	1:1000	Invitrogen (Waltham, Massachusetts, USA)
AlexaFluor™ 555 anti-rabbit	goat	1:1000	Invitrogen (Waltham, Massachusetts, USA)
DyLight 680 anti-Mouse	goat	1:15.000	Thermo Fisher Scientific Inc. (Waltham, Massachusetts, USA)
DyLight 800 anti-Chicken	goat	1:15.000	Thermo Fisher Scientific Inc. (Waltham, Massachusetts, USA)
DyLight 800 anti-Mouse	goat	1:15.000	Thermo Fisher Scientific Inc. (Waltham, Massachusetts, USA)
DyLight 800 anti-rat	goat	1:15.000	Thermo Fisher Scientific Inc. (Waltham, Massachusetts, USA)

**Table 16: SOFTWARE**

<b>SOFTWARE</b>	<b>MANUFACTURER</b>
FIJI ImageJ®	National Institutes of Health (Rockville, Maryland, USA)
GenomeStudio 2.0.4	Illumina® (San Diego, California, USA)
GraphPadPrism 8.0	GraphPad Software (San Diego, California, USA)

ImageStudioVer2.0	LI-COR Bioscience (Lincoln, Nevada, USA)
Leica Application Suite 2.3.1	Leica Microsystems GmbH (Wetzlar, Germany)
Microsoft Excel 2010	Microsoft Corporation (Redmond, Washington, USA)
Microsoft PowerPoint 2010	Microsoft Corporation (Redmond, Washington, USA)
Microsoft Word 2010	Microsoft Corporation (Redmond, Washington, USA)
SnapGene®	GSL Biotech LLC (Chicago, Illinois, USA)

## **3. Methods**

### **3.1. Cell culture protocols**

The cells used in this study were feeder-free human iPSC, reprogrammed from fibroblasts employing Sendai Virus technology and with no known associated disorders. All experiments performed in this project were completed in compliance with Germany's legal provisions and ethical guidelines and the 'Declaration of Helsinki – Ethical Principles for Medical Research Involving Human Subjects' from the World Medical Association. This study was completed at the Life and Brain Institute (Bonn, Germany) and at the Hector Institute for Translational Brain Research (Mannheim, Germany) and the use of the human cell lines employed were in full ethical agreement with the institutions' regulations. Cells were cultivated in sterile conditions and regularly tested for Mycoplasma. List of media and buffer compositions can be found in the Material section.

#### **3.1.1. Coating**

##### **3.1.1.1. GelTrex™ coating**

To culture cells in 2D, GelTrex™ was used. GelTrex™ was thawed on ice and diluted 1:100 (for hiPSC) or 1:50 (for NSC or neurons) in 4°C wash medium. Plates were coated 24 h prior to usage with sufficient volume to cover the surface area of the vessel. Diluted GelTrex™ was stored at 4°C until further use for a maximum of one week.

##### **3.1.1.2. Pluronic® coating**

For organoid culture conditions and to avoid attachment of cells on wells and dishes Pluronic® solution diluted in Dulbecco's Phosphate Buffered Saline (PBS) (50 mg/ml, sterile filtered) was used. Wells and dishes were coated with prediluted Pluronic® and incubated for 15 min at 37°C or room temperature (RT) until use.

#### **3.1.2. Maintenance and passaging of human iPSCs (hiPSCs)**

hiPSCs were cultured in 6-well plates previously coated with GelTrex™. They were maintained at a constant temperature of 37°C and 5% CO<sub>2</sub> in stem cell medium. The media was changed on a daily basis to promote their growth in colonies. When cells



reached 80% confluency, they were passaged in a 1:12 to 1:20 ratio using 0.5 mM ethylenediamine tetra acetic acid (EDTA) diluted in PBS (1:1.000). Specifically, hiPSCs were washed twice with PBS before adding 1 ml of EDTA for 4 min at RT. EDTA was aspirated and cells were mechanically detached using 1 ml of stem cell medium. To promote cell survival during/after passaging, Rho-associated coiled-coil containing protein kinase inhibitor (RI) was added in a concentration of 1:1000 to the media.

### **3.1.3. Generation of neural stem cells in 2D**

hiPSC were grown to 90% confluency and stem cell media was replaced with neural progenitor induction medium (Day 0). Media was changed daily to sustain the culture with all the necessary components. On day 10, cells were passaged 1:2 on 6-well plates previously coated with GelTrex™. Neural progenitor induction medium was aspirated, 600 µl of TrypleE Phenol Red added and cells were incubated at 37°C for 4 min. TrypleE is a dissociation reagent, disaggregating hiPSCs colonies to single cells. Cells were detached and collected in a Falcon™ tube containing 4.4 ml wash medium and RI (1:1000). Cells were centrifuged at 800 xg at RT for 3:30 min. Finally, cells were resuspended in 1 ml of progenitor induction medium and 1:1000 RI and plated accordingly in 2 ml of medium. RI was withdrawn after 24 h. On day 15, cells were passaged again using TrypleE at a 1:2 ratio. The obtained cortical progenitors can be passaged as described for up to one month.

### **3.1.4. Generation of dorsal forebrain organoids**

#### **3.1.4.1. Embryonic Body formation**

EBs, were generated when hiPSCs reached a maximum of 70-80% confluency. Stem cell medium was aspirated, 600 µl of TrypleE was added to the cells and incubated at 37°C for 4 min. Cells were detached and collected in a tube containing wash medium. The cell suspension was centrifuged at 800 x g at RT for 4 min. The pellet was resuspended in 1 ml of stem cell medium and the concentration of cells in suspension was quantified using the Luna™ Automated Cell Counter. EBs were generated in 96-well plates previously coated with Pluronic® solution. For each well 9000 cells were plated in 150 µl of stem cell medium supplemented with RI (1:100). EB formation took just a couple of hours under these conditions. RI was removed after 48 h.

#### **3.1.4.2. Neuroectoderm induction & matrix embedding**

EBs were kept in stem cell medium for 5 days. Every second day, 100  $\mu$ l were carefully replaced with fresh medium. Within 4 to 6 days, EBs were expected to grow up to 350-450  $\mu$ m in diameter. If they exhibited smooth edges and reached the desired size, the neuroectodermal fate could be induced by replacing the stem cell medium with forebrain organoids induction medium for 5 days. Medium was changed every other day until day 10. To increase the stability of organoids it is important to cover every EB with a layer of matrix, in our case GelTrex™, with a procedure called embedding. EBs were embedded as previously described by Qian et al. <sup>147</sup>. Briefly, up to 20 EBs were collected in 67  $\mu$ l induction media. 100  $\mu$ l of cold GelTrex™ (3:2 ratio) were added and carefully mixed. The cell suspension was transferred into a 6 cm dish coated with Pluronic® solution, and evenly distributed to avoid fusions of EBs. Subsequently, the dish was incubated for 30 min at 37°C to let the GelTrex™ form a layer of matrix around the EBs. Medium was then added to the dishes and stored in the incubator overnight. 24 h later the dish was moved to an orbital shaker with a constant shaking speed of 70 rpm.

#### **3.1.4.3. Differentiation and maturation**

Around day 10 the EBs should be embedded in GelTrex™, placed on the orbital shaker and media was shifted in forebrain organoids differentiation medium. This media was replaced twice a week until day 35. At this stage components to support neuronal maturation and organoids stability have been added to the culture though the forebrain organoids maturation media. Media was replaced every 3 to 4 days and up to day 100.

#### **3.1.5. Organoids single cell dissociation and RNA-sequencing**

Organoids were dissociated with Papain following a protocol developed in our lab. Single loops were cut from an organoid using a single-use sterile scalpel. Those fragments were collected and resuspended in 1 ml Papain solution supplemented with 31.8  $\mu$ l DNase. Samples were maintained at 37°C for 20 min in agitation to dissociate it in single cell. 2 ml of prewarmed N2 media was added, and the samples were resuspended to mechanically help the complete dissociation of the sample. Following centrifugation at 400 xg for 4 min, the pellet was resuspended in ice cold PBS supplemented with 0.04% BSA and filtered through a 30  $\mu$ m filter to ensure a single cell suspension. Samples were then

processed according to the 10X Genomic kit in a specialized facility at the University of Heidelberg. Bioinformatic analysis was performed following pipelines on R.

### **3.1.6. Fixation & dehydration**

Samples were fixed with paraformaldehyde (PFA) for imaging purpose. For fixation, neuronal cells or forebrain organoids were first washed twice with 1x PBS (pH 7.4) and then exposed to PFA for 10 min. Neuronal 2D cells were washed twice and stored at 4°C until further use. Organoids were washed twice with PBS after PFA fixation, 20 min at RT. Organoids were subsequently dehydrated by addition of 30% (w/v, PBS based) sucrose solution incubated at 4°C overnight.

## **3.2. Cryopreservation and cryosectioning**

For long-term conservation organoids were embedded in tissue embedding solution. The solution was heated up to 55°C for 2 hours. Each organoid was carefully transferred into a 2 ml centrifuge tube filled with warm tissue embedding solution. Then, the embedded organoids were carefully transferred into embedding molds, on ice. Once the solution had polymerized, the molds were placed and snap frozen in a 100% ethanol dry ice-cold bath for at least 1 min and stored long-term at -80°C. Embedded organoids were cut into 20 µm slices using the LEICA CM3050S cryostat and OCT™ tissue freezing medium. The sections were attached on SuperFrost™ microscope slides, air-dried and long-term conserved at -20°C.

## **3.3. Immunofluorescence (IF)**

Slides with organoids sections were incubated 1 hour at RT with blocking solution (0.1% - 0.5% Triton, 10% fetal bovine serum diluted in PBS). Primary antibodies were diluted in blocking solution (0.5% Triton for nuclear antibodies, 0.1% Triton for membrane and cytoplasmic antibodies) and incubated overnight at 4°C. After 3 washes with PBS, the slides were exposed to the secondary antibody solutions, and incubated for 1h at RT. The slides were washed twice, incubated for 5 minutes with DAPI and washed again twice before mounting them with mowiol. Samples were air-dried overnight at RT and stored at 4°C. Images were taken using the Leica DM6B fluorescence microscope. All the images were processed with ImageJ (Fiji).

### **3.4. DNA extraction**

To isolate genomic DNA, hiPSCs, neuronal cells or organoids were harvested in 1.5 ml tubes and washed two times with PBS. Samples were centrifuged 5 min at 3000 xg at RT and lysed with 150  $\mu$ l gDNA isolation lysis buffer supplemented with 1  $\mu$ l Proteinase K. Samples were incubated at 37 °C for 1 h at 500 rpm to promote the lysis. After 10 minutes at 95°C to inactivate the Proteinase K, samples were ready for the DNA precipitation. 105  $\mu$ l of 98.8% (v/v) isopropanol was added and mixed by hand for 15 sec. Samples were incubated for 1 h at 4°C or overnight at -20°C and then centrifuged for 10 min at 12000 xg. Samples were washed twice with 70% (v/v) ethanol and centrifuged for 5 min at 12000 xg. DNA pellet was dried at RT for 20-30 min or until the pellet became transparent. Depending on the pellet size, samples were resuspended in 20-50  $\mu$ l ddH<sub>2</sub>O water and incubated 30 min at 37°C and 500rpm. Finally, DNA concentration and purity were measured at the Nanodrop® ND-1000. The isolated DNA was stored at -20°C until further use. For high-resolution SNP array karyotyping the purified DNA was sent to an external company (Life&Brain, Bonn, Germany). Data was processed using GenomeStudio software v2.0.4, module Genotyping v2.0.4.

### **3.5. RNA isolation**

RNA was isolated following peqGOLD TriFAST™ instructions. Briefly, organoids were collected in 1.5 ml Eppendorf tubes, washed with PBS and lysed with the peqGOLD TriFAST™ agent. Chloroform was added and mixed to allow the separation of RNA from proteins and DNA. After centrifugation the clear upper layer containing RNA was isolated. Isopropanol was added and incubated at 4°C to allow the RNA precipitation. The RNA was pelleted and washed twice with 75% ethanol. Finally, the pellet was air-dried and resuspended in RNase free-H<sub>2</sub>O. To avoid DNA contamination the sample was treated with DNase (Sigma-Aldrich AMPD1-DNaseI kit) according to the manufacturers' instructions. Final RNA concentration was measured using the NanoDrop™ ND-1000 Spectrophotometer. The samples were stored at -80°C until further use.

#### **3.5.1. Reverse Transcriptase for cDNA synthesis**

cDNA was generated employing the Bio-RAD iScript kit, following the manufacturers' instructions. In brief, 500 ng of RNA was diluted in 15  $\mu$ l of RNase free-

H<sub>2</sub>O and supplemented with 1 µl of the reverse transcription enzyme, and 4 µl of reaction buffer (5X). The reverse transcription was run in the Peltier Thermal Cycler PTC-200 with the following program: 1) Priming at 25 °C for 10 min, 2) Reverse transcription at 46°C for 20 min, and 3) Inactivation at 95 °C for 1 minute (35 cycles). The final cDNA product was diluted in ddH<sub>2</sub>O and stored at -20 °C.

### **3.5.2. Polymerase Chain Reaction (PCR)**

cDNA was amplified with the Biozym Taq DNA Polymerase kit, following the manufacturer's instructions. In brief, the reaction mix contained: 2 µl primers (10µM forward; 10 µM reverse), 0.25 µl dNTPs (100 mM; 25 mM each), 2.5 µl 10X Taq Reaction Buffer, 19.125 µl H<sub>2</sub>O (or 20,125 µl H<sub>2</sub>O for control samples), 1 µg cDNA, 0.125 µl Taq DNA Polymerase. The sample were exposed to the following program in the Peltier Thermal Cycler PTC-200:

**Table 17: POLYMERASE CHAIN REACTION PROGRAM**

<b>Cycle step</b>	<b>Temperature</b>	<b>Time</b>	<b>Cycles</b>
Initial denaturation	95°C	1 min	1
Denaturation	95°C	15 s	35
Annealing	60°C	15 s	
Extension	72°C	15 s/kb	

Each PCR product was loaded with 6x loading buffer dye on an agarose gel (1.5% agarose in TAE-buffer, 1:5000 PeqGREEN intercalating dye), and run for 1 h (80 V and 400 mA). Finally, the agarose gel was exposed to UV-light to visualize DNA bands and images were acquired.

#### **3.5.2.1. Gel extraction and sequencing**

For sequencing analysis, cDNA and genomic DNA were extracted using the GoldPeqlab Gel extraction kit. DNA was loaded and run in 1.5% agarose gel. Bands were visualized with UV light, excised, and collected in 1.5 ml tubes. The samples were weighted, and binding buffer was added in equal amount. After 5 min incubation at 55°C and 500 rpm, the liquid solution was loaded on a DNA collection column, centrifuged and washed multiple times. The column was dried, and DNA was eluted with addition of

ddH<sub>2</sub>O. Final DNA concentration and quality was measured using the NanoDrop™ ND-1000 Spectrophotometer. The samples were stored at -20°C until further use. For Sanger Sequencing sample were shipped and processed in an external company (Mycrosynth Seqlab Göttingen, Germany).

### **3.5.3. Gene expression characterization by qRT-PCR**

The quantitative Reverse Transcriptase - Polymerase Chain Reaction (qRT-PCR) was used to quantify the expression levels of different genes, following the instruction of the GoTaq® Probe qPCR Master Mix kit. 18s was used as housekeeping gene for all the analyses. Relative expression was analyzed with the  $\Delta\Delta C_T$ -method.

## **3.6. Western Blot**

To extract protein, cells or organoids were lysed in lysis buffer, sonicated and incubated on ice for 30 min prior centrifugation at 12.000 xg for 4 min at 4°C. A bicinchoninic acid assay (BCA) was performed according to the manufactures' instructions to determine the protein concentration, using the BioTEK PowerWaveXS. Samples were diluted in SB buffer and heated for 5 min at 95°C. Sodium dodecyl sulfate polyacrylamide gel electrophoresis (SDS-PAGE, 10% separating gel and 4% stacking gel) were used to separate the proteins by size. Once the proteins had been separated, they were blotted on a polyvinylidene fluoride (PVDF) membrane using the BioRad Trans-Blot Turbo for 30 min at 0.5 A and 15 V. The membrane was incubated for 1h with Tris-buffered saline with Tween20 (TBST) containing 5 % milk powder as a blocking agent. Primary antibodies were prepared in the same solution and incubated on a rotor overnight at 4°C. After 3 washes with TBST for 10 min, the secondary antibody was incubated in secondary antibody solution (0.01%SDS in TBST) for 1h at RT. After 3 additional washes with TBST, membranes were visualized and analyzed at the LiCOR Odyssey and ImageStudio.

## **3.7. Statistical analyses**

For statistical analysis and graph generation Prism8.0 was used. Unpaired two-tailed Student's t-test was used to compare two groups (KO compared to control cell line). The criterion for significance was set at 5%. Error bars represent the standard deviation ( $\pm$  SD), unless stated otherwise.

## 4. RESULTS

### 4.1. Generation of CRISPR/Cas9-based hiPSCs KO lines

In this study hiPSC lines 80#6 and 28#4 (Table 1), previously reprogrammed using Sendai Virus, were used. A commercially available KO-kit based on CRISPR/Cas9 technology was chosen to generate single gene KO. The commercial kit consists of a mix of six plasmids: the first three, the CRISPR/Cas9 plasmids, express the Cas9 machinery, a GFP reporter gene, and three different guide RNAs (one for each plasmid); the other three, called homology-directed repair (HDR) plasmids, containing the homology arm (one for each gRNA), LoxP sites, an RFP reporter gene, and Puromycin resistance cassette (Figure 16A).

The gRNAs were commercially designed to tag early exons of the gene. The choice of having three gRNA instead of one was to increase the rate of success of the CRISPR/Cas9 mediated KO. This plasmid mix was nucleofected in young hiPSCs (below 20 passages) to generate single-cell clones carrying the desired mutation (Figure 16B). Already after two days, cells expressing the reporter genes GFP and/or RFP could be identified confirming successful nucleofection (Figure 16C). To be noted, while the HDR plasmid integrated into the newly engineered lines, the CRISPR/Cas9 plasmids maintained a transient expression. For this reason, seven days after nucleofection, GFP expression could no longer be detected in the culture. Puromycin selection and low-density passaging allowed the generation of single-cell clones that were expanded for genotypic characterization.

Approximately 70 clones were picked and expanded under Puromycin selection for every engineered line. The single clones that survived this phase were analyzed by PCR to assess if and where the integration of the cassette had occurred in the genome (Figure 17). The primers were designed as follows: the forward primer was located a few hundred base pairs before the gRNA sequence and outside of the homology arms; the reverse primer was located in the sequence of the HDR plasmid (Figure 17A). Three primer pairs, one for every gRNA from the commercial kit, were designed for every newly obtained KO iPSC line, except for *TBR2*-KO and *NIF1*-KO. For these conditions, the two gRNAs were

designed too close to each other and thus just one primer pair was designed for two integration sites.

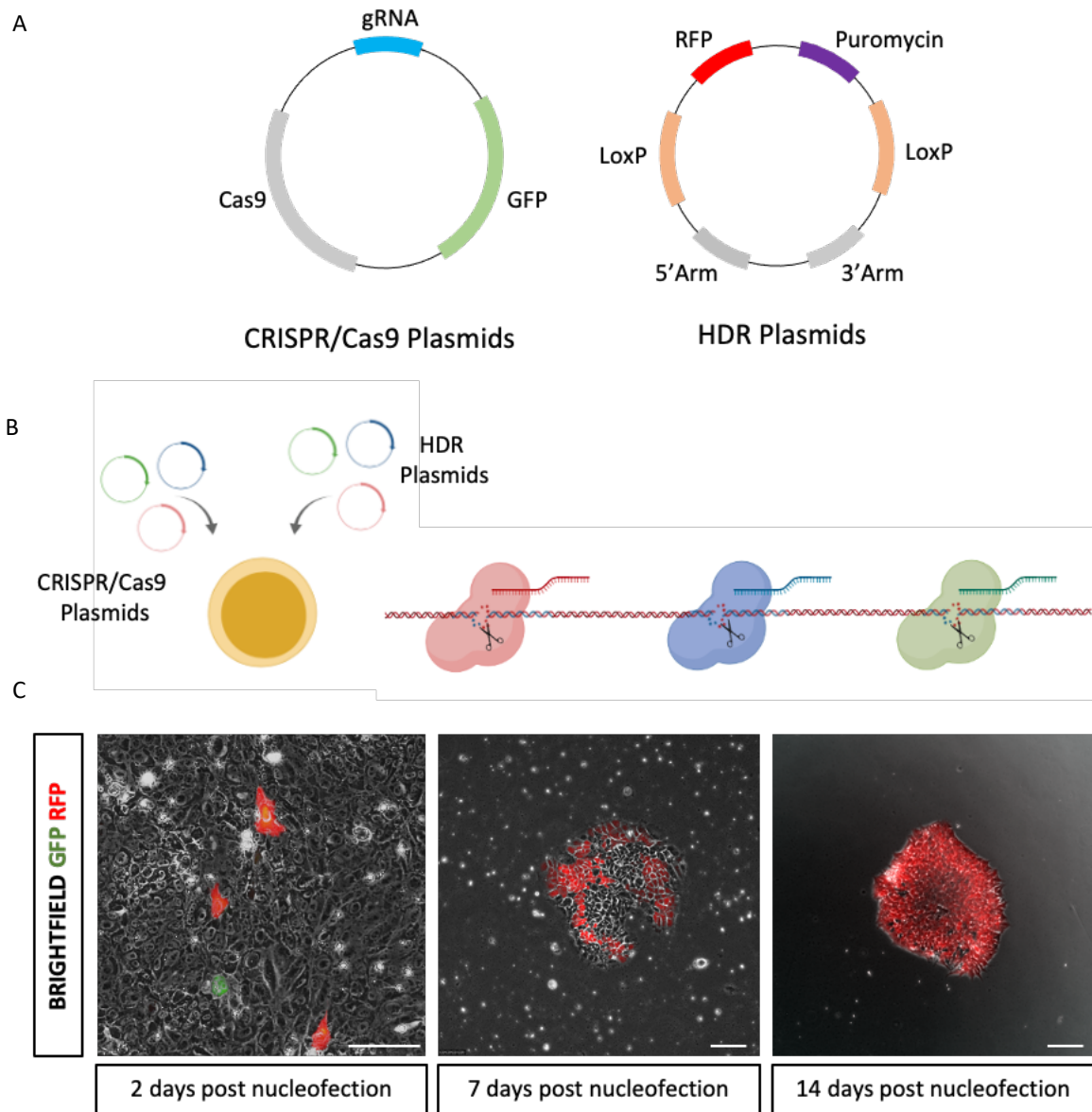


**Figure 16: GENERATION OF hiPSCs KNOCKOUT (KO) CELL LINES.**

(A) To genetically engineer hiPSCs, a combination of commercially available CRISPR/CAS9 and HDR plasmids has been used. (B) The CRISPR/Cas9 plasmid is designed to express the CRISPR/Cas9 machinery and cut the DNA strand according to the guide RNA (gRNA) sequence. The homology directed repair (HDR) plasmids insert the sequence of interest in the targeted DNA region. (C) The presence of GFP or RFP reporters allows to visualize the cells expressing the plasmids (C). Scale bar: 50µm.



The majority of clones analyzed showed integration of the HDR cassette in one of the three sites targeted by the gRNA, except for the clones targeting the *TBR2* gene. In this case only two clones correctly integrated the HDR plasmid, both at the target site of gRNA 3 (Figure 17B).

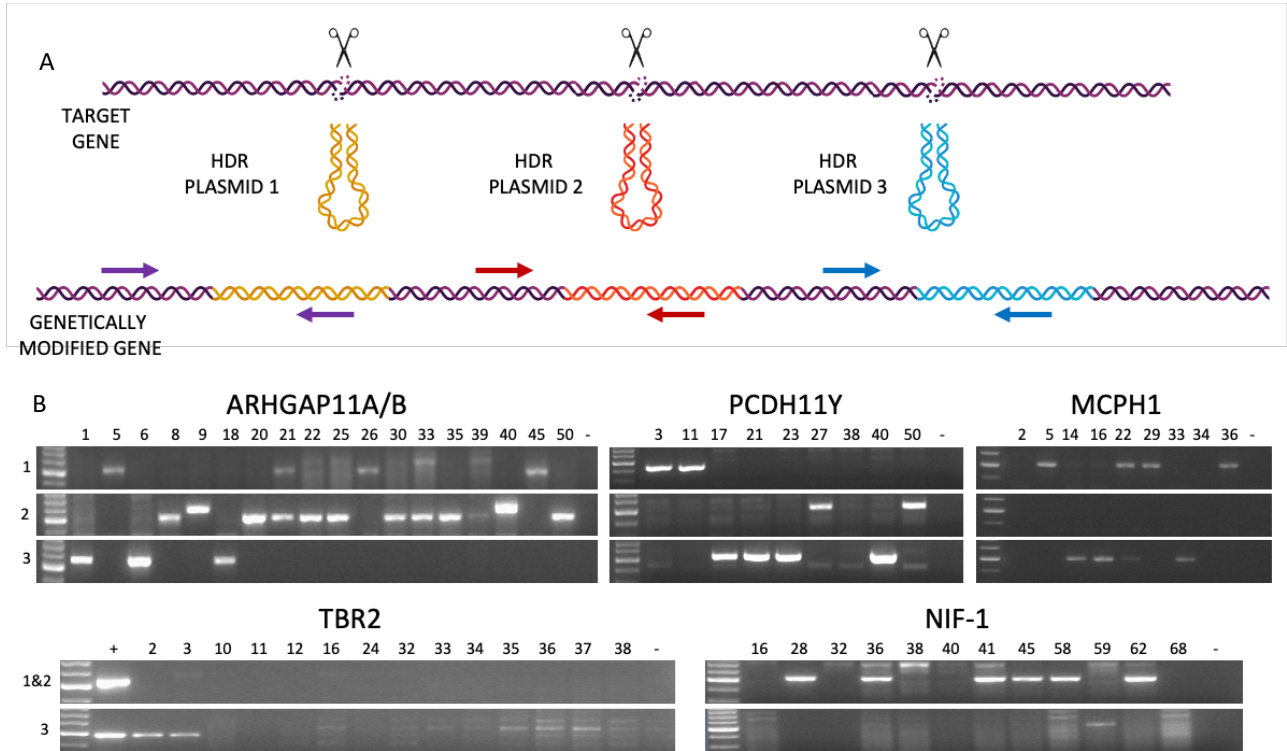


**Figure 17 CHARACTERIZATION OF hiPSC KO LINES.**

(A) Different sets of primers have been designed to investigate the integration site in the gene of interest. (B) Polymerase Chain Reaction (PCR) analysis of different clones revealed the success of the integration of the HDR plasmids in different loci in all the targeted genes.

The subsequent work focused on two out of the five candidates' genes investigated so far, namely: *ARHGAP11B* and *TBR2*. To identify the homozygous or heterozygous integration of the HDR cassette in the different clones, we performed quantitative Reverse Transcriptase – Polymerase Chain Reaction (qRT-PCR) targeting the gene of interest for all clones. Only one clone for each gene of interest showed homozygous integration of the cassette, as quantified by an absence of mRNA expression by qRT-PCR or demonstrated by Sanger sequencing, namely: *ARHGAP11B* KO clone number 40 (#40) (Figure 18) and *TBR2* KO clone number 3 (#3) (Figure 19). As these clones were intended to be the primary models for this project, additional validation was carried out.

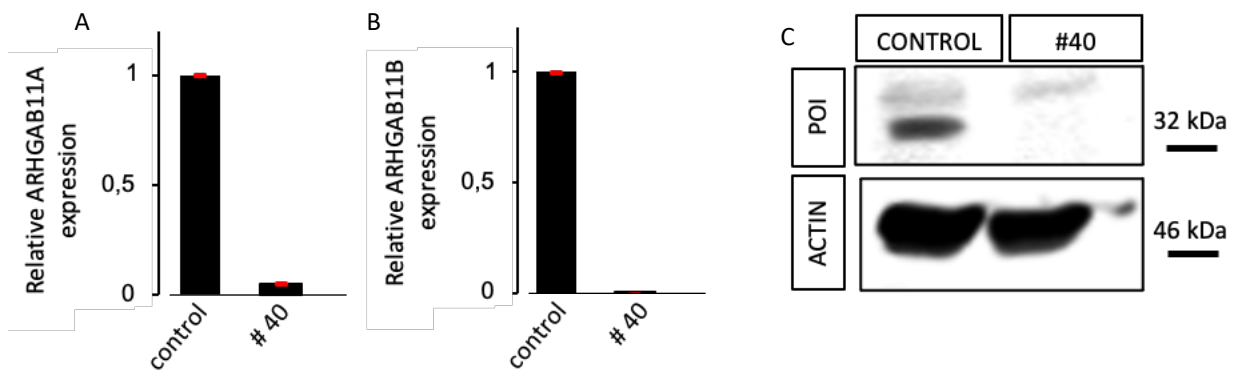


**Figure 18 VALIDATION OF *ARHGAP11A/BKO***

*ARHGAP11A/B* clones have been selected and further characterized according to the RNA expression levels. In one clone (#40) no *ARHGAP11A* (A) nor *ARHGAP11B* (B) expression was detected. Similarly, western blot analysis shows the absence of *ARHGAP11B* protein in clone #40 (C). POI: protein of interest.

Because *ARHGAP11B* shares the same genomic sequence as its ancestor gene, *ARHGAP11A*, which is also present in the human genome, and only differs by one base pair, it was not feasible to selectively target the *ARHGAP11B* variant of the gene with CRISPR/Cas9 technology. Both *ARHGAP11A* and *ARHGAP11B* gene expression levels were analyzed by qRT-PCR, which confirmed that both genes were homozygously knocked out in clone #40 (Figure 18A,B). No other clones carried a homozygous mutation exclusively targeting just one of the two genes. Western Blot analysis further confirmed the success of the KO of clone #40 (Figure 18C).

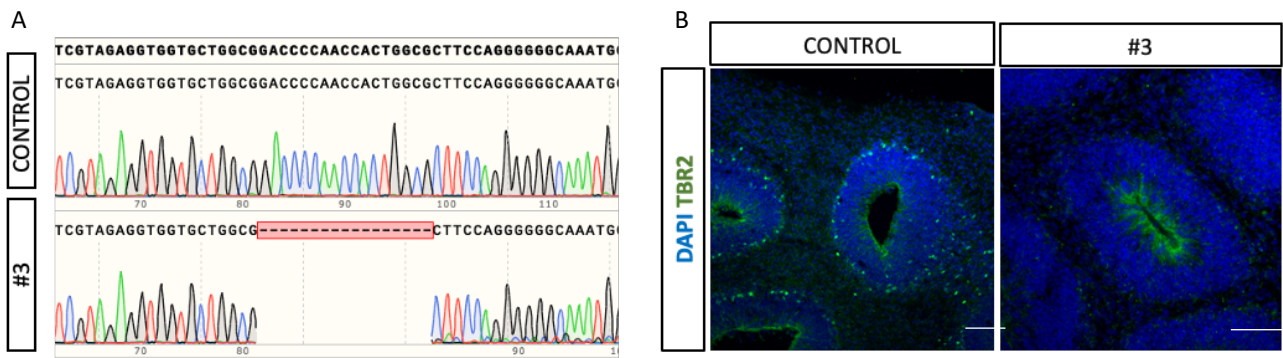


**Figure 19 VALIDATION OF *TBR2KO***

(A) Sanger sequencing confirmed a 17bp mutation in the coding region of the gene for the selected clone#3. (B) Immunofluorescence (IF) validated the absence of *TBR2* protein in 55 days old dorsal forebrain organoids (B). Scale bar: 100  $\mu$ m

Clone #3 underwent analysis by qRT-PCR and Sanger sequencing to validate the successful mutation of *TBR2*. The sequencing demonstrated a 17-base pair (bp) deletion

in the mRNA sequence of *TBR2*, which resulted in a frameshift mutation and hence created a premature stop codon (Figure 19A). Commercially available antibodies did not perform well in western blot analysis, so the KO could not be confirmed with this assay. The absence of the expression of *TBR2* in clone #3 was confirmed by immunofluorescence (IF) staining of 55 old dorsal forebrain organoids (Figure 19B). In the control organoid, *TBR2* positive cells localized between the ventricular-like zone and the cortical plate, as expected (Figure 19B, left panel). No positive signal was observed in *TBR2*#3KO derived organoids (Figure 19B, right panel).

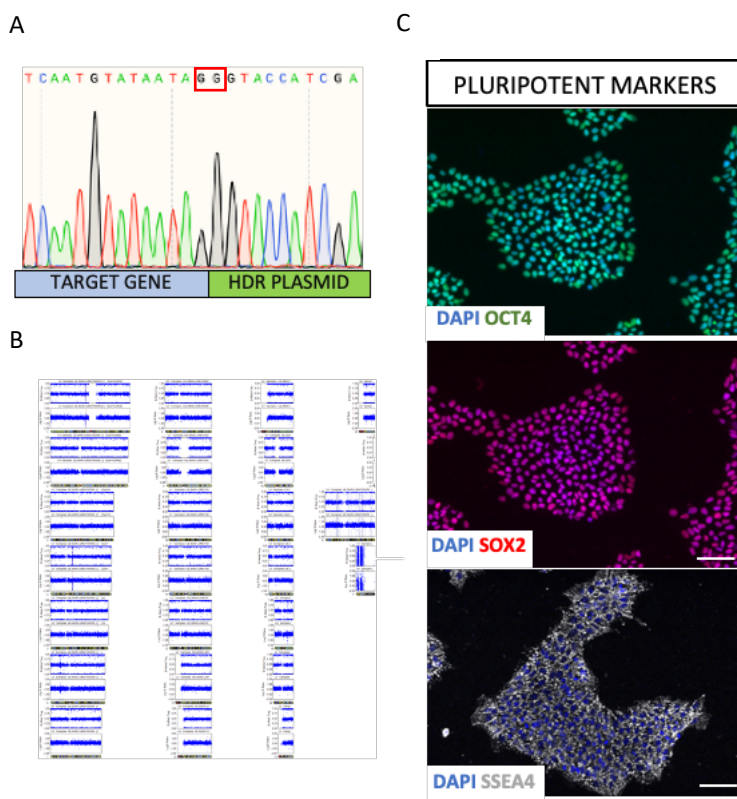


### Figure 18 KARYOTYPE AND PLURIPOTENCY CHARACTERIZATION OF THE SELECTED CLONES.

(A) Sanger sequencing analysis was performed to assess the exact integration site of the HDR plasmid. The highlighted sequence in red marks the PAM sequence, beginning of the integration site. (B) Karyotypic analysis of *ARHGAP11*KO clone #40 and *TBR2*KO clone #3 compared to the isogenic control hiPSC line excluded chromosomal aberration during the CRISPR/Cas9 process. (C) The expression of pluripotent markers like OCT4, SOX2 and SSEA4 confirms the pluripotency of the cells of clone #3 of the *TBR2*KO line, as representative images. Scale bar: 50µm (C).

Moreover, PAM sequence at the start site of integration of the HDR cassette for both clones were identified by Sanger sequenced (Figure 20A). Karyotyping of both clones as compared to the isogenic control hiPSC line demonstrated that no chromosomal aberrations incurred during gene editing (Figure 20B). Furthermore, both clonal lines expressed markers of pluripotency OCT4, SOX2 and SSEA4 as expected from a healthy hiPSC line (Figure 20C, representative images from the *TBR2*KO cell line, clone #3).

Taken together, these results show that homozygous hiPSC KO lines for *ARHGAP11A/B* and *TBR2* were generated and fully characterized. These lines were

further used to assess the roles of *ARHGAP11A/B* and *TBR2* in human cortical development.

## 4.2. Organoid generation and characterization

Organoids were generated employing a protocol developed by Krefft, O. *et al.*<sup>163</sup> (Figure 21A). Shortly, human iPSCs (hiPSCs) were detached from the cultivation plate at day 0 and seeded in 96 well U-bottom plates to generate EBs. The EBs were first induced to neuroectoderm using a combination of small molecules (A83 500nM, LDL193189 200nM, XAV939 2µM) and subsequently toward dorsal forebrain organoids. Organoids were maintained in a maturation medium for long-term cultivation on an orbital shaker.

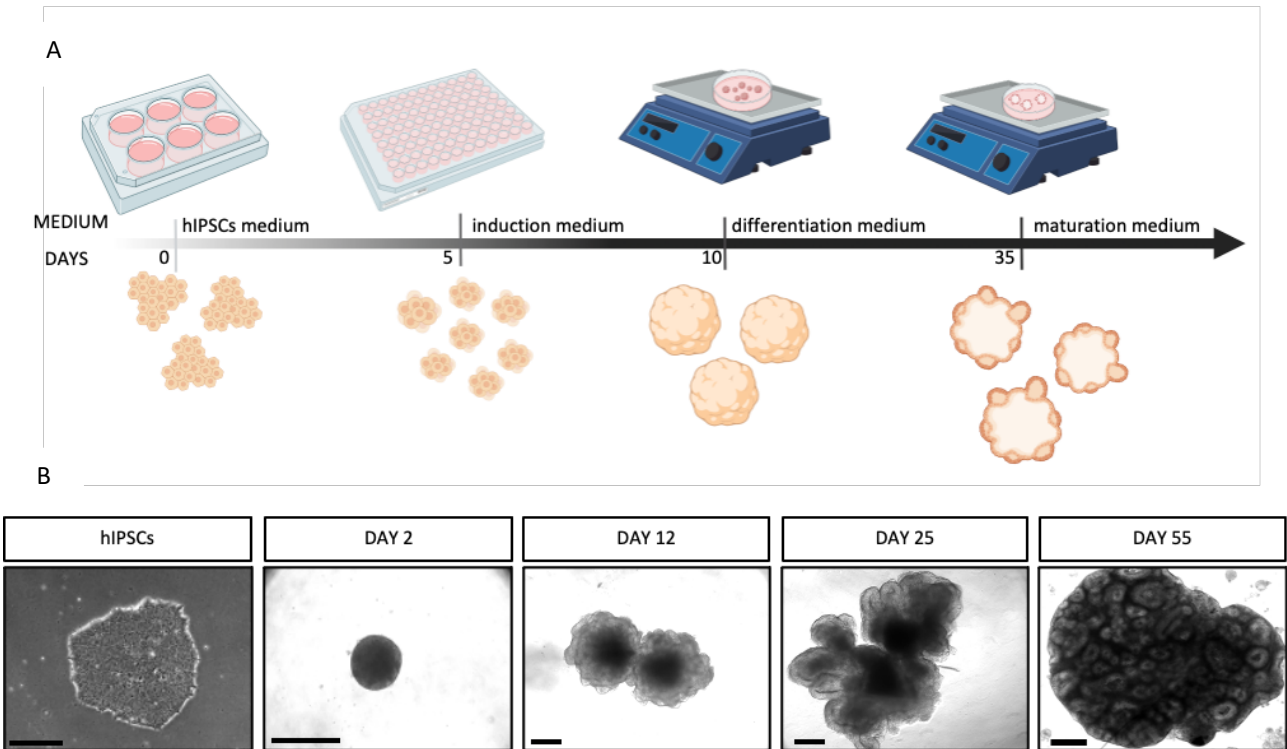


### Figure 19 GENERATION OF DORSAL FOREBRAIN ORGANIDS.

(A) Schematic representation of the organoids protocol developed by Krefft, O. *et al.*<sup>163</sup>. Starting from hiPSCs, embryoid bodies (EBs) have been generated and induced into neuroectoderm for 5 days. At day 10 they were moved on an orbital shaker with differentiation medium. After 25 days in differentiation media, the organoids are shifted to maturation media to maintain them in culture over a longer period. (B) Brightfield images of the different stages, from the hiPSCs to organoids 55 days old. Scale bar:100µm.

Morphologically the EBs grew over time and acquired the specific appearance of cortical-like structures. The first sign of neuroectoderm was observed between weeks 1 and 2 of

the protocol and is associated with the appearance of a bright layer surrounding the EBs (Figure 21B, day 12). Around 1 month after the start of the protocol cortical loops could be observed protruding from the EB itself. Every loop is considered to be the *in vitro* counterpart of one developing human cortex. They consist of one central ventricular-like structure and a layer of progenitor cells radially arranged around it. Those expand and differentiate giving rise to RGs and cortical neurons. Those structures are maintained over time (Figure 21B, day 55).

To characterize the cellular composition of the generated organoids, single cell RNA sequencing (scRNA-seq) was performed. This analysis revealed that the cells that form the organoids could be divided into 3 main types: progenitor cells, mature neurons, and cells in an intermediate stage referred as young neurons (Figure 22A). This data confirmed the efficiency of the protocol to generate organoids with neuronal fate. To verify that the organoid has a dorsal forebrain phenotype, the expression of genes specific for this region, including *FOXP1*, *LHX2*, *PAX6* and *EMX2*, was quantified. scRNA-seq analysis demonstrated high expression of these genes. The expression of region-specific genes in CNS such as *OTX2* and *LMX1a*, expressed in midbrain and hindbrain, respectively, exhibited relatively low expression levels and, in some cases, were not detected (Figure 22A).

Morphologically, the organoids were characterized according to the development of cortical regions and their spatial distribution at day 55 of differentiation (Figure 22B). At this time point, clusters of SOX2<sup>+</sup> progenitor cells can be identified (Figure 22B, in grey, left panel), surrounded by HUC/D positive neurons (Figure 22B, in red, left panel), recreating what in the literature has been described and referred to as cortical loop<sup>164</sup>. In this dense and highly populated region, called the ventricular-like zone (VZ), all the proliferating cells were radially distributed around a central empty cavity. The outermost part of the cortical structure is formed by a layer of neurons, the majority of them positive for CTIP2 (or BCL11B) (Figure 22B, in red, right panel) and TBR1 (Figure, 22B in green, middle panel), which are expressed *in vivo* in cortical layers V and VI. Intermediate progenitor cells positive for TBR2 (EOMES) (Figure 22B, in grey, right panel) were observed and they were physiologically aligned just outside of the VZ, in the so-called subventricular-like zone, between the radial glial cells and the layer of more differentiated CTIP2<sup>+</sup> neuronal cells (Figure 22B, in red, right panel).

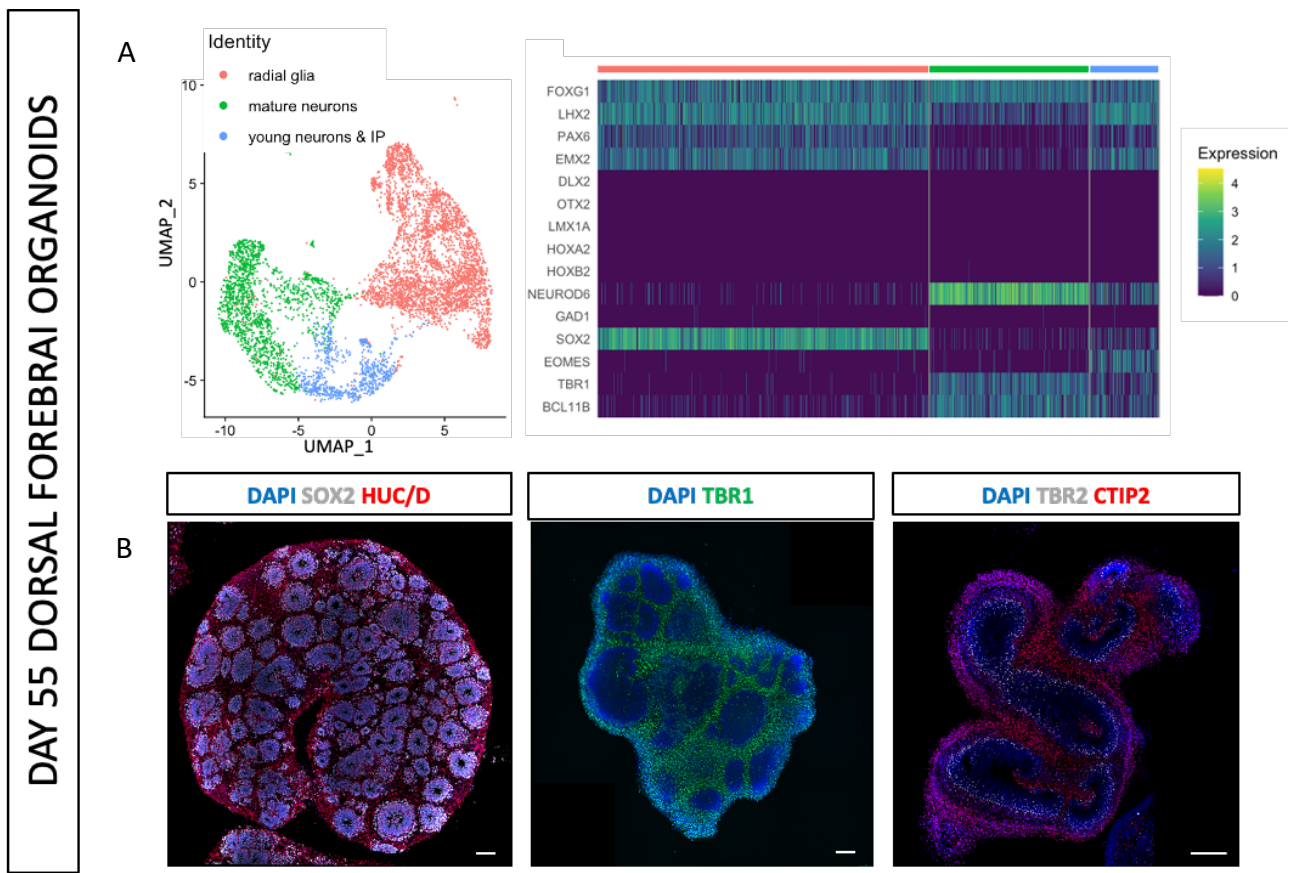


**Figure 20 MATURE DORSAL FOREBRAIN ORGANOID CHARACTERIZATION.**

(A) Cells derived from organoids processed by scRNA-seq group in 3 clusters (left): radial glia (red), intermediate progenitors and young neurons (blue) and cortical neurons (red). Every cluster is characterized by the expression of specific set of genes (right). (B) Morphologically the obtained dorsal forebrain organoids express progenitors marker like SOX2 (in grey left panel) in the cortical loop like area surrounded by general neuronal markers like HUC/D (in red, left panel). Cortical markers like TBR1 (green, middle panel) and CTIP2 (in red, right panel) are expressed in the cortical plate-like area, while intermediate progenitors markers like TBR2 (in grey right panel) are located in the subventricular-like area. Scale bar: 100 $\mu$ m

ScRNA-seq was also performed to confirm the efficiency of this protocol in generating organoids with dorsal forebrain fate (Figure 23). Interestingly, by analyzing the UMAP plot from this scRNA-seq experiment, genes associated with dorsal forebrain identity were homogeneously distributed in the whole sample (Figure 23, positive expression shown in violet). This trend was not observed for expression of genes associated with other brain region identity. In particular, the high expression of *FOXP1* and the absence of *OTX2* confirmed that the cells within the organoids were of forebrain origin and not from the midbrain.

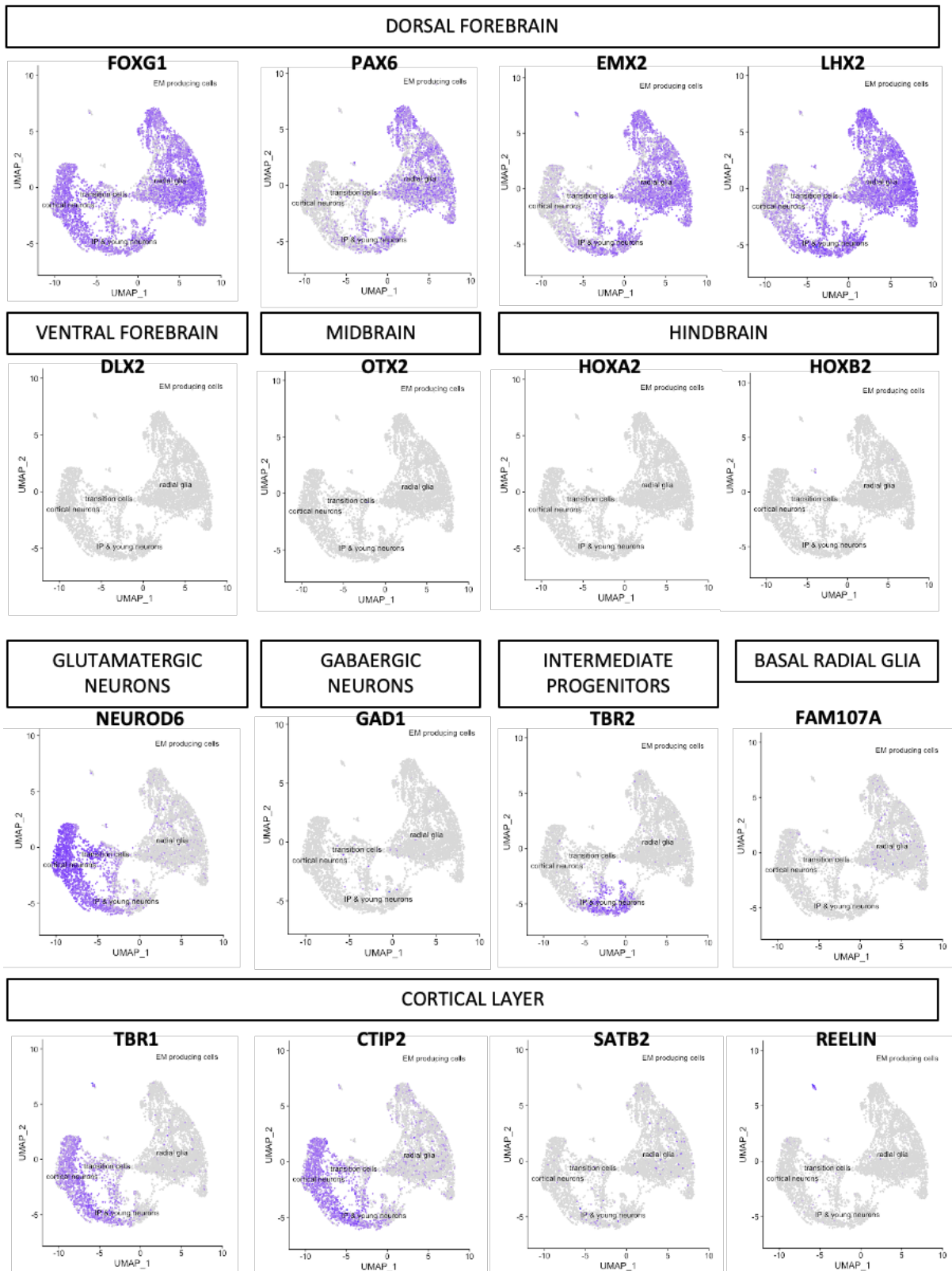


**Figure 21 ANALYSIS OF CORTICAL MARKERS IN DORSAL FOREBRAIN ORGANIDS.** Single cell sequencing data generated from dorsal forebrain organoids 55 days old. Purple dots in the dots plot are single cell positive for the respective marker. (Legend continued on next page)

(continue) All dorsal forebrain markers are expressed throughout the sample. No positive cells for ventral forebrain, midbrain, or hindbrain markers as well as GABAergic neurons were detected. TBR2<sup>+</sup> cells cluster together as intermediate progenitors. Basal radial glial cells (FAM107A<sup>+</sup>) are localized in the radial glia cluster. Cortical layer markers like CTIP2 and TBR1 are widely expressed in the cells clustering as neurons, where instead SATB2<sup>+</sup> cells are rare.

Similarly, the expression of *PAX6* in our samples and the absence of *DLX2* strongly confirmed that the organoids were correctly patterned dorsally rather than ventrally. No hindbrain markers (*HOXA2*, *HOXB2*) were detected (Figure 23). scRNA-seq data confirmed that glutamatergic neurons were generated almost exclusively, characterized by *NEUROD6*<sup>+</sup> expression. In contrast, no *GAD1*<sup>+</sup> cells were detected, which characterize GABAergic neurons. At this stage of differentiation, the cortical markers expressed in the cells were mostly from layers V (*CTIP2*) and VI (*TBR1*). Only some spars *SATB2* positive cells were detected, representing the cortical layer IV. Important for this work was the presence of bRGs and IPs. bRG cells were visualized in the progenitor cluster using the bona-fide marker *FAM107A*. IPs, characterized by TBR2 expression, are clustering together and are localized between the RGs and differentiated neurons (Figure 23).

Taken together, this data suggests that this *in vitro* organoid model shows promise in mimicking certain aspects of human cortical development. Morphologically, the model successfully recapitulated key features of neural tube development, such as the formation of the cortical loops as well as the presence of ventricular- and subventricular-like zone. From a transcriptional point of view, the homogeneous expression of dorsal forebrain markers in the organoids was confirmed by scRNA-seq together with the presence of cortical layers markers and glutamatergic neuron.

### **4.3. ARHGAP11KO**

In order to investigate the potential role of *ARHGAP11B* in driving evolutionary changes in the human brain, organoids deficient in *ARHGAP11A/B* (*ARHGAP11KO*) were generated and subjected to a 60-day differentiation process. Around day 10, when the neuroectodermal layer and the first cortical-like loops usually develop, the KO lines appeared to have larger neuroectodermal loops compared to the isogenic control (Figure 24A). To further investigate the effect of the knockout of *ARHGAP11B*, cryosectioning and IF staining was performed on both the *ARHGAP11KO* organoids and the control organoids. Immunostaining of N-Cadherin, specifically targeting the junction within the



lumen of the ventricular-like structure, provided confirmation that in the isogenic control line, a greater number of loops, albeit smaller in size, could be observed compared to the *ARHGAP11KO* line (Figure 24A).

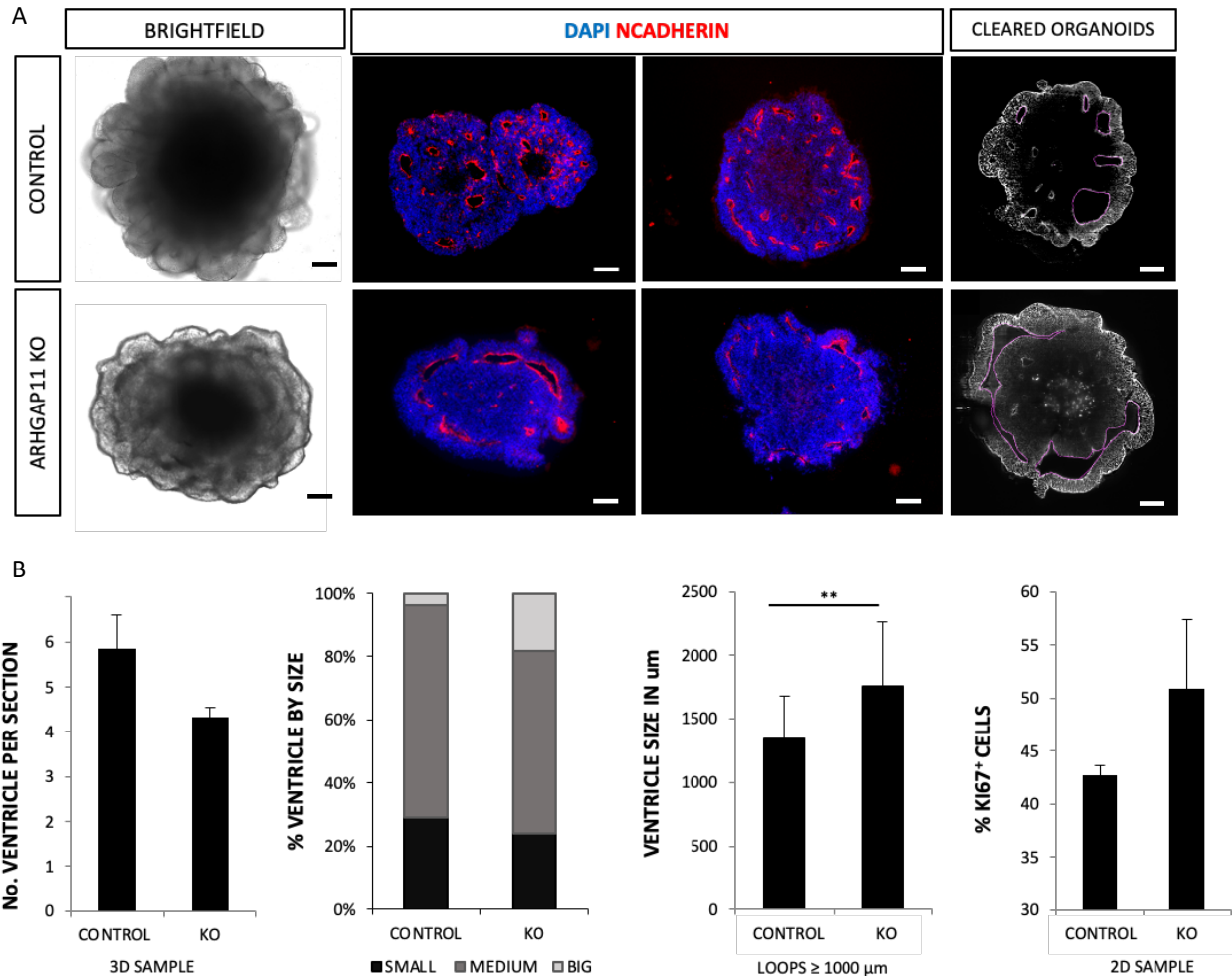


**Figure 22 ARHGAP11KO ORGANOID CHARACTERIZATION AT DAY 10.**

Comparison of *ARHGAP11KO* organoids vs isogenic control after 10 days of culture shows (A) phenotypical differences in brightfield images as well as IF and cleared organoids. (B) Differences in the development of the ventricle-like structures have been quantified. In *ARHGAP11KO*-derived organoids there are less size ventricle per section (B, left graph). The ventricles have been divided according to their size in small, medium or big, and in *ARHGAP11KO* organoids a higher percentage of big ventricles was observed (B, second graph from the left). The average size of the ventricles is also significantly bigger in *ARHGAP11KO* derived organoids compared to control organoids (B second graph from the right). NSC proliferation assay shows an increased percentage of KI67+ cells in KO cells compared to isogenic control (B, right graph). Scale bar: 100 $\mu\text{m}$ . \*\*  $p < 0.01$

Moreover, to have an overview of the overall structure and architecture of organoid, the organoids were cleared to achieve transparency and allow imaging of the whole

organoid. Various parameters, including the number and size of loops, were quantified based on these whole organoid images (Figure 24, right panel).

Consistent with the observation of the immunostaining for N-Cadherin, the analysis on the cleared organoids revealed that a greater number of loops were present in control organoids, compared to the *ARHGAP11KO* organoids (Figure 24B). Interestingly, a larger percentage of large loops (ventricle > 1000 μm) was observed in *ARHGAP11KO* compared to the isogenic control organoids (Figure 24B). Furthermore, the analysis of the mean size of the 'big loop' population revealed a significantly increased ventricular size in *ARHGAP11KO* organoids compared to the control organoids (1786 μm +/- 526 μm vs 1341 μm +/- 310 μm) (Figure 24B).

The observed increase in ventricular size of the bigger loops of the *ARHGAP11KO* organoids may potentially be attributed to an increased proliferation capacity of the neural stem cells within the *ARHGAP11KO* cell line. Quantification by immunocytochemistry (ICC) of the neural stem cell proliferation against the cell proliferation marker KI67 revealed a trend towards increased proliferation in the *ARHGAP11KO* cells (Figure 24B). Surprisingly, 20 days post differentiation, the differences in proliferation capacity of the neural stem cells between *ARHGAP11KO* cells and control cells disappeared (data not shown). Further characterization of the *ARHGAP11KO* organoids was performed on day 55 (Figure 25). IF on cryosections of *ARHGAP11KO* organoids and control organoids showed no difference in the number of cells expressing cortical layers markers TBR1 and CTIP2 (Figure 25A). Interestingly, HOPX and PTPRZ1, markers characterizing bRG, appeared enriched in the *ARHGAP11KO* organoids (Figure 25A, B). A significant increase in cells positive for PTPRZ1 was observed in the *ARHGAP11KO* organoids compared to the control. This experiment was repeated with a second *ARHGAP11KO* line, generated with a different genetic background, as a second validation of the results. (Figure 25C).

ScRNA-seq performed on *ARHGAP11KO* organoids and their isogenic control at developmental day 55 was analyzed (Figure 26). From this experiment, no significant differences were observed in the cell clusters forming the *ARHGAP11KO* organoids and their isogenic control organoid, as indicated by the UMAP plot (Figure 26). This suggests that the KO of *ARHGAP11* did not lead to substantial alterations in the cell clustering patterns within the organoids.

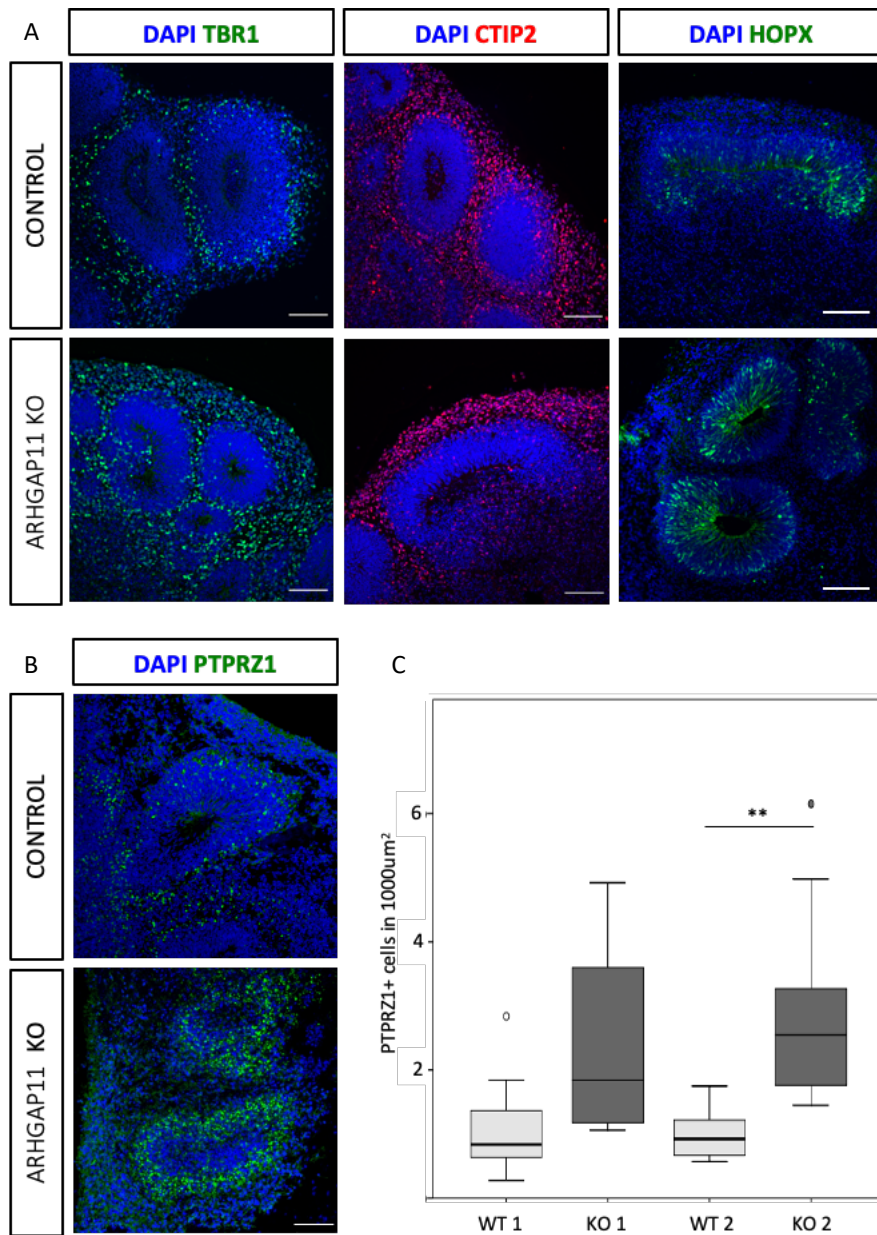


**Figure 23 ARHGAP11KO ORGANIDS CHARACTERIZATION AT DAY 55.**

Comparison of *ARHGAP11KO* derived organoids and isogenic control after 55 days of culture. (A) IF of neuronal marker TBR1 (in green, left image) and CTIP2 (in red, middle image) show similar distribution in *ARHGAP11KO* – and isogenic control- derived organoids. HOPX (in green, right image) is enriched in *ARHGAP11KO*. (B) Basal radial glial marker PTPRZ1 (in green) is also enriched in *ARHGAP11KO* derived organoids. (C) Quantification of PTPRZ1<sup>+</sup> cells in the subventricular zone confirmed the increased expression in *ARHGAP11KO* organoids compared to controls in two different genetic background. Scale bar: 100µm. \*\*: p-value < 0.01. WT: wild type, KO: Knockout.

Upon analyzing the expression profile of bRG cells, notable differences were observed in the gene expression pattern typically associated with bRG cells between the

*ARHGAP11KO* organoids and the isogenic control (Figure 27A). Specifically, a general increase in the number of bona fide bRG genes per cell was present in the *ARHGAP11KO* organoids compared to the control (Figure 27B). The most enriched genes associated with basal radial glia were *PTPRZ1*, *HOPX*, *TNC*, and *ETV5*. Additionally, genes related to the proliferation pathway of bRG, like *YAP1*, *Notch2*, and *BMP7* were upregulated in the *ARHGAP11KO* organoids, compared to the isogenic control (Figure 27C).

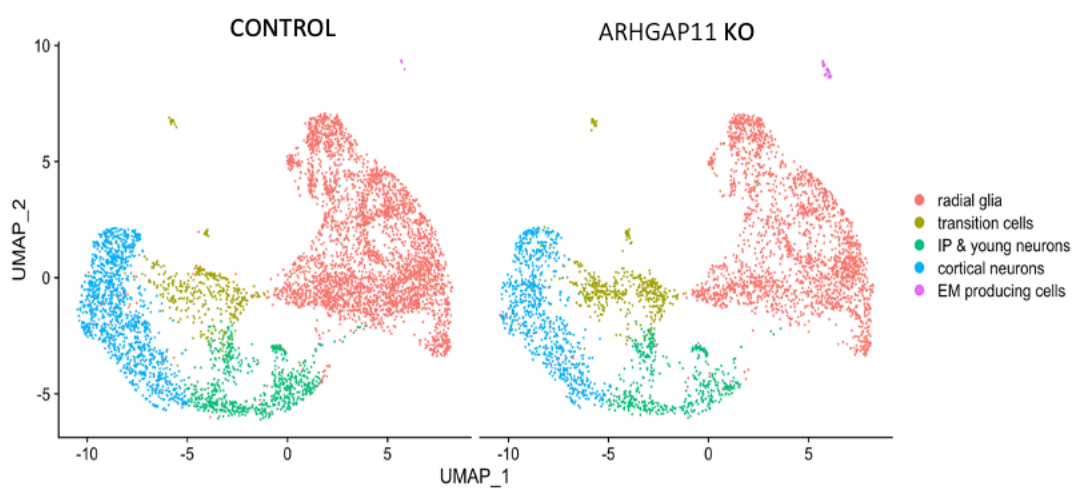


**Figure 24 SINGLE CELL RNA SEQUENCING (scRNA-seq) DATA FROM *ARHGAP11KO* AND ISOGENIC CONTROL ORGANIDS.**

UMAP plot generated from scRNA-seq comparing control versus *ARHGAP11KO* derived organoids at days 55. Cells are clustered in radial glia (red), transition cells (olive green), IP and young neurons (emerald green), cortical neuron (blue) and extracellular matrix (EM) producing cells.

Taken together, these results demonstrate that *ARHGAP11A/B* play an important role in the proliferation of the bRG population, although the specific contribution of *ARHGAP11A* and *ARHGAP11B* is still unclear.

#### **4.3.1. *ARHGAP11A* vs *ARHGAP11B***

To gain a better understanding of the individual contribution of *ARHGAP11A* and *ARHGAP11B* to the observed phenotype, additional investigations were conducted. This involved electroporation of GFP-reporter plasmids together with plasmids containing *ARHGAP11A* alone, *ARHGAP11B* alone, both *ARHGAP11A* and *ARHGAP11B*, or an empty vector in *ARHGAP11KO* organoids as well as in the isogenic control organoids.

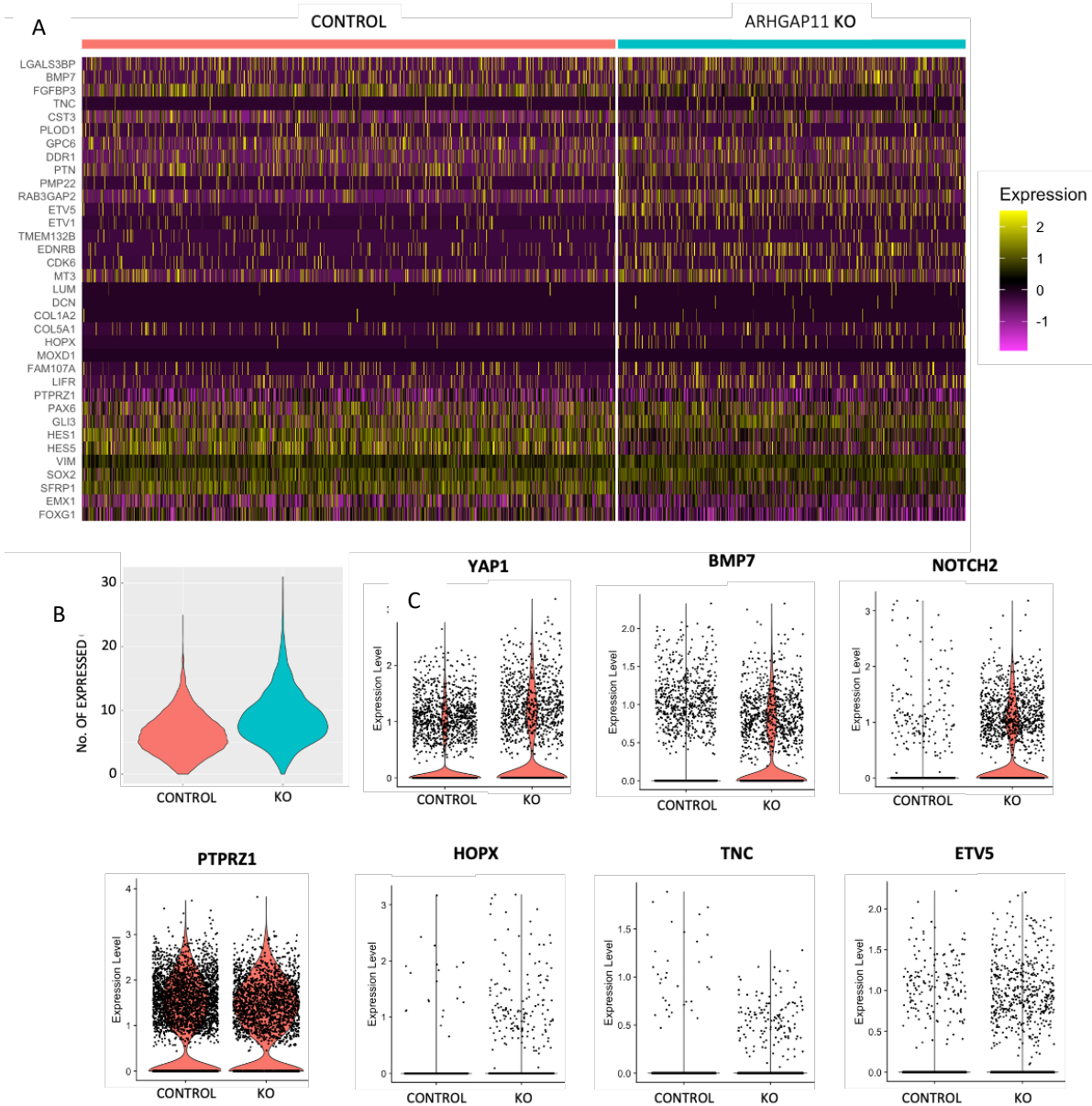


**Figure 25 BASAL RADIAL GLIA CELLS (bRG) IN 55 DAYS OLD ORGANIDS.**

(A) Expression plot of bona-fide bRGs markers in control- and ARHGAP11KO- derived organoids. (B) Violin plot summarizing the number and intensity of genes expressed in the plot A. (C) Example of genes with enriched expression in ARHGAP11KO derived organoids compared to the isogenic control (C).

The electroporation was specifically performed in the ventricle-like structure of the organoids, thus targeting aRGs, and the samples were fixed and analyzed 10-days post electroporation (Figure 28A,B). At first, we analysed the control condition to understand the behavior of the cells transfected only with the GFP plasmid and the empty vector 10 days post electroporation.

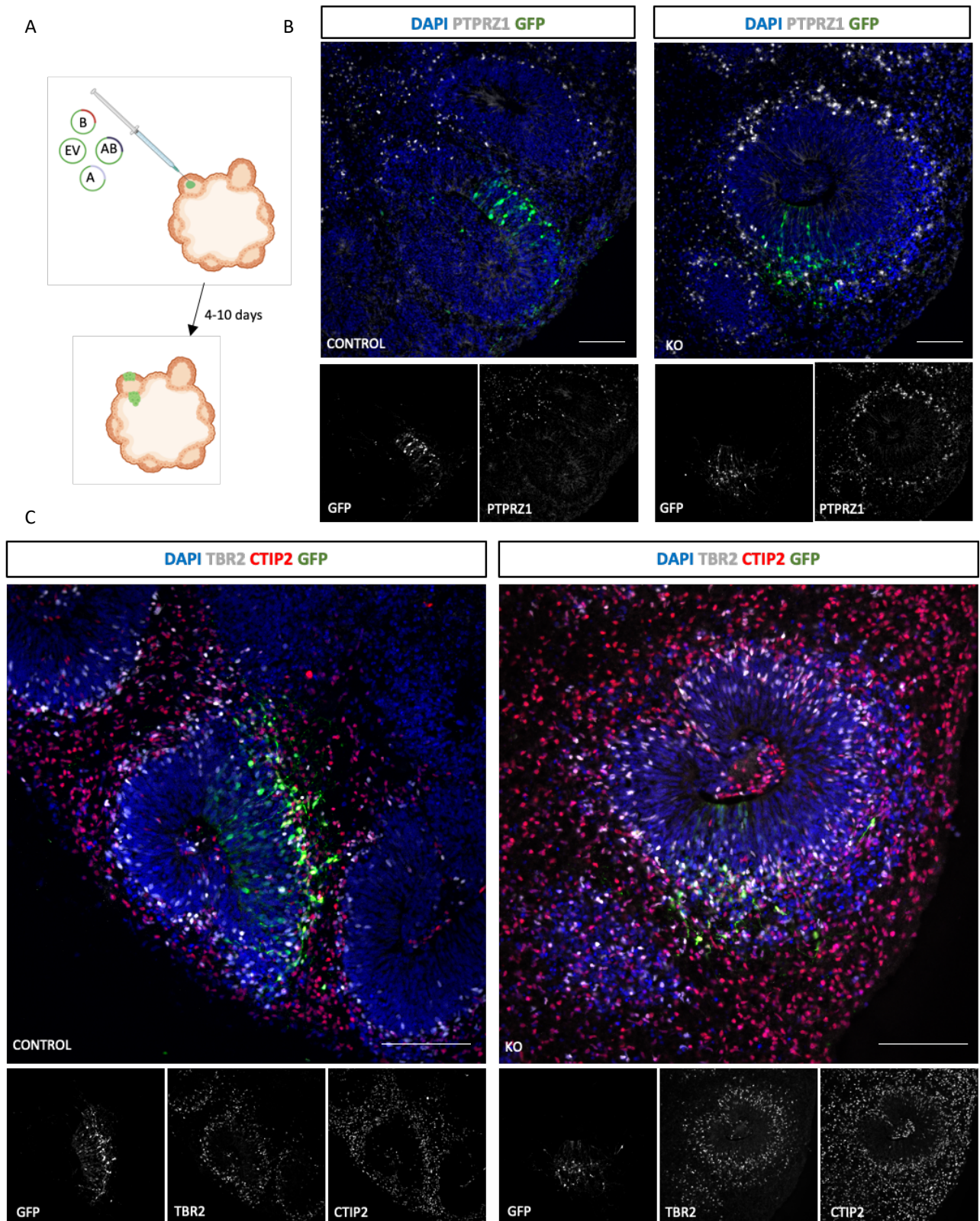


**Figure 26 ELECTROPORATION OF D55 DORSAL FOREBRAIN ORGANIDS.**

(A) Schematic of the rescue experiment. A GFP plasmid together with a plasmid encoding for *ARHGAP11A* (plasmid A), *ARHGAP11B* (plasmid B), *ARHGAP11A* and *ARHGAP11B* (plasmid AB) or empty vector (plasmid EV) has been microinjected and electroporated in the center of cortical loops (Legend continued on next page).

(continue) (B) Ten days after electroporation IF analysis confirmed that the control cells transfected with the empty vector (GFP<sup>+</sup> cell, in green) managed to migrate into the SVZ, were bRG PTPRZ1<sup>+</sup> cells (in grey) are localized both in control and *ARHGAP11KO* organoids. (C) IF of the transfected GFP<sup>+</sup> cells (in green) localizing in the SVZ together with TBR2<sup>+</sup> cells (in grey) and in the cortical plate with cortical neurons CTIP2<sup>+</sup> cells (in red) in control and *ARHGAP11KO* organoids. Scale bar: 100µm

IF performed on *ARHGAP11KO* organoids and control organoids confirmed that the electroporation did not interfere with radial migration and differentiation of transduced cells. It was possible to identify GFP<sup>+</sup> cells expressing PTPRZ1, TBR2 and/or CTIP2 10 days after electroporation both in control and *ARHGAP11KO* derived organoids (Figure 28B,C). To assess whether expression of either *ARHGAP11A* or *ARHGAP11B* or both could impact corticogenesis, IF was performed on control and *ARHGAP11KO* organoids to trace cells transduced with the one or other plasmid. The expected differences were in (I) the expansion of the intermediate progenitors, (II) early neurogenesis and (III) bRG generation.

First, co-staining of TBR2 and the transduced GFP<sup>+</sup> cells did not show any difference in amount of colocalizing cells between empty vector, overexpression of *ARHGAP11A* alone, *ARHGAP11B* alone or overexpression of both genes in the *ARHGAP11KO* organoids (Figure 29). Secondly, no difference could be detected in the analysed markers affecting early neurogenesis, as rescue of either *ARHGAP11A*, *ARHGAP11B* or both did not alter the percentage of GFP<sup>+</sup>/CTIP2<sup>+</sup> co-expressing cells (Figure 29). Overall, this data suggests that neither *ARHGAP11A* nor *ARHGAP11B* play a significant role in the expansion of intermediate progenitors or the corticogenesis of newborn neurons.

Lastly, we investigated the role of these genes on bRG generation. For this purpose, PTPRZ1 was chosen as a reference marker. Overexpression of either *ARHGAP11A* or *ARHGAP11B* in control organoids did not lead to any difference in the percentage of transfected (GFP<sup>+</sup>) colocalizing with PTPRZ1<sup>+</sup> cells (Figure 30). Interestingly, the overexpression of *ARHGAP11A* in the *ARHGAP11KO* organoids led to a significant decrease in the number of bRG cells (PTPRZ1<sup>+</sup>/GFP<sup>+</sup>), compared to the rescue of *ARHGAP11B* only or both *ARHGAP11A* and *ARHGAP11B* genes (Figure 30).

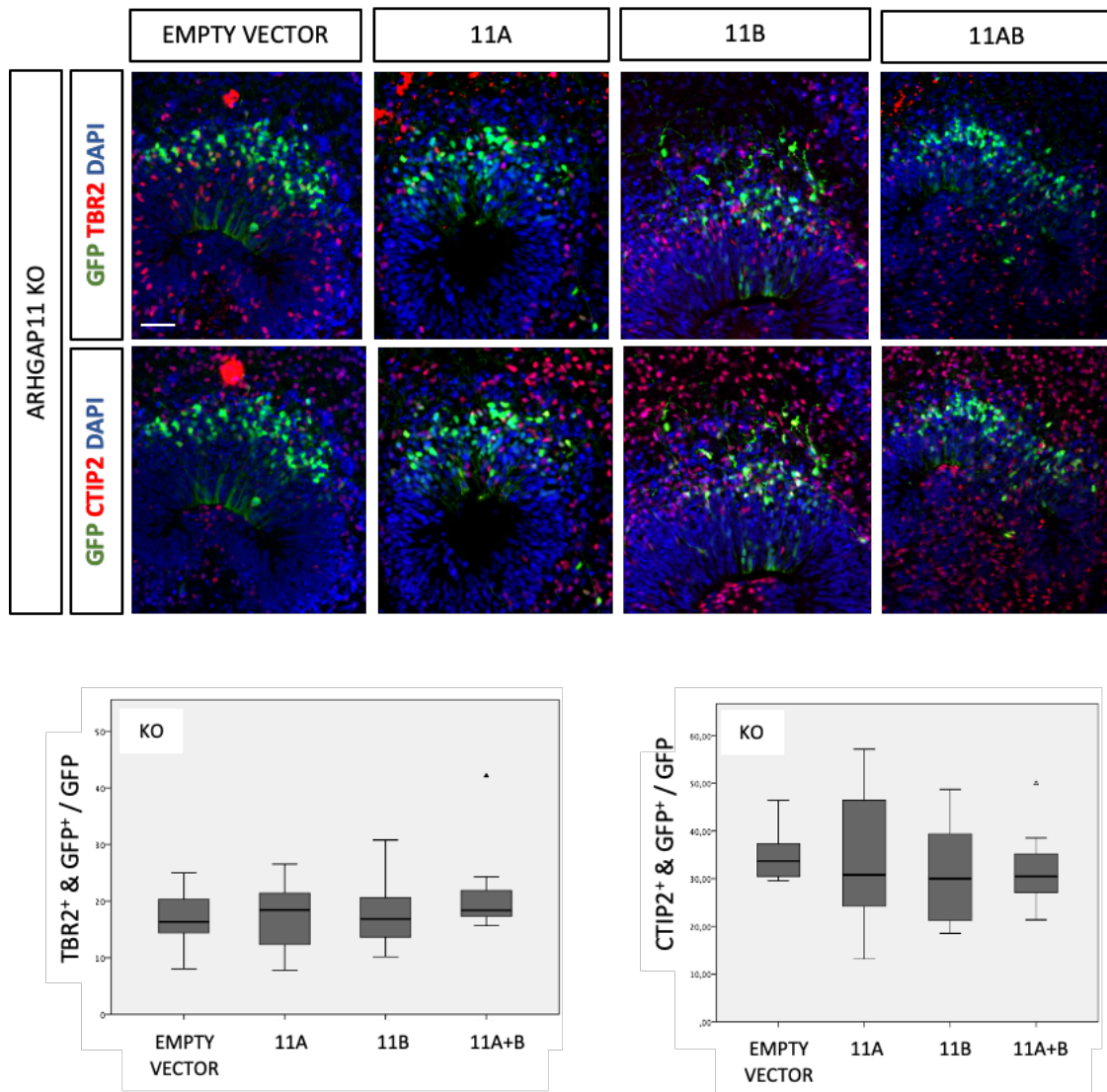


**Figure 27 RESCUE OF *ARHGAP11A* AND/OR *ARHGAP11B* IN INTERMEDIATE PROGENITORS AND CORTICAL NEURONS.**

IF analysis of the localization of the transfected GFP<sup>+</sup> cells (green) with TBR2 (red, top) and CTIP2 (red, bottom) in *ARHGAP11KO* derived organoids. Four different conditions have been evaluated: empty vector as control and rescue or *ARHGAP11A* alone, or *ARHGAP11B* alone, or *ARHGAP11A* and *ARHGAP11B* together. Plots summarize the amount of colocalization of the transfected cells with TBR2 (left) or CTIP2 (right). No significant difference can be observed. Scale bar: 100 $\mu$ m

This data strongly suggests that *ARHGAP11B* is responsible for maintaining the heightened level of basal progenitors, both in the presence or absence of *ARHGAP11A*.



Taken together, this data highlights novel roles of *ARHGAP11A* and *ARHGAP11B* in human brain development and evolution, impacting mostly bRG cells proliferation and maintenance. Specifically, this data shows that *ARHGAP11B* plays an important role in the maintenance and proliferation of bRG cells in brain organoids. In this model, *ARHGAP11A* and/or *ARHGAP11B* expression does not seem to have a noticeable impact on other cell types, like intermediate progenitors or newborn cortical neurons.

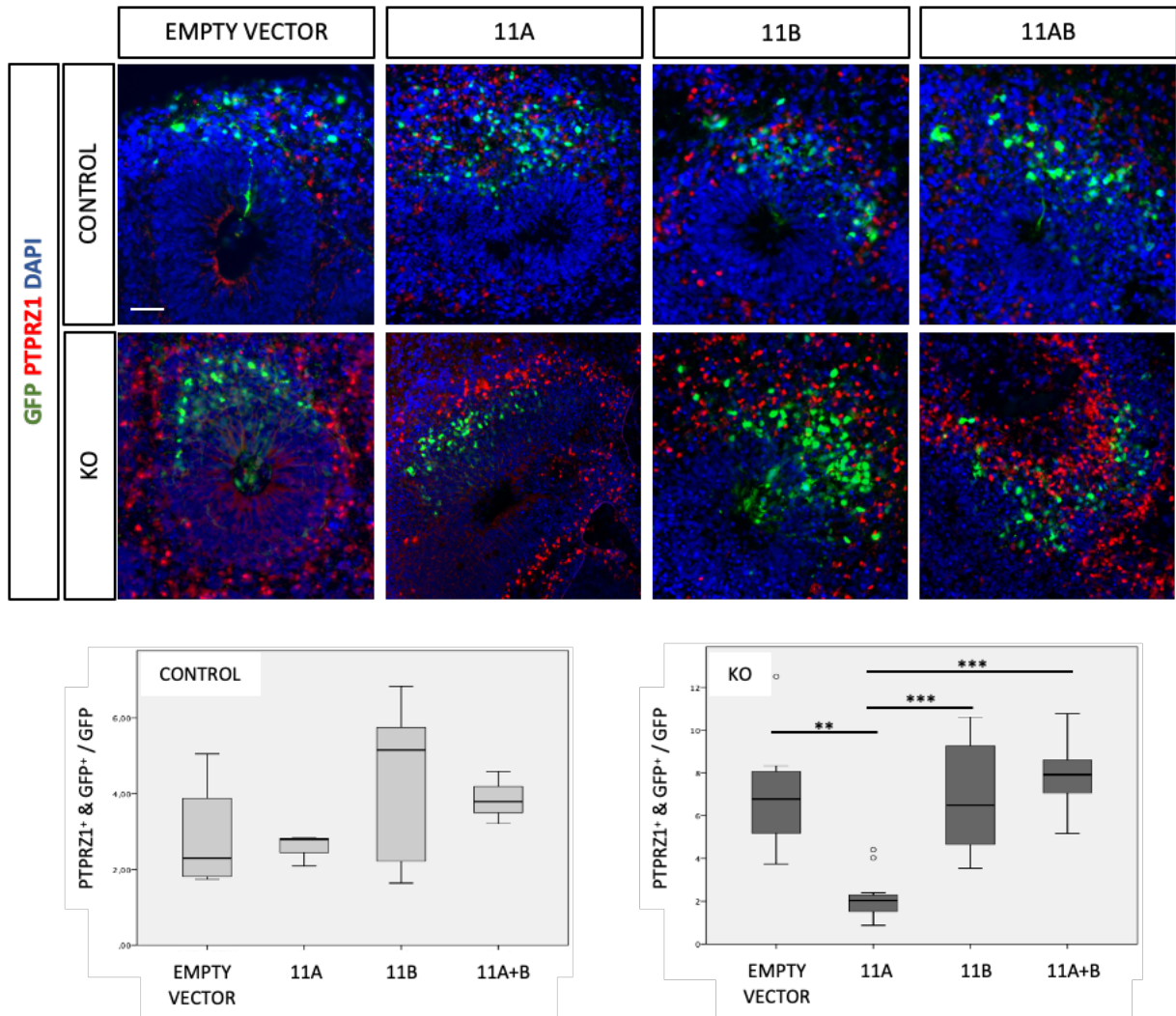


**Figure 28 RESCUE OF *ARHGAP11A* AND/OR *ARHGAP11B* IN BASAL RADIAL GLIA.** IF analysis of the localization of the transfected GFP<sup>+</sup> cells (green) with PTPRZ1 (red) in control (top) and ARHGAP11KO (bottom) derived organoids. Four different conditions have been evaluated: empty vector as control and rescue or ARHGAP11A alone, or ARHGAP11B alone, or ARHGAP11A and ARHGAP11B together. Plots summarize the amount of colocalization of the transfected cells with PTPRZ1 in control (left) or ARHGAP11KO (right) organoids. Scale bar:100 $\mu$ m. \*\*: p-value<0.01; \*\*\*: p-value <0.001

## 4.4. TBR2

The role of *TBR2* has been previously investigated using a conditional KO mice model<sup>100</sup>. However, its specific function in human brain is still largely unknown. For this purpose, dorsal forebrain organoids were generated, and subsequent investigation was carried out to explore potential phenotypic changes between the *TBR2*KO lines compared to the isogenic control lines.

Firstly, the proliferation potential of cells from the apical lumen of the ventricular-like zone was investigated, as previously shown in the mice<sup>104</sup>. IF against phosphorylated Vimentin (pVIM), expressed in mitotic cells, showed a miss localization of proliferating cells at early developmental stages (Figure 31A) in *TBR2*KO organoids compared to the isogenic control. In the *TBR2*KO organoids, a significantly higher number of dividing cells outside the ventricular-like zone was observed (Figure 31A,C) at day 25. The same analysis at later time points (day 35, 45 and 55) shows the same trend.

These results suggest an abnormal migration of dividing cells from the apical ventricular zone to the pial surface at early developmental stage in *TBR2*KO organoids.

### 4.4.1. *Plane of division of apical radial glial cells*

To understand if *TBR2* plays a role in the proliferative or differentiation capacity of aRG cells, the mitotic spindle was analyzed. Organoids at day 25 were stained to target one protein required for the assembly of the mitotic spindle itself, TPX2 (Figure 32A). The percentage of vertical (or symmetrical) division was 16% higher in control organoids (61%) compared to the *TBR2*KO organoids (45%). Conversely, asymmetrical oblique division was reduced by 18% in control organoids (17%) compared to *TBR2*KO organoids (35%) (Figure 32B). Horizontal division was not affected (22% in control organoids vs 20% in *TBR2*KO organoids).

Taken together these results suggest that *TBR2* plays a role in maintaining the ratio of symmetrical/asymmetrical proliferation. In this scenario, the increased asymmetrical oblique division in *TBR2*KO organoids suggests that neurons would be inclined in developing earlier in the absence of *TBR2* expression, leading to a decrease progenitor pool and ultimately resulting in fewer neurons. This observation is in line with previous studies where disruptions in proliferative behavior have been shown to result in a decreased generation of cortical neuronal layers<sup>101,104,110</sup>.

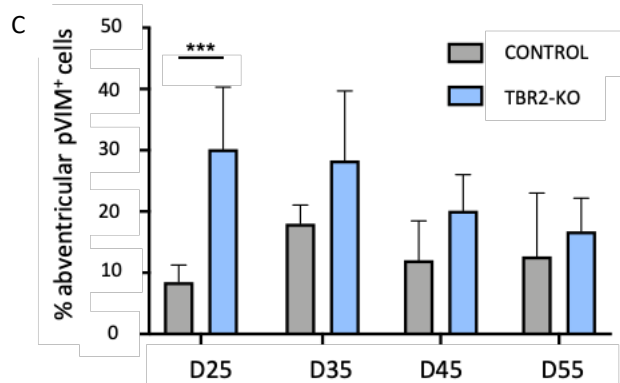
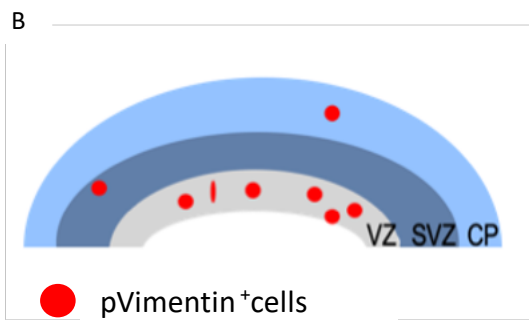
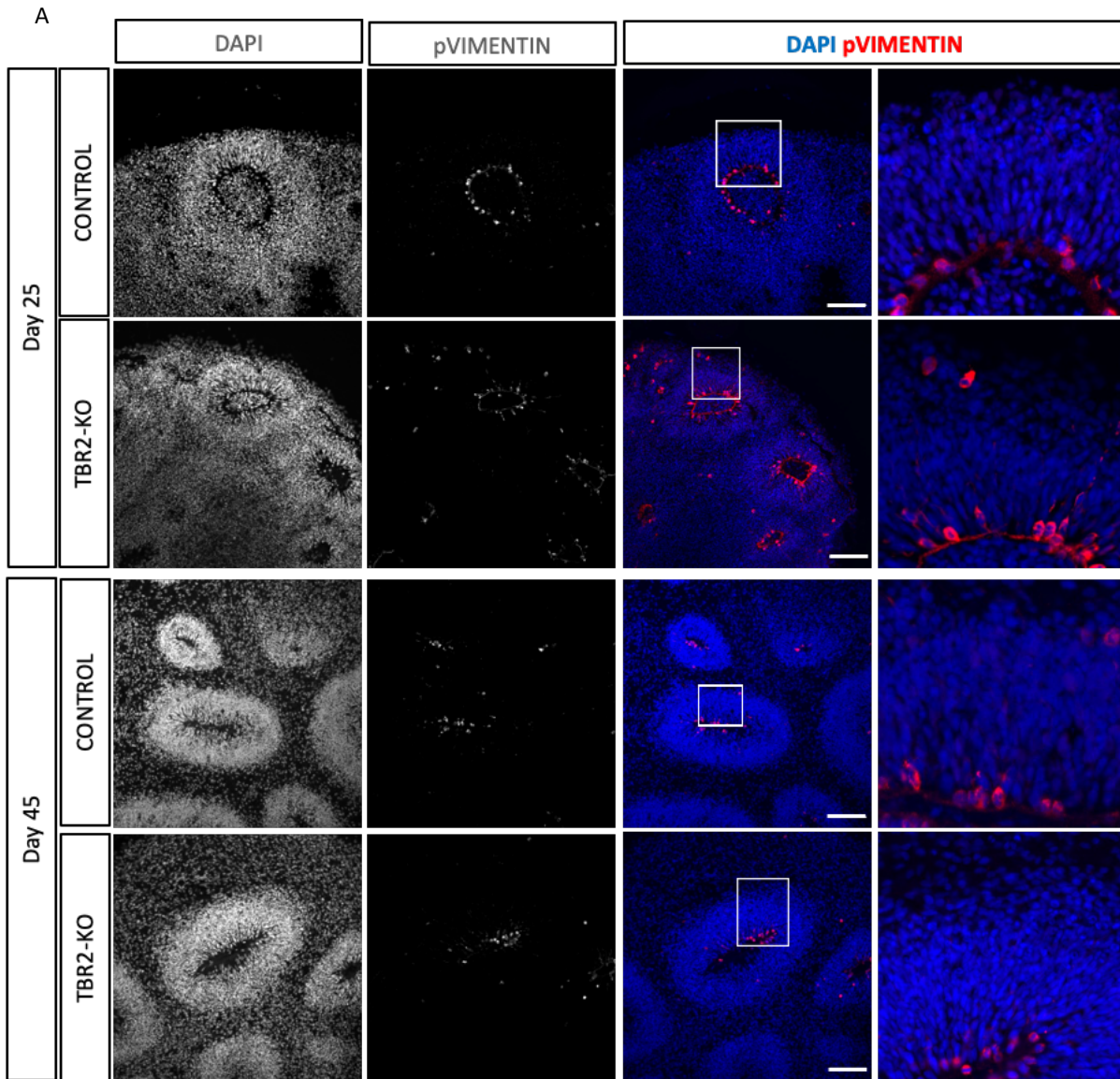


**Figure 29 ABVENTRICULAR MITOTIC CELLS IN *TBR2KO* DERIVED ORGANIDS.**

(A) IF showing the localization of pVIM (grey/red) in control and *TBR2KO* derived organoids at day 25 and day 55. (B) Schematic of the physiological distribution of the pVIM<sup>+</sup> cells, mostly localized in the VZ with rare examples of cells located in the SVZ and cortical plate. (C) Quantification of the percentage of cells with abventricular localization in control and *TBR2KO* derived organoids over time (Day 25, 35, 45, 55). Scale bar: 100µm; \*\*\*: p-value < 0.001

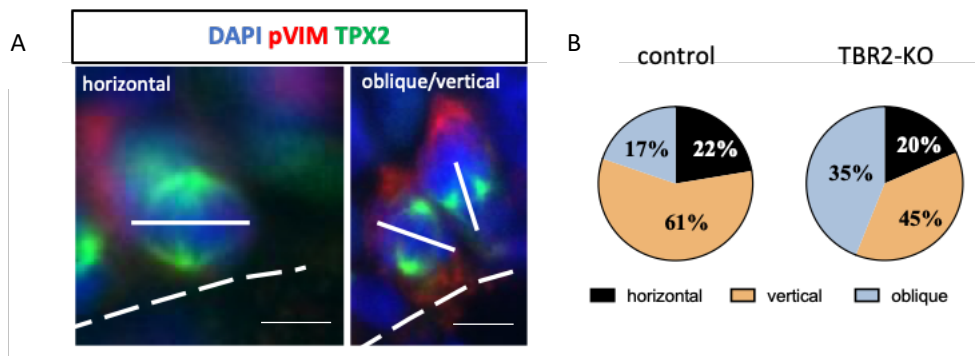


**Figure 30 PLANE OF DIVISION CHANGES IN VENTRICULAR MITOTIC CELLS.**

(A) Mitotic cells (pVIM+, red) in the ventricular lining divide according to the orientation of their spindle apparatus (TPX2+, green). The three orientations are horizontal, vertical or oblique. (B) Quantification of the cells division in the ventricular lining of control and *TBR2KO* derived organoids. Scale bar: 10  $\mu$ m.

#### 4.4.2. Corticogenesis

To investigate, whether a disrupted proliferative behavior could result in reduced generation of cortical neuronal layers in *TBR2KO* organoids, IF was performed to assess the expression of proteins expressed in cortical layers VI, V and IV in *TBR2KO* organoid vs isogenic control organoids (Figure 33A). Quantification of the amount of TBR1, CTIP2 and SATB2 positive cells at developmental day 55 only showed a significant reduction of layer VI marker *TBR1* neurons in *TBR2KO* organoids, compared to the isogenic control (Figure 33C). A time course analysis starting from day 25 up to day 55 demonstrated that the difference in TBR1 expression cells in control vs *TBR2KO* organoids remained unchanged over time (Figure 33B).

To further study this, we performed scRNA-seq at day 55 of the organoid development. The results from the scRNA-seq were in line with the IF observation and gene expression data, where a reduction in TBR1-expressing cells was noted in the *TBR2KO* organoids compared to the isogenic control (Figure 33D). As *TBR2* is known to characterize intermediate progenitors<sup>86</sup>, no *TBR2*-positive cells were detected in the cultured *TBR2KO* organoids (Figure 33A). Furthermore, genes such as PPP1R17, which are typically expressed in this population, exhibited a significant reduction in *TBR2KO*-derived organoids compared to the isogenic control (Figure 33E).

Taken together this data show the impact of *TBR2* on the plane of division of the aRG cells. In the *TBR2KO* model, there is an increased asymmetrical division (Figure 32) which could explain the presence of mitotic cells in the abventricular zone (Figure 31).

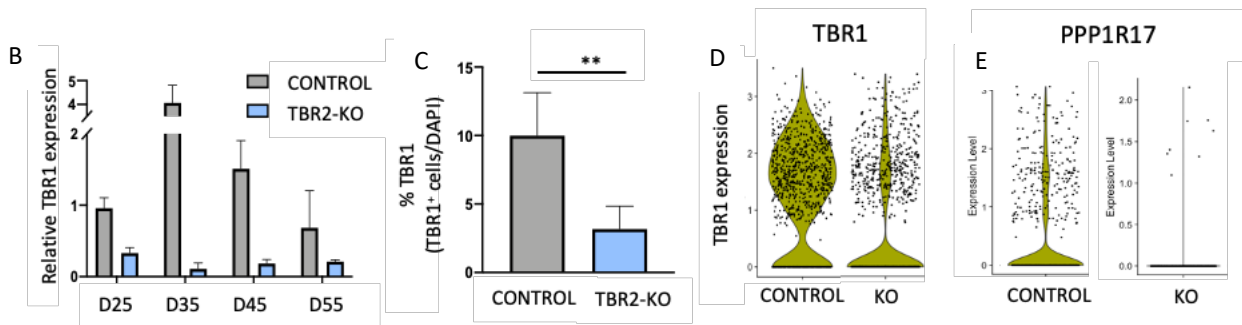
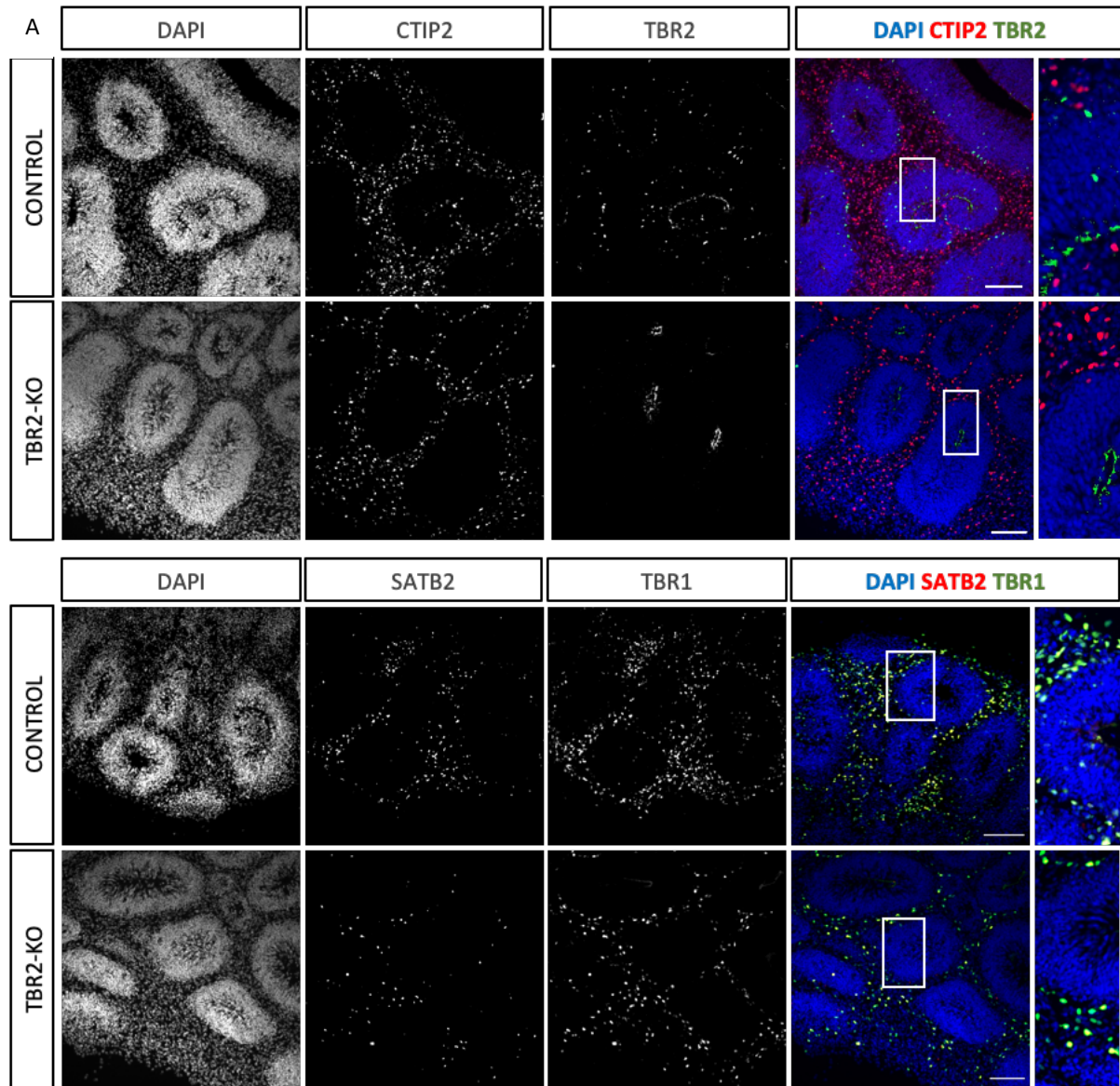


**Figure 31 CORTICAL DEVELOPMENT IN *TBR2*KO ORGANIDS.**

(A) IF of control and *TBR2*KO derived organoids at day 55. In the top panel are depicted representative images of the distribution of CTIP2+ cells (red) and TBR2 + cells (green). The bottom panel depicts representative images of the distribution of SATB2+ cells (red) and TBR1+ cells (green). (B) RNA expression level of TBR1 in control and *TBR2*KO organoids at day 25, 35, 45, 55. (C) Quantification of the percentage of TBR1+ cells in control and *TBR2*KO organoids. (D) Violin plot based on scRNA-seq data showing the expression of TBR1 and PPP1R17 in control and *TBR2*KO organoids. Scale bar:100µm; \*\*: p-value < 0.01

Later in the development, once cortical neurons are present in culture, the absence of *TBR2* was shown to have an impact mainly on intermediate progenitors and cortical layer VI (Figure 33). In the first case, this result confirms the fundamental role of *TBR2* in the generation and maintenance of intermediate progenitors, further confirmed by the lower expression of another important intermediate progenitor markers, *PPP1R17* (Figure 33E). Lastly, there is a strong effect of *TBR2* on cortical layer VI, evident from the reduction of *TBR1*<sup>+</sup> cells (Figure 33D).

## 4.5. Contributors

All the studies described within this thesis were conducted by me with the following exceptions:

Prof. Dr. Wieland Huttner and Dr. Michael Heide helped in the design of the *ARHGAP11A/B* rescue experiments. Dr. Michael Heide also performed the electroporation of the organoids at the Max Planck Institute of Molecular Cell Biology and Genetics (MPI-CBG) in Dresden.

Dr. Anne Hoffrichter helped me with the bioinformatics analysis at the Hector institute of Translational Brain research (HITBR) in Mannheim.

Annasara Artioli cultivated, cryosectioned and stained organoids for Figure 30 at the Hector institute of Translational Brain research (HITBR) in Mannheim.

Stefan Backes, Miriam Wanders and Davide D'Angelo supported the research on *TBR2* as master students, under my supervision. They generated, analysed and interpreted data generated from *TBR2*KO organoids at the Hector institute of Translational Brain research (HITBR) in Mannheim.

## 5. Discussion

In the past decades the evolution of the human brain has been a major challenge to unravel, due to the lack of reliable models. The discovery of efficient and adaptable gene editing techniques, like CRISPR/Cas9<sup>167</sup> and the generation of human pluripotent stem cells<sup>123</sup>, opened new perspectives in the field<sup>168</sup>. This study focused on the role of *ARHGAP11B* and *TBR2* to unravel mechanisms behind human brain evolution, employing brain organoids as a model system<sup>164,169,170</sup>

### 5.1. Human *in vitro* gene editing with organoids

Editing human cells has been a major challenge until the advent of CRISPR-associated gene engineering<sup>167</sup>. Beforehand, several other techniques, mainly based on homology recombination, were employed, with a sufficiently high efficiency for non-human model organisms<sup>171</sup>. It is estimated that 11.000 genes have been knocked out in mice in the last twenty years, to understand their biological role<sup>172</sup>. The advent of hiPSC now allows the investigation of the role of single genes also in human cells<sup>123,168</sup>. Additionally, isogenic controls permit the generation of a very clean system to discriminate between biological effects or possible biological artifacts. For this reason, hiPSC technology has complemented data from *in vivo* experiments, and made it possible to take a step forward in disease modeling, drug screening, and personalized medicine<sup>168,173–175</sup>. In this study, CRISPR/Cas9-based hiPSC KO clones were generated for *ARHGAP11B* and *TBR2* genes and the differences between KO and isogenic controls were mainly assessed with 3D neuronal culture, namely brain organoids.

Brain organoid cultures allow to recreate and investigate brain development, including cell differentiation, spatial patterning, and morphogenesis<sup>176</sup>. Moreover, organoids can mimic gene expression patterns of fetal brain development up to the first trimester<sup>162,177</sup>.

This study mainly focuses on corticogenesis, thus dorsal forebrain organoids, also referred to as cortical organoids, were generated via an innovative protocol that required the establishment of the right conditions to achieve homogeneous cultures, stable over time, and expressing cortical layer markers (Figure 21)<sup>164</sup>. Single cell sequencing data was employed to confirm the reliability of the system (Figure 22). After 2 months in culture,

all cell populations of interest for this work (RG, IP, and cortical neurons) could be identified (Figure 23). Taken together, these results show that hiPSC KO derived organoids were successfully generated to study human corticogenesis.

This doctoral project aims to explore the evolutionary superiority of the human brain in comparison to other species. While attributing these differences to a single event may be challenging due to their complexity, investigating one or more contributing factors can provide insights into the underlying mechanisms responsible for the evolutionary advantage of the human brain. Given the multitude of potential targets for the investigation, it became evident that genes exhibiting specific characteristics had to be prioritized. It is well established that cells in the human subventricular zone (SVZ) play a role in cortical enlargement as compared to other species, a key aspect of brain evolution<sup>98</sup>. Consequently, genes associated with the generation and maintenance of SVZ cells hold significant potential for this investigation. Several datasets are available to investigate the expression profile of genes in cells from different species. Specifically, Florio *et al.*<sup>178</sup> described *ARHGAP11B* to be specifically expressed in cells located in the SVZ, namely bRG. Notably, the expression of this gene was found to be exclusive to the human brain, indicating that it is a unique feature of the human species. Lastly, this work described how the expression of *ARHGAP11B* in bRG cells may have contributed to cortical enlargement, crucial for human brain evolution, making it an ideal target for this project. At the same time, the *TBR2* gene holds importance in human brain evolution for several reasons. Mostly, *TBR2* is involved in the regulation of the intermediate progenitors (IPs) which play a crucial role in the generation of neurons in the developing brain. IPs, together with bRG, form the SVZ. It is important to note that there is a lack of human-specific data regarding *TBR2*, requiring a comprehensive investigation into its function and significance in humans. Further research is needed to explore the specific mechanisms and functions of *TBR2* in the context of human brain development and evolution.

## **5.2. Role of *ARHGAP11B* in human brain evolution**

Approximately 5 million years ago, a novel gene known as *ARHGAP11B* emerged through a partial duplication event of the highly conserved gene *ARHGAP11A*<sup>178</sup>. The high homology of the *ARHGAP11B* gene with its ancestor *ARHGAP11A* posed a challenge in generating hiPSCs KO lines for *ARHGAP11B*. The similarity between the two



genes, differing for just one base pair (C to G), made it difficult to specifically target and disrupt the expression of *ARHGAP11B* without affecting *ARHGAP11A*. The single different base pair results in a point mutation in the GAP domain of *ARHGAP11B*, which occurred during the gene duplication. This point mutation leads to a frameshift and a short novel C-terminal sequence on mRNA level <sup>178</sup>. To distinguish between the two genes, the experiments focused on targeting the unique C-terminal sequence of *ARHGAP11B* <sup>178</sup>. However, despite efforts to selectively disrupt *ARHGAP11B*, every clone obtained from the CRISPR/Cas9 experiment targeting *ARHGAP11B* also showed a reduction in *ARHGAP11A* expression. Thus, a clone carrying a homozygous double KO was at the end selected for downstream experiments investigating their role on the human brain development.

*ARHGAP11B* was initially characterized by Florio *et al.* in 2015 <sup>178</sup>. Since then, and in parallel with this doctoral work, further research has been conducted to have a better understanding of its function <sup>115</sup>. In the *ARHGAP11KO* organoids with less but bigger loops compared to the isogenic control could be observed by imaging and were therefore quantified (Figure 24). At the same time, 2D cultures of neural stem cells carrying the double KO showed increased proliferation (Figure 24). Interestingly, this effect could be observed in a specific timepoint of the organoid/neural stem cell protocol. Once the differentiation process started, the organoid morphology was rescued within one week, and no structural differences could be observed anymore between the *ARHGAP11KO* organoid and the controls. This can be explained by the fact that *ARHGAP11A* and *ARHGAP11B* are member of a larger family of Rho-GTPases, which are involved in a wide array of molecular and cellular pathways. During neuronal differentiation, several members of the Rho-GTPase family remain active, and it is plausible that some of these members are activated in order to rescue the phenotype caused by *ARHGAP11KO*. Previous studies have reported that alteration of Rho-GTPases can impact embryonic development, cell migration, cell adherence, and actin reorganization (Figure 34) <sup>179</sup>. The interplay between various Rho-GTPases may therefore contribute to the compensatory effect observed in response to *ARHGAP11A/B* disruption in the *ARHGAP11KO* organoid during neuronal differentiation. Further studies will follow to find evidence on this theory.

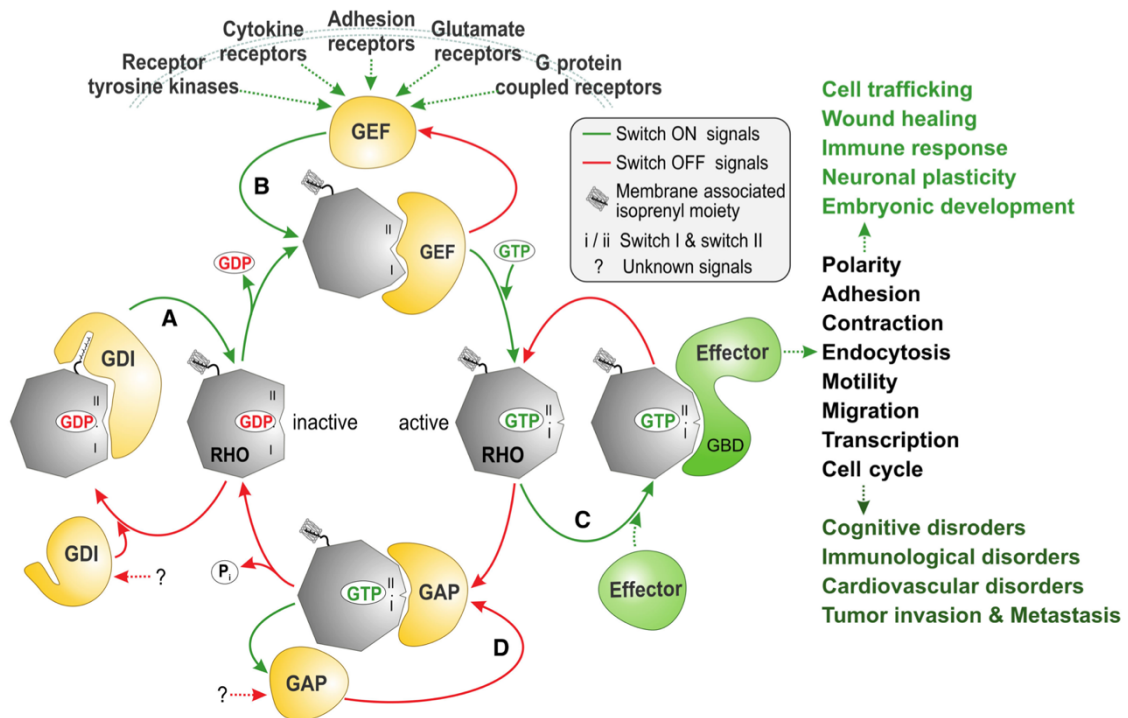


**Figure 32 RHO GTPase REGULATION.**

Rho GTPases play a role in a big variety of process in the cells. The abundance in isoforms and subtypes made them available in different tissues with activation or repressor activity. From Mosaddeghzadeh and Ahmadian, 2021

Around two months after the start of organoids differentiation protocol, an increase in RG cells in the SVZ was observed by IF (Figure 25) and scRNA-seq (Figure 27). Previous work has reported that knock-in of *ARHGAP11B* in non-human cells results in increased bRG proliferation<sup>117,119,178</sup>. The results from this doctoral work contradict these previous findings, as a reduction in bRG proliferation was not observed in *ARHGAP11KO* cells. A possible explanation is that in none of the other works an altered expression of *ARHGAP11A* has been induced<sup>117,119,178</sup>. This was the main reason of performing the rescue experiments and have a better understanding of the different roles of *ARHGAP11A* and *ARHGAP11B* in our model.

This experiment involved *ARHGAP11B* overexpression in *ARHGAP11KO* organoids, together with or without the overexpression of *ARHGAP11A* (Figure 30). The results highlighted the importance of *ARHGAP11B* for bRG amplification, independent of the presence of *ARHGAP11A*, in human cells (Figure 30) and in line with all the previous findings<sup>117,119,178</sup>. It was thus confirmed that *ARHGAP11B* plays a critical role in the

generation and amplification of bRG in human cells, reinforcing the understanding of *ARHGAP11B*'s significance in human brain development.

Additionally, these results raise new questions about the role of *ARHGAP11A* in corticogenesis, specifically how *ARHGAP11A* could influence the bRG abundance in the double KO organoids. Limited studies have been published so far regarding *ARHGAP11A* expression in the brain. Most of the research on the gene has focused on its involvement in cell cycle progression and cell migration in cancer cells <sup>180</sup>. The only study of *ARHGAP11A* on brain tissue was performed by Pilaz *et al.* <sup>181</sup>, demonstrating that the expression of *ARHGAP11A* was enriched in RGs but absent in the cortical neurons of human fetal brains and mice. Moreover, *ARHGAP11A* mRNA was discovered to exhibit distinct subcellular localization patterns within RGs, with enrichment in the basal processes and the ventricular zone (VZ). Disruptions of its expression were shown to alter cellular morphology, impair radial glial cell function, disrupt cortical layer formation and most importantly delamination <sup>181</sup>. The only plausible theory is thus that absence of *ARHGAP11A* leads to delamination of aRG cells, which are then populating the SVZ, as observed in Figure 24. In the future, generation of hiPSCs deficient of *ARHGAP11A* alone will help with the understanding of their specific role independently of the status of *ARHGAP11B*.

### **5.3. *TBR2* in corticogenesis**

*Tbr2* is a transcription factor involved in the generation and development of intermediate progenitors (IPs) in the mouse brain, more specifically having a fundamental role in the differentiation and migration of IP-derived neurons. Therefore, *Tbr2* is crucial for the establishment of the layered structure of the cerebral cortex <sup>86,114</sup>. Moreover, previous publications implicated *Tbr2* in the role of IPs differentiating into neurons of all cortical layers, while others have suggested that IPs can only drive differentiation into upper layer neurons <sup>99,101,104,106,111,182</sup>. Additionally, the downregulation of *Tbr2* in ferrets has been shown to impact IPs and bRGs and thus decrease cortical folding <sup>78</sup>.

So far, studies on *Tbr2* have focused on mice models, and there is a lack of research specifically evaluating its role in human neuronal cells and human brain development. As it is essential to investigate the function and significance of *TBR2* in the

context of human brain development, human-specific model systems such as hiPSCs and brain organoids were exploited.

Firstly, during this doctoral project, the generation of hiPSCs carrying *TBR2* mutation was challenging, as it seemed to have a heavy toll on cell survival, therefore only a few clones survived the process. Only one carried a homozygous KO of 17bp at the mRNA level, blocking its translation into a functional protein (Figure 19). Moreover, functional organoids were generated carrying the homozygous deletion of *TBR2* and they were successfully cultured for up to 2 months, in contrast with previous work showing that homozygous KO in mice was not compatible with life <sup>101,102</sup>.

The main goal of this doctoral project was to investigate the role of *TBR2* in cortical development, focusing on its function in the human context for the first time. To pursue this objective, *TBR2*KO organoids were utilized as a model system. One key objective investigated in this project was to validate if the observation in mice studies could be reproduced in cortical organoids.

One of the observation was the non-physiological abventricular localization of mitotic cells <sup>104</sup>. Within the first 30 days of development of the *TBR2*KO organoids, an increased amount of misplaced proliferative cells was observed (Figure 31). This finding aligns with the observations from Mihalas *et al.* in conditional KO mice <sup>104</sup>. In contrast, studies on different animal models have shown the opposite effect, where absence of *TBR2* caused a reduction in mitosis <sup>101,182</sup>. In the study from Lv *et al.* <sup>183</sup> a possible explanation of the phenomenal is proposed, though the interaction between *Tbr2* and the cell adhesion protein Protocadherin19 (*Pcdh19*). *Pcdh19* is shown to be localized in the apical lumen of developing VZ and it is directly regulated by *Tbr2*. Reduction in *Tbr2* levels led to decreased in *PCDH19* expression and disperse tangential distribution of RG cells. Based on these published data, one of the hypotheses was that this cell adhesion molecule could be the link between *Tbr2* and the observed abventricular localization of mitotic cells as well as the shift in asymmetrical cell division observed in *TBR2*KO organoids (Figure 32).

A second observation in *in vivo* studies was a decrease in thickness of layer VI <sup>101,104,182,183</sup> in *Tbr2* deficient mice, associated with a downregulation of *Tbr1*. *Tbr1* was then identified as one of the first downstream targets of *Tbr2* <sup>86</sup>. The influence of *Tbr2* on other layers of the cerebral cortex is not clear <sup>101,104 182</sup>. Also, in cortical organoids a

different expression of *TBR1* was observed in the *TBR2*KO organoids compared to the isogenic control. Immunostaining as well as expression data provided evidence that *TBR2* deficiency resulted in the downregulation of *TBR1* (Figure 33). In this doctoral work, *TBR2*KO organoids did not exhibit significant differences in the expression of *CTIP2* (predominantly expressed in layer V of the cerebral cortex) by IF (Figure 33). Our data could therefore not clarify if *TBR2* deficiency has an influence in other layers of the cerebral cortex.

In conclusion, this study shows that a human model was successfully established to study for the first time the role of *TBR2* in human corticogenesis. Some phenotypes previously observed *in vivo* could be reproduced in the human organoid model<sup>101,104,182,183</sup>. This suggests that *TBR2* effects may be conserved during evolution. Further studies on cortical organoids are ongoing to elucidate the upstream and downstream regulators of *TBR2*.

## 6. Abstract

The human brain is remarkably complex and has been subject to noteworthy changes throughout evolution. An expansion of progenitor cells is thought to contribute to the complexity and increase in cortical size that is observed in the human cortex as compared to non-human primates. The developmental mechanisms underlying the evolutionary changes are, however, poorly understood.

In this doctoral work, gene editing on hiPSCs and hiPSCs-derived organoids was exploited to study the function of *ARHGAP11B* and *TBR2*. *ARHGAP11B* is a human-specific gene expressed in radial glial cells, *TBR2* expression is characteristic of intermediate progenitors, conserved during evolution, and highly enriched in humans. In the human neocortex both genes play an important role in establishing the outer subventricular zone (oSVZ). Using CRISPR/Cas9 mediated gene editing, *ARHGAP11B* and *TBR2* hiPSC lines were generated. Following validation, forebrain-type organoid was generated from these KO lines to investigate morphologic and transcriptomic differences between the KO and the isogenic controls. An optimized protocol to generate homogenous organoids up to 2 months of age was developed.

Deficiency of *ARHGAP11B* had an important effect on the expansion of proliferative cells. At early time points the effects could be observed on neuroepithelial (NES) cells while at later stages basal radial glial cells (bRGC) were mainly affected. *TBR2* KO derived organoids showed a shift in asymmetrical plane of division of apical radial glial cells (aRG) at early stages. At more mature stages the *TBR2* deficiency had an impact on the generation of intermediate progenitors and significantly reduced the amount of layer VI *TBR1*<sup>+</sup> cortical neurons.

Taken together, this data indicates that both genes are fundamental for the correct development of the human brain. In their absence the amount of bRG and neurogenesis is impaired. Further studies will focus on their effects in older and or more mature organoids to assess their role in upper layer neurons. Importantly, this doctoral work highlights how transgenic organoids represent a powerful tool to map human-specific gene function in brain development, correlate genetics to functional phenotypes and to complement the long tradition of KO models in developmental biology and neuroscience.

## 7. List of Figures

FIGURE 1 NEURULATION.....	- 8 -
FIGURE 2 MORPHOGENS PATTERNING THE NEURAL TUBE.....	- 9 -
FIGURE 3 DETERMINATION OF BRAIN REGIONAL IDENTITIES .....	- 10 -
FIGURE 4 GROWTH OF THE NEURAL TUBE .....	- 11 -
FIGURE 5 SYMMETRIC VS ASYMMETRIC DIVISION OF RADIAL GLIAL CELLS .....	- 12 -
FIGURE 6 INTERKINETIC NUCLEAR MIGRATION IN THE VENTRICULAR ZONE .....	- 13 -
FIGURE 7 CELL MIGRATION AND CORTICOGENESIS.....	- 14 -
FIGURE 8 MOUSE VS HUMAN CORTEX .....	- 15 -
FIGURE 9 CELL DYNAMICS IN HUMAN CORTEX DEVELOPMENT.....	- 16 -
FIGURE 10 TRANSCRIPTION FACTORS TRANSITION DURING CORTICOGENESIS .....	- 17 -
FIGURE 11 NETWORK AND SIGNALING CASCADE AROUND TBR2.....	- 18 -
FIGURE 12 ARHGAP11B IMPACT IN DIFFERENT MODELS .....	- 20 -
FIGURE 13 IMPACT OF ARHGAP11B IN MITOCHONDRIA.....	- 21 -
FIGURE 14 PATTERNING OF PLURIPOTENT STEM CELL DERIVED NEURONS.....	- 23 -
FIGURE 15 3D NEURONAL CULTURES IN VITRO .....	- 25 -
FIGURE 16: GENERATION OF HIPSCs KNOCK-OUT (KO) CELL LINES. ....	- 56 -
FIGURE 17 CHARACTERIZATION OF HUMAN IPSC KO LINES. ....	- 57 -
FIGURE 18 VALIDATION OF TBR2KO. ....	- 58 -
FIGURE 19 VALIDATION OF ARHGAP11A/B-KO .....	- 58 -
FIGURE 20 KARYOTYPE AND PLURIPOTENCY CHARACTE-RIZATION OF THE SELECTED CLONES. ....	- 59 -
FIGURE 21 GENERATION OF DORSAL FOREBRAIN ORGANIDS.....	- 60 -
FIGURE 22 MATURE DORSAL FOREBRAIN ORGANIDS CHARACTERIZATION.....	- 62 -
FIGURE 23 ANALYSIS OF CORTICAL MARKERS IN DORSAL FOREBRAIN ORGANIDS. .	- 63 -
FIGURE 24 ARHGAP11KO ORGANIDS CHARACTERIZATION AT DAY 10.....	- 65 -
FIGURE 25 ARHGAP11KO ORGANIDS CHARACTERIZATION AT DAY 55.....	- 67 -
FIGURE 26 SINGLE CELL SEQUENCING DATA FROM ARHGAP11KO AND ISOGENIC CONTROL ORGANIDS. ....	- 68 -
FIGURE 27 BASAL RADIAL GLIA CELLS IN 55 DAYS OLD ORGANIDS. ....	- 69 -
FIGURE 28 ELECTROPORATION OF D55 DORSAL FOREBRAIN ORGANIDS.....	- 70 -
FIGURE 29 EFFECTS OF THE RESCUE OF ARHGAP11A AND/OR ARHGAP11B IN INTERMEDIATE PROGENITORS AND CORTICAL NEURONS. ....	- 72 -
FIGURE 30 EFFECTS OF THE RESCUE OF ARHGAP11A AND/OR ARHGAP11B IN BASAL RADIAL GLIA.....	- 73 -
FIGURE 31 ABVENTRICULAR MITOTIC CELLS IN TBR2KO DERIVED ORGANIDS.....	- 75 -
FIGURE 32 PLANE OF DIVISION CHANGES IN VENTRICULAR MITOTIC CELLS.....	- 76 -
FIGURE 33 CORTICAL DEVELOPMENT IN TBR2KO ORGANIDS. ....	- 77 -
FIGURE 34 RHO GTPASE REGULATION.....	- 82 -

## 8. List of Tables

TABLE 1: CELL LINES .....	- 28 -
TABLE 2: CELL CULTURE .....	- 28 -
TABLE 3: CELL CULTURE MEDIUM COMPOSITION .....	- 30 -
TABLE 4: EQUIPMENT .....	- 33 -
TABLE 5 CONSUMABLES .....	- 36 -
TABLE 6 REAGENTS AND CHEMICAL COMPOUNDS .....	- 37 -
TABLE 7 SELF-MADE BUFFER AND SOLUTIONS .....	- 39 -
TABLE 8 COMMERCIAL BUFFER AND SOLUTIONS .....	- 41 -
TABLE 9 ENZYMES .....	- 41 -
TABLE 10 REAGENTS .....	- 42 -
TABLE 11 KITS .....	- 42 -
TABLE 12 DATA PROCESSING .....	- 43 -
TABLE 13 PRIMERS .....	- 44 -
TABLE 14: PRIMARY ANTIBODIES .....	- 44 -
TABLE 15: SECONDARY ANTIBODIES .....	- 46 -
TABLE 16: SOFTWARE .....	- 46 -
TABLE 17: POLYMERASE CHAIN REACTION PROGRAM .....	- 53 -



## 9. References

1. Geschwind, D. H. & Rakic, P. Cortical evolution: Judge the brain by its cover. *Neuron* **80**, 633–647 (2013).
2. Douglas, R. J. & Martin, K. A. C. Neuronal circuits of the neocortex. *Annu. Rev. Neurosci.* **27**, 419–451 (2004).
3. Lui, J. H., Hansen, D. V. & Kriegstein, A. R. Development and evolution of the human neocortex. *Cell* **146**, 18–36 (2011).
4. Rakic, P. Evolution of the neocortex: A perspective from developmental biology. *Nat. Rev. Neurosci.* **10**, 724–735 (2009).
5. Azevedo, F. A. C. *et al.* Equal numbers of neuronal and nonneuronal cells make the human brain an isometrically scaled-up primate brain. *J. Comp. Neurol.* **513**, 532–541 (2009).
6. Eccles, J. C. Evolution of consciousness. *Proc. Natl. Acad. Sci. U. S. A.* **89**, 7320–7324 (1992).
7. Bear, M. F., Connors, B. W. & Paradiso, M. A. *Neuroscience: Exploring the brain.* (2016).
8. Florio, M. & Huttner, W. B. Neural progenitors, neurogenesis and the evolution of the neocortex. *Dev.* **141**, 2182–2194 (2014).
9. Sahara, S., Yanagawa, Y., O’Leary, D. D. M. & Stevens, C. F. The fraction of cortical GABAergic neurons is constant from near the start of cortical neurogenesis to adulthood. *J. Neurosci.* **32**, 4755–4761 (2012).
10. Stiles, J. & Jernigan, T. L. The basics of brain development. *Neuropsychol. Rev.* **20**, 327–348 (2010).
11. Lu, C. C., Brennan, J. & Robertson, E. J. From fertilization to gastrulation: Axis formation in the mouse embryo. *Curr. Opin. Genet. Dev.* **11**, 384–392 (2001).
12. Robb, L. & Tam, P. P. L. Gastrula organiser and embryonic patterning in the mouse. *Semin. Cell Dev. Biol.* **15**, 543–554 (2004).
13. Schoenwolf, G. C. & Smith, J. L. Mechanisms of neurulation: Traditional viewpoint and recent advances. *Development* **109**, 243–270 (1990).
14. Mangold, V. O. Über die Induktionsfähigkeit der verschiedenen Bezirke der Neurula von Urodelen. *Naturwissenschaften* **27**, (1933).
15. Placzek, M. The role of the notochord and floor plate in inductive interactions. *Curr. Opin. Genet. Dev.* **5**, 499–506 (1995).
16. Simoes-Costa, M. & Bronner, M. Establishing neural crest identity: a gene regulatory recipe. *Development* **142**, 242–257 (2015).
17. Larsen, W. J. *Human Embryology.* (2001).
18. Tanabe, Y. & Jessell, T. M. Diversity and pattern in the developing spinal cord. *Science (80- )*. **274**, 1115–1122 (1996).
19. Wilson, P. A. & Hemmati-Brivanlou, A. Vertebrate neural induction: Inducers, inhibitors, and a new synthesis. *Neuron* **18**, 699–710 (1997).
20. Le Douarin, N. & Kalcheim, C. *The neural crest.* (1999).
21. Ericson, J. *et al.* Sonic hedgehog induces the differentiation of ventral forebrain neurons: A common signal for ventral patterning within the neural tube. *Cell* **81**, 747–756 (1995).
22. Liem, K. F., Tremml, G., Roelink, H. & Jessell, T. M. Dorsal differentiation of neural plate cells induced by BMP-mediated signals from epidermal ectoderm. *Cell* **82**, 969–979 (1995).
23. Basler, K., Edlund, T., Jessell, T. M. & Yamada, T. Control of cell pattern in the neural tube: Regulation of cell differentiation by dorsalin-1, a novel TGF $\beta$  family member. *Cell* **73**, 687–702 (1993).
24. Shimamura, K. & Rubenstein, J. L. R. Inductive interactions direct early regionalization of

- the mouse forebrain. *Development* **124**, 2709–2718 (1997).
25. Marcelle, C., Stark, M. R. & Bronner-Fraser, M. Coordinate actions of BMPs, Wnts, Shh and noggin mediate patterning of the dorsal somite. *Development* **124**, 3955–3963 (1997).
  26. Chiang, C. *et al.* Mice lacking Sonic hedgehog gene function. *Nature* **383**, 407–413 (1996).
  27. Echelard, Y. *et al.* Sonic hedgehog, a member of a family of putative signaling molecules, is implicated in the regulation of CNS polarity. *Cell* **75**, 1417–1430 (1993).
  28. Briscoe, J. & Ericson, J. The specification of neuronal identity by graded sonic hedgehog signalling. *Semin. Cell Dev. Biol.* **10**, 353–362 (1999).
  29. Alberts, B. *et al.* *Molecular biology of the cell, Sixth edition.* ed. Garland Science, Taylor and Francis Group, New York, NY. (2015).
  30. Vieira, C. *et al.* Molecular mechanisms controlling brain development: An overview of neuroepithelial secondary organizers. *Int. J. Dev. Biol.* **54**, 7–20 (2010).
  31. Houart, C. *et al.* Establishment of the telencephalon during gastrulation by local antagonism of Wnt signaling. *Neuron* **35**, 255–265 (2002).
  32. Xuan, S. *et al.* Winged helix transcription factor BF-1 is essential for the development of the cerebral hemispheres. *Neuron* **14**, 1141–1152 (1995).
  33. Crossley, P. H., Martinez, S. & Martin, G. R. Midbrain development induced by FGF8 in the chick embryo. *Nature* **380**, 66–68 (1996).
  34. Martinez-Ferre, A. & Martinez, S. Molecular regionalization of the diencephalon. *Front. Neurosci.* **6**, 1–10 (2012).
  35. Scholpp, S., Wolf, O., Brand, M. & Lumsden, A. Hedgehog signalling from the zona limitans intrathalamica orchestrates patterning of the zebrafish diencephalon. *Development* **133**, 855–864 (2006).
  36. Tole, S. & Patterson, P. H. Regionalization of the developing forebrain: A comparison of FORSE-1, Dlx- 2, and BF-1. *J. Neurosci.* **15**, 970–980 (1995).
  37. Alexander, P. & Wassef, M. The isthmic organizer links anteroposterior and dorsoventral patterning in the mid/hindbrain by generating roof plate structures. *Development* **130**, 5331–5338 (2003).
  38. Nakamura, H., Sato, T. & Suzuki-Hirano, A. Isthmus organizer for mesencephalon and metencephalon. *Dev. Growth Differ.* **50**, (2008).
  39. Gavalas, A. & Krumlauf, R. Retinoid signalling and hindbrain patterning. *Curr. Opin. Genet. Dev.* **10**, 380–386 (2000).
  40. Halilagic, A., Zile, M. H. & Studer, M. A novel role for retinoids in patterning the avian forebrain during presomite stages. *Development* **130**, 2039–2050 (2003).
  41. Molotkova, N., Molotkov, A. & Gregg, D. Role of retinoic acid during forebrain development begins late when Raldh3 generates retinoic acid in the ventral subventricular zone. *Dev. Biol.* **303**, 601–610 (2007).
  42. Schneider, R. A., Hu, D., Rubenstein, J. L. R., Maden, M. & Helms, J. A. Local retinoid signaling coordinates forebrain and facial morphogenesis by maintaining FGF8 and SHH. *Development* **128**, 2755–2767 (2001).
  43. Siegenthaler, J. A. *et al.* Retinoic Acid from the Meninges Regulates Cortical Neuron Generation. *Cell* **139**, 597–609 (2009).
  44. Götz, M. & Huttner, W. B. The cell biology of neurogenesis. *Nat. Rev. Mol. Cell Biol.* **6**, 777–788 (2005).
  45. Florio, M. & Huttner, W. B. Neural progenitors, neurogenesis and the evolution of the neocortex. *Development* **141**, 2182–2194 (2014).
  46. Chenn, A. & McConnell, S. K. Cleavage Orientation and the Asymmetric Inheritance of Notch1 Immunoreactivity in Mammalian Neurogenesis. *Cell* **82**, 631–641 (1995).
  47. Huttner, W. B. & Kosodo, Y. Symmetric versus asymmetric cell division during neurogenesis in the developing vertebrate central nervous system. *Curr. Opin. Cell Biol.*

- 17, 648–657 (2005).
48. Rakic, P. A small step for the cell, a giant leap for mankind: a hypothesis of neocortical expansion during evolution. *Trends Neurosci.* **18**, 383–388 (1995).
  49. Rakic, P. & Swaab, D. F. Defects of neuronal migration and the pathogenesis of cortical malformations. *Prog. Brain Res.* **73**, 15–37 (1988).
  50. Arai, Y. & Taverna, E. Neural progenitor cell polarity and cortical development. *Front. Cell. Neurosci.* **11**, 1–11 (2017).
  51. Malatesta, P., Appolloni, I. & Calzolari, F. Radial glia and neural stem cells. *Cell Tissue Res.* **331**, 165–178 (2008).
  52. Schnitzer, J., Franke, W. W. & Schachner, M. Immunocytochemical demonstration of vimentin in astrocytes and ependymal cells of developing and adult mouse nervous system. *J. Cell Biol.* **90**, 435–447 (1981).
  53. Zecevic, N. Specific characteristic of radial glia in the human fetal telencephalon. *Glia* **48**, 27–35 (2004).
  54. Malatesta, P., Hartfuss, E. & Götz, M. Isolation of radial glial cells by fluorescent-activated cell sorting reveals a neural lineage. *Development* **127**, 5253–5263 (2000).
  55. Baye, L. M. & Link, B. A. Interkinetic nuclear migration and the selection of neurogenic cell divisions during vertebrate retinogenesis. *J. Neurosci.* **27**, 10143–10152 (2007).
  56. Del Bene, F. Interkinetic nuclear migration: Cell cycle on the move. *EMBO J.* **30**, 1676–1677 (2011).
  57. Miyata, T. *et al.* Asymmetric production of surface-dividing and non-surface-dividing cortical progenitor cells. *Development* **131**, 3133–3145 (2004).
  58. Noctor, S. C., Martinez-Cerdeño, V., Ivic, L. & Kriegstein, A. R. Cortical neurons arise in symmetric and asymmetric division zones and migrate through specific phases. *Nat. Neurosci.* **7**, 136–144 (2004).
  59. Sauer, F. C. Mitosis in the neural tube. *J. Comp. Neurol.* **62**, 377–405 (1935).
  60. Miyata, T., Okamoto, M., Shinoda, T. & Kawaguchi, A. Interkinetic nuclear migration generates and opposes ventricular-zone crowding: Insight into tissue mechanics. *Front. Cell. Neurosci.* **8**, 1–11 (2015).
  61. Del Bene, F., Wehman, A. M., Link, B. A. & Baier, H. Regulation of Neurogenesis by Interkinetic Nuclear Migration through an Apical-Basal Notch Gradient. *Cell* **134**, 1055–1065 (2008).
  62. Caviness, V. S. Neocortical histogenesis in normal and reeler mice: A developmental study based upon [3H]thymidine autoradiography. *Dev. Brain Res.* **4**, 293–302 (1982).
  63. Zecevic, N. & Rakic, P. Development of layer I neurons in the primate cerebral cortex. *J. Neurosci.* **21**, 5607–5619 (2001).
  64. Rakic, S. & Zecevic, N. Emerging complexity of layer I in human cerebral cortex. *Cereb. Cortex* **13**, 1072–1083 (2003).
  65. Soriano, P. The PDGF $\alpha$  receptor is required for neural crest cell development and for normal patterning of the somites. *Development* **124**, 2691–2700 (1997).
  66. Nichols, A. J. & Olson, E. C. Reelin promotes neuronal orientation and dendritogenesis during preplate splitting. *Cereb. Cortex* **20**, 2213–2223 (2010).
  67. Zecevic, N., Chen, Y. & Filipovic, R. Contributions of cortical subventricular zone to the development of the human cerebral cortex. *J. Comp. Neurol.* **491**, 109–122 (2005).
  68. Budday, S., Steinmann, P. & Kuhl, E. Physical biology of human brain development. *Front. Cell. Neurosci.* **9**, 1–17 (2015).
  69. Allendoerfer, K. L. & Shatz, C. J. The subplate, a transient neocortical structure: Its role in the development of connections between thalamus and cortex. *Annu. Rev. Neurosci.* **17**, 185–218 (1994).
  70. Kostovic, I. & Rakic, P. Developmental history of the transient subplate zone in the visual and somatosensory cortex of the macaque monkey and human brain. *J. Comp. Neurol.* **297**, 441–470 (1990).

71. Raybaud, C., Ahmad, T., Rastegar, N., Shroff, M. & Al Nassar, M. The premature brain: Developmental and lesional anatomy. *Neuroradiology* **55**, (2013).
72. Goldman, S. A. & Kuypers, N. J. How to make an oligodendrocyte. *Dev.* **142**, 3983–3995 (2015).
73. Clowry, G., Molnár, Z. & Rakic, P. Renewed focus on the developing human neocortex. *J. Anat.* **217**, 276–288 (2010).
74. Molnár, Z. & Clowry, G. Cerebral cortical development in rodents and primates. *Prog. Brain Res.* **195**, 45–70 (2012).
75. Herculano-Houzel, S. The human brain in numbers: a linearly scaled-up primate brain. *Front. Hum. Neurosci.* **3**, 1–11 (2009).
76. Hofman, M. A. Size and shape of the cerebral cortex in mammals: II. The cortical volume. *Brain. Behav. Evol.* **32**, 17–26 (1988).
77. Zilles, K., Palomero-Gallagher, N. & Amunts, K. Development of cortical folding during evolution and ontogeny. *Trends Neurosci.* **36**, 275–284 (2013).
78. Toda, T., Shinmyo, Y., Dinh Duong, T. A., Masuda, K. & Kawasaki, H. An essential role of SVZ progenitors in cortical folding in gyrencephalic mammals. *Sci. Rep.* **6**, 1–12 (2016).
79. Nonaka-Kinoshita, M. *et al.* Regulation of cerebral cortex size and folding by expansion of basal progenitors. *EMBO J.* **32**, 1817–1828 (2013).
80. Gertz, C. C. & Kriegstein, A. R. Neuronal migration dynamics in the developing ferret cortex. *J. Neurosci.* **35**, 14307–14315 (2015).
81. Nowakowski, T. J. *et al.* Spatiotemporal gene expression trajectories reveal developmental hierarchies of the human cortex. *Science (80-. ).* **358**, 1318–1323 (2017).
82. Mora-Bermúdez, F. *et al.* Differences and similarities between human and chimpanzee neural progenitors during cerebral cortex development. *Elife* **5**, 1–24 (2016).
83. Smart, I. H. M., Dehay, C., Giroud, P., Berland, M. & Kennedy, H. Unique morphological features of the proliferative zones and postmitotic compartments of the neural epithelium giving rise to striate and extrastriate cortex in the monkey. *Cereb. Cortex* **12**, 37–53 (2002).
84. Fish, J. L., Dehay, C., Kennedy, H. & Huttner, W. B. Making bigger brains - The evolution of neural-progenitor-cell division. *J. Cell Sci.* **121**, 2783–2793 (2008).
85. Penisson, M., Ladewig, J., Belvindrah, R. & Francis, F. Genes and Mechanisms Involved in the Generation and Amplification of Basal Radial Glial Cells. *Front. Cell. Neurosci.* **13**, 1–21 (2019).
86. Englund, C. *et al.* Pax6, Tbr2, and Tbr1 are expressed sequentially by radial glia, intermediate progenitor cells, and postmitotic neurons in developing neocortex. *J. Neurosci.* **25**, 247–251 (2005).
87. Haubensak, W., Attardo, A., Denk, W. & Huttner, W. B. Neurons arise in the basal neuroepithelium of the early mammalian telencephalon: A major site of neurogenesis. *Proc. Natl. Acad. Sci. U. S. A.* **101**, 3196–3201 (2004).
88. Noctor SC, Flint AC, Weissman TA, Dammerman RS, K. A. Neurons derived from radial glial cells establish radial units in neocortex. *Nature* **409**, 714–720 (2001).
89. Martínez-Martínez, M. Á. *et al.* A restricted period for formation of outer subventricular zone defined by Cdh1 and Trnp1 levels. *Nat. Commun.* **7**, (2016).
90. Kawaue, T. *et al.* Lzts1 controls both neuronal delamination and outer radial glial-like cell generation during mammalian cerebral development. *Nat. Commun.* **10**, 1–18 (2019).
91. Hansen, D. V., Lui, J. H., Parker, P. R. L. & Kriegstein, A. R. Neurogenic radial glia in the outer subventricular zone of human neocortex. *Nature* **464**, 554–561 (2010).
92. Kalebic, N. *et al.* Neocortical Expansion Due to Increased Proliferation of Basal Progenitors Is Linked to Changes in Their Morphology. *Cell Stem Cell* **24**, 535-550.e9 (2019).
93. Pollen, A. A. *et al.* Molecular Identity of Human Outer Radial Glia during Cortical Development. *Cell* **163**, 55–67 (2015).

94. Betizeau, M. *et al.* Precursor Diversity and Complexity of Lineage Relationships in the Outer Subventricular Zone of the Primate. *Neuron* **80**, 442–457 (2013).
95. Reillo, I., De Juan Romero, C., García-Cabezas, M. Á. & Borrell, V. A Role for intermediate radial glia in the tangential expansion of the mammalian cerebral cortex. *Cereb. Cortex* **21**, 1674–1694 (2011).
96. Liu, J. *et al.* The Primate-Specific Gene TMEM14B Marks Outer Radial Glia Cells and Promotes Cortical Expansion and Folding. *Cell Stem Cell* **21**, 635–649.e8 (2017).
97. Fiddes, I. T. *et al.* Human-Specific NOTCH2NL Genes Affect Notch Signaling and Cortical Neurogenesis. *Cell* **173**, 1356–1369.e22 (2018).
98. Florio, M. *et al.* Evolution and cell-type specificity of human-specific genes preferentially expressed in progenitors of fetal neocortex. *Elife* **7**, 1–37 (2018).
99. Kowalczyk, T. *et al.* Intermediate neuronal progenitors (basal progenitors) produce pyramidal-projection neurons for all layers of cerebral cortex. *Cereb. Cortex* **19**, 2439–2450 (2009).
100. Mihalas, A. B. & Hevner, R. F. *Control of Neuronal Development by T-Box Genes in the Brain. Current Topics in Developmental Biology* **122**, (Elsevier Inc., 2017).
101. Arnold, S. J. *et al.* The T-box transcription factor Eomes/Tbr2 regulates neurogenesis in the cortical subventricular zone. *Genes Dev.* **22**, 2479–2484 (2008).
102. Russ, A. P. *et al.* Eomesodermin is required for mouse trophoblast development and mesoderm formation. *Nature* **404**, 95–99 (2000).
103. Sessa, A. *et al.* The Tbr2 Molecular Network Controls Cortical Neuronal Differentiation Through Complementary Genetic and Epigenetic Pathways. *Cereb. Cortex* **27**, 3378–3396 (2017).
104. Mihalas, A. B. *et al.* Intermediate Progenitor Cohorts Differentially Generate Cortical Layers and Require Tbr2 for Timely Acquisition of Neuronal Subtype Identity. *Cell Rep.* **16**, 92–105 (2016).
105. Elsen, G. E. *et al.* The protomap is propagated to cortical plate neurons through an Eomes-dependent intermediate map. *Proc. Natl. Acad. Sci. U. S. A.* **110**, 4081–4086 (2013).
106. Martínez-Cerdeño, V., Noctor, S. C. & Kriegstein, A. R. The role of intermediate progenitor cells in the evolutionary expansion of the cerebral cortex. *Cereb. Cortex* **16**, (2006).
107. Pontious, A., Kowalczyk, T., Englund, C. & Hevner, R. F. Role of intermediate progenitor cells in cerebral cortex development. *Dev. Neurosci.* **30**, 24–32 (2007).
108. Baala, L. *et al.* Homozygous silencing of T-box transcription factor EOMES leads to microcephaly with polymicrogyria and corpus callosum agenesis. *Nat. Genet.* **39**, 454–456 (2007).
109. Abe, P. *et al.* Intermediate progenitors facilitate intracortical progression of thalamocortical axons and interneurons through CXCL12 chemokine signaling. *J. Neurosci.* **35**, 13053–13063 (2015).
110. Sessa, A. *et al.* Tbr2-positive intermediate (basal) neuronal progenitors safeguard cerebral cortex expansion by controlling amplification of pallial glutamatergic neurons and attraction of subpallial GABAergic interneurons. *Genes Dev.* **24**, 1816–1826 (2010).
111. Vasistha, N. A. *et al.* Cortical and clonal contribution of Tbr2 expressing progenitors in the developing mouse brain. *Cereb. Cortex* **25**, 3290–3302 (2015).
112. Arnò, B. *et al.* Neural progenitor cells orchestrate microglia migration and positioning into the developing cortex. *Nat. Commun.* **5**, (2014).
113. Hevner, R. F., Hodge, R. D., Daza, R. A. M. & Englund, C. Transcription factors in glutamatergic neurogenesis: Conserved programs in neocortex, cerebellum, and adult hippocampus. *Neurosci. Res.* **55**, 223–233 (2006).
114. Hevner, R. F. Intermediate progenitors and Tbr2 in cortical development. *J. Anat.* **235**, 616–625 (2019).

115. Ding, J. & Pollen, A. A. Filling an ARHGAP in our knowledge of human brain evolution . *EMBO Rep.* **23**, 10–12 (2022).
116. Florio, M. *et al.* Human-specific gene ARHGAP11B promotes basal progenitor amplification and neocortex expansion. *Science (80-. )*. **347**, 1465–1470 (2015).
117. Namba, T. *et al.* Human-Specific ARHGAP11B Acts in Mitochondria to Expand Neocortical Progenitors by Glutaminolysis. *Neuron* **105**, 867-881.e9 (2020).
118. Kalebic, N. *et al.* Human-specific ARHGAP11B induces hallmarks of neocortical expansion in developing ferret neocortex. *Elife* **7**, 1–25 (2018).
119. Heide, M. *et al.* Human-specific ARHGAP11B increases size and folding of primate neocortex in the fetal marmoset. *Science (80-. )*. **369**, 546–550 (2020).
120. Marsoner, F. *et al.* Human-specific ARHGAP11B ensures human-like basal progenitor levels in hominid cerebral organoids. *EMBO Rep.* **23**, 1–19 (2022).
121. Sousa, A. M. M., Meyer, K. A., Santpere, G., Gulden, F. O. & Sestan, N. Evolution of the Human Nervous System Function, Structure, and Development. *Cell* **170(2)**, 226–247 (2017).
122. Takahashi, K. & Yamanaka, S. Induction of pluripotent stem cells from mouse embryonic and adult fibroblast cultures by defined factors. *Cell* **126 VN-**, 663–676 (2006).
123. Takahashi, K. *et al.* Induction of pluripotent stem cells from adult human fibroblasts by defined factors. *Cell* **131**, 861–72 (2007).
124. Marsoner, F. *et al.* Generation and characterization of an induced pluripotent stem cell (iPSC) line from a patient with clozapine-resistant Schizophrenia. *Stem Cell Res.* **17**, 661–664 (2016).
125. Fusaki, N., Ban, H., Nishiyama, A., Saeki, K. & Hasegawa, M. Efficient induction of transgene-free human pluripotent stem cells using a vector based on Sendai virus, an RNA virus that does not integrate into the host genome. *Proc. Jpn. Acad. Ser. B. Phys. Biol. Sci.* **85**, 348–62 (2009).
126. Zeltner, N. & Studer, L. Pluripotent stem cell-based disease modeling: Current hurdles and future promise. *Curr. Opin. Cell Biol.* **37**, 102–110 (2015).
127. Reynolds, B. A., Tetzlaff, W. & Weiss, S. A multipotent EGF-responsive striatal embryonic progenitor cell produces neurons and astrocytes. *J. Neurosci.* **12**, 4565–4574 (1992).
128. Reynolds, B. A. & Weiss, S. Generation of neurons and astrocytes from isolated cells of the adult mammalian central nervous system. *Science (80-. )*. **255**, 1707–1710 (1992).
129. Conti, L. *et al.* Niche-independent symmetrical self-renewal of a mammalian tissue stem cell. *PLoS Biol.* **3**, 1594–1606 (2005).
130. Koch, P., Opitz, T., Steinbeck, J. A., Ladewig, J. & Brüstle, O. A rosette-type, self-renewing human ES cell-derived neural stem cell with potential for in vitro instruction and synaptic integration. *Proc. Natl. Acad. Sci. U. S. A.* **106**, 3225–3230 (2009).
131. Falk, A. *et al.* Capture of neuroepithelial-like stem cells from pluripotent stem cells provides a versatile system for in vitro production of human neurons. *PLoS One* **7**, 1–13 (2012).
132. Elkabetz, Y. *et al.* Human ES cell-derived neural rosettes reveal a functionally distinct early neural stem cell stage. *Genes Dev.* **22**, 1257 (2008).
133. Shi, Y., Kirwan, P. & Livesey, F. J. Directed differentiation of human pluripotent stem cells to cerebral cortex neurons and neural networks. *Nat. Protoc.* **7**, 1836–1846 (2012).
134. Chambers, S. M. *et al.* Highly efficient neural conversion of human ES and iPS cells by dual inhibition of SMAD signaling. *Nat. Biotechnol.* **27**, 275–80 (2009).
135. Paşca, S. P., Panagiotakos, G. & Dolmetsch, R. E. Generating human neurons in vitro and using them to understand neuropsychiatric disease. *Annu. Rev. Neurosci.* **37**, 479–501 (2014).
136. Espuny-Camacho, I. *et al.* Pyramidal Neurons Derived from Human Pluripotent Stem Cells Integrate Efficiently into Mouse Brain Circuits In Vivo. *Neuron* **77**, 440–456 (2013).
137. Suzuki, I. K. & Vanderhaeghen, P. Is this a brain which i see before me? Modeling human

- neural development with pluripotent stem cells. *Dev.* **142**, 3138–3150 (2015).
138. Quadrato, G., Brown, J. & Arlotta, P. The promises and challenges of human brain organoids as models of neuropsychiatric disease. *Nat. Med.* **22**, 1220–1228 (2016).
  139. Watanabe, K. *et al.* Directed differentiation of telencephalic precursors from embryonic stem cells. *Nat. Neurosci.* **8**, 288–296 (2005).
  140. Eiraku, M. *et al.* Self-Organized Formation of Polarized Cortical Tissues from ESCs and Its Active Manipulation by Extrinsic Signals. *Cell Stem Cell* **3**, 519–532 (2008).
  141. Eiraku, M. *et al.* Self-organizing optic-cup morphogenesis in three-dimensional culture. *Nature* **472**, 51–58 (2011).
  142. Lancaster, M. A. *et al.* Cerebral organoids model human brain development and microcephaly. *Nature* **501**, 373–379 (2013).
  143. Marsoner, F., Koch, P. & Ladewig, J. Cortical organoids: why all this hype? *Curr. Opin. Genet. Dev.* **52**, 22–28 (2018).
  144. Qian, X., Song, H. & Ming, G. L. Brain organoids: Advances, applications and challenges. *Dev.* **146**, (2008).
  145. Iefremova, V. *et al.* An Organoid-Based Model of Cortical Development Identifies Non-Cell-Autonomous Defects in Wnt Signaling Contributing to Miller-Dieker Syndrome. *Cell Rep.* **19**, 50–59 (2017).
  146. Mariani, J. *et al.* Modeling human cortical development in vitro using induced pluripotent stem cells. *Proc. Natl. Acad. Sci. U. S. A.* **109**, 12770–12775 (2012).
  147. Qian, X. *et al.* Brain-Region-Specific Organoids Using Mini-bioreactors for Modeling ZIKV Exposure. *Cell* **165**, 1238–1254 (2016).
  148. Jo, J. *et al.* Midbrain-like Organoids from Human Pluripotent Stem Cells Contain Functional Dopaminergic and Neuromelanin-Producing Neurons. *Cell Stem Cell* **19**, 248–257 (2016).
  149. Qian, X. *et al.* Generation of human brain region-specific organoids using a miniaturized spinning bioreactor. *Nat. Protoc.* **13**, 565–580 (2018).
  150. Fligor, C. M. *et al.* Three-Dimensional Retinal Organoids Facilitate the Investigation of Retinal Ganglion Cell Development, Organization and Neurite Outgrowth from Human Pluripotent Stem Cells. *Sci. Rep.* **8**, 1–14 (2018).
  151. Xiang, Y. *et al.* Fusion of Regionally Specified hPSC-Derived Organoids Models Human Brain Development and Interneuron Migration. *Cell Stem Cell* **21**, 383-398.e7 (2017).
  152. Kadoshima, T. *et al.* Self-organization of axial polarity, inside-out layer pattern, and species-specific progenitor dynamics in human ES cell-derived neocortex. *Proc. Natl. Acad. Sci.* **110**, 20284–20289 (2013).
  153. Pasca, A. M. *et al.* Functional cortical neurons and astrocytes from human pluripotent stem cells in 3D culture. *Nat. Methods* **12**, 671–678 (2015).
  154. Heymann, D. L. *et al.* Zika virus and microcephaly: Why is this situation a PHEIC? *Lancet* **387**, 719–721 (2016).
  155. Mlakar, J. *et al.* Zika Virus Associated with Microcephaly. *N. Engl. J. Med.* **374**, 951–958 (2016).
  156. Ventura, C. V., Maia, M., Bravo-Filho, V., Góis, A. L. & Belfort, R. Zika virus in Brazil and macular atrophy in a child with microcephaly. *Lancet* **387**, 228 (2016).
  157. Gabriel, E. *et al.* Recent Zika Virus Isolates Induce Premature Differentiation of Neural Progenitors in Human Brain Organoids. *Cell Stem Cell* **20**, 397-406.e5 (2017).
  158. Bershteyn, M. *et al.* Human iPSC-Derived Cerebral Organoids Model Cellular Features of Lissencephaly and Reveal Prolonged Mitosis of Outer Radial Glia. *Cell Stem Cell* **20**, 435-449.e4 (2017).
  159. Qian, X., Nguyen, H. N., Jacob, F., Song, H. & Ming, G. L. Using brain organoids to understand Zika virus-induced microcephaly. *Dev.* **144**, 952–957 (2017).
  160. Gonzalez, C. *et al.* Modeling amyloid beta and tau pathology in human cerebral organoids. *Mol. Psychiatry* **23**, 2363–2374 (2018).

161. Luo, C. *et al.* Cerebral Organoids Recapitulate Epigenomic Signatures of the Human Fetal Brain. *Cell Rep.* **17**, 3369–3384 (2016).
162. Camp, J. G. *et al.* Human cerebral organoids recapitulate gene expression programs of fetal neocortex development. *Proc. Natl. Acad. Sci.* **112**, 201520760 (2015).
163. Krefft, O., Jabali, A., Iefremova, V., Koch, P. & Ladewig, J. Generation of standardized and reproducible forebrain-type cerebral organoids from human induced pluripotent stem cells. *J. Vis. Exp.* **2018**, 1–8 (2018).
164. Krefft, O., Jabali, A., Iefremova, V., Koch, P. & Ladewig, J. Generation of Standardized and Reproducible Forebrain-type Cerebral Organoids from Human Induced Pluripotent Stem Cells Video Link. *J. Vis. Exp* **56768**, 1–8 (2017).
165. Kanton, S. *et al.* Organoid single-cell genomic atlas uncovers human-specific features of brain development. *Nature* **574**, (2019).
166. Huch, M. & Koo, B. K. Modeling mouse and human development using organoid cultures. *Dev.* **142**, 3113–3125 (2015).
167. Jinek, M. *et al.* A Programmable Dual-RNA–Guided DNA Endonuclease in Adaptive Bacterial Immunity. *Science (80- )*. **337**, 816–822 (2012).
168. McTague, A., Rossignoli, G., Ferrini, A., Barral, S. & Kurian, M. A. Genome Editing in iPSC-Based Neural Systems: From Disease Models to Future Therapeutic Strategies. *Front. Genome Ed.* **3**, (2021).
169. Lancaster, M. A. *et al.* Cerebral organoids model human brain development and microcephaly. *Nature* **501**, 373–379 (2013).
170. Iefremova, V. *et al.* An Organoid-Based Model of Cortical Development Identifies Non-Cell-Autonomous Defects in Wnt Signaling Contributing to Miller-Dieker Syndrome. *Cell Rep.* **19**, 50–59 (2017).
171. Hall, B., Limaye, A. & Kulkarni, A. B. Overview: Generation of Gene Knockout Mice. *Curr. Protoc. Cell Biol.* (2009). doi:10.1002/0471143030.cb1912s44
172. Vogel, G. A knockout Award in Medicine. *Science (80- )*. **318**, 179–179 (2007).
173. Ellis, J. & Bhatia, M. iPSC technology: Platform for drug discovery. *Clin. Pharmacol. Ther.* **89**, 639–641 (2011).
174. Kim, C. iPSC technology-Powerful hand for disease modeling and therapeutic screen. *BMB Rep.* **48**, 256–265 (2015).
175. Chun, Y. S., Byun, K. & Lee, B. Induced pluripotent stem cells and personalized medicine: current progress and future perspectives. *Anat. Cell Biol.* **44**, 245 (2011).
176. Sasai, Y., Eiraku, M. & Suga, H. In vitro organogenesis in three dimensions: self-organising stem cells. *Development* **139**, 4111–21 (2012).
177. Kelava, I. & Lancaster, M. A. Dishing out mini-brains: Current progress and future prospects in brain organoid research. *Dev. Biol.* **420**, 199–209 (2016).
178. Florio, M. *et al.* Human-specific gene ARHGAP11B promotes basal progenitor amplification and neocortex expansion. *Science (80- )*. **347**, 1465–1470 (2015).
179. Mosaddeghzadeh, N. & Ahmadian, M. R. The rho family gtpases: Mechanisms of regulation and signaling. *Cells* **10**, (2021).
180. Kagawa, Y. *et al.* Cell cycle-dependent Rho GTPase activity dynamically regulates cancer cell motility and invasion in vivo. *PLoS One* **8**, (2013).
181. Pilaz, L. J. *et al.* Subcellular mRNA localization and local translation of ARHGAP11A in radial glial cells regulates cortical development. *bioRxiv Juli* **31**, 1–55 (2020).
182. Sessa, A., Mao, C. an, Hadjantonakis, A. K., Klein, W. H. & Broccoli, V. Tbr2 Directs Conversion of Radial Glia into Basal Precursors and Guides Neuronal Amplification by Indirect Neurogenesis in the Developing Neocortex. *Neuron* **60**, 56–69 (2008).
183. Lv, X. *et al.* TBR2 coordinates neurogenesis expansion and precise microcircuit organization via Protocadherin 19 in the mammalian cortex. *Nat. Commun.* **10**, 1–15 (2019).



## 10. Acknowledgements

A lot of people have to be acknowledged for their help and support during my PhD.

First my supervisor Julia Ladewig and Philipp Koch. I learned a lot from you during those years, and I will always be grateful for giving me the possibility to join the lab in the first place and also to support my decision to leave the lab to start a new career. I'm happy about what we achieved together, and I wish you all the best for your bright future career.

A big thanks also to Prof. Dr. Wieland Huttner and Dr. Michael Heide. Our collaboration gave me a new perspective on the project itself. I'm proud of our work and the article we managed to publish together. I think it was a perfect example of how collaboration in science is key in reach your goal and helping others to reach theirs. Also, thanks to your colleagues in Dresden, who collaborate on the paper we published together.

The first one and a half years in Bonn have been probably the most joyful months of my PhD., so I really have to thank Prof. Dr. Brüstle for giving me a chance to start working at Life and Brain, but also to all the amazing colleagues I met there. Kevin, Fredi, Marianna, and Jasmin in particular, thanks for all the great moments we spent together, in the lab but also outside. We built a strong friendship and I'm really looking forward to celebrating with you in Bonn one more time!

Moving to Mannheim and leaving such good friends behind was not easy but has been the chance to meet other fantastic people. Thanks to all the people in the lab and especially Elena, Julia, Klara, Karen, Malin, Andrea, Annasara, Raquel, and Ruven. Thanks for the beautiful memories I have in my mind when thinking about every each of you. It was great to know that I could count on you when I needed some support. I'm sure there will be many more moments that we will share together.

An enormous thanks to Sonia and Foro, who have been my truly best friends in the last few years. You have been the anchor to reach out in difficult times and the perfect people to party and share happy moments with. Apparently, we keep following each other around Germany and now even Nederland! I cannot be happier about that. Sonia, I really appreciate your time and effort in reading and giving input on this thesis! Love you, guys.

Obviously, I cannot leave my family out of the acknowledgment, since they are the most important people in my life. For sure it has not been easy for you to see me going abroad, but I hope that I have made you proud. Grazie di tutto mami, papi e Chiara <3. Last but not least a big thanks to Kim, who had to experience the last stressful time of the PhD, with the writing of the thesis and the submission. Thank you for your encouragement and motivation, I love you.